THERMIONIC EMISSION FROM AND SURFACE STRUCTURE OF SINGLE CRYSTALS OF TUNGSTEN

Thesis by

George Foster Smith

In Partial Fulfillment of the Requirements

for the Degree of

Doctor of Philosophy

California Institute of Technology

Pasadena, California

1952

ABSTRACT

Surface structure of and thermionic emission from single crystals of tungsten grown in 5-mil wires by the Robinson method (2) were investigated. Photomicrographic evidence points to the existence of "plateaus" on the surface normal to the (110), (112), and (001) directions of a crystal heated sufficiently in vacuum to evaporate 3.5 to 4 percent of the wire diameter; these plateaus were about 11°, 6°, and 7°, respectively, in angular width. Superimposed upon the plateaus was to be found a "shingle" structure previously observed by Nichols (7) in the (110) direction. A crystal wire subjected to only mild heat treatment (22 hrs. at 1980°K. and 20 min. at 2280°K.) also showed both types of structure, indicating that evaporation cannot be the only mechanism involved. All wires were heated by a.c. exclusively, to avoid the "d.c. etch." (5,6,7).

Polar plots of the thermionic emission vs. angle about the wire show "flats" of emission, confirming the existence of the plateaus. New values of the thermionic constants for different crystal directions were measured on a crystal having a minimum of shingling, in the same tube used by Nichols (7), modified to eliminate an anomalous effect discovered during preliminary tests. The modification did not appreciably alter the emission constants for the (111), (112), (116), and (001) directions, which constants are in good agreement with Nichols' values (7,8). A second anomalous effect contributed to the currents measured in the low emission (110) direction, rendering normally obtained values erroneous (including those of Nichols'). Although the true (110)

constants could not be obtained, an upper limit for the emission is characterized by $\phi^{**} = 4.72$, $A^{**} = 9.7$, and a 5.26 volt estimate is deduced for ϕ^{**}.

Contact potentials, determined by comparing retarding potential curves taken in different directions, failed to agree in general with apparent work function differences. The disagreement can be explained by (a) assuming uniform surfaces with temperature dependent work functions, in which case the temperature derivatives obtained also account for departure of the A^{**} values from 120; or (b) assuming patchy surfaces with temperature independent patch work functions; two-patch surfaces are demonstrated which can account for the observed data. There was no evidence in general for patchiness of the single crystal surfaces investigated; however, the usual tests cannot conclusively deny the existence of patchiness.

ACKNOWLEDGMENTS

Especial gratitude is due to Professor M. H. Nichols, who suggested the problem, for his continued interest and inspiration, for stimulating discussions, and for his many suggestions.

I should also like to thank Professors W. R. Smythe and H. V. Neher for helpful discussions.

Mr. Trueman Robbins assisted with the glass blowing connected with the problem. Mr. T. W. Harvey and Miss Dorothy Denhard assisted with the preparation of the illustrations.

I am grateful to the Standard Oil Company of California for the Standard Oil Company Fellowship, during the tenure of which part of this work was done. The work was also assisted by a Research Corporation grant and by Office of Naval Research sponsorship.

Finally, I should like to thank my wife, without whose assistance and encouragement the work could not have been completed.

TABLE OF CONTENTS

PART I. GROWTH AND SURFACE STRUCTURE OF SINGLE CRYSTALS OF TUNGSTEN

The technique of producing crystals of centimeter length in tungsten wire is by now well known. As a result of about 1 percent of "dope" consisting of Na_2O, K_2O, $CaCl_2$, Al_2O_3 and SiO_2 added before the sintering process (1), the "non-sag" type of tungsten wire recrystallizes into crystals occupying the entire cross section of the wire. Robinson (2) has shown that under a favorable vacuum heat treatment schedule one can produce crystals several centimeters long in prewar non-sag tungsten wire.* Chemical analyses of the doped tungsten wire after the usual heat treatment connected with thermionic emission measurements show about the same very small relative impurity content as in undoped wire (3). This fact along with thermionic emission stability through all temperature cycles after sufficient heat treatment, gives assurance that emission studies of doped wire are actually characteristic of pure tungsten (3). As a result of the working given the wire during the drawing process, the crystals grown in doped wire are normally oriented with a face diagonal very nearly parallel to the wire axis. This orientation is particularly favorable to emission studies, since if the wire is smooth and round the placing of the face diagonal along the wire axis causes directions emerging normal to the surface to include all directions with Miller indices of the form (hhk). Martin's work (4) with thermionic emission from a single crystal sphere

---

* According to Mr. George Moore, of the Bell Telephone Laboratories, there is a difference in the properties of prewar "non-sag" tungsten wire and the corresponding postwar production in that it is very difficult to produce large crystals in the latter. This may be due to different impurities occurring in the ores or manufacturing process.

of tungsten showed that the directions of principal interest, namely the maxima and minima of emission are all of the form (hhk).*

Two kinds of surface structure have been observed on single crystals of tungsten heated in vacuum: (a) a so-called "d.c. etch," and (b) a "shingle" structure. The former effect was first reported by Johnson (5), and has been studied by Schmidt (6). It consists of a step-like structure found on wires subjected to prolonged heating on direct current; it also occurs near the supports of a wire heated on alternating current, where strong thermal gradients exist. As yet this process is not understood theoretically. The shingle structure was reported by Nichols (7), and was observed in the (110) crystal direction. Both structure effects were to be found on the crystal from which Nichols (7) obtained his emission constants as a function of crystallographic direction. Moreover, it has appeared plausible to explain the emission data for the (110) direction as being characteristic of a patch surface (7,8) contributory evidence of the patchy nature deriving from the existence of the shingle structure on that surface. Among the objectives of this research was to make thermionic measurements from a crystal (a) free from the d.c. etch and (b) with minimized shingle structure. Freedom from d.c. etch could readily be achieved by using only a.c. heating power. Indeed, Johnson (5) has reported that tungsten wires heated on a.c. in vacuum develop surfaces which appear to be free from any structure visible under a light microscope, even after heating sufficient to evaporate away 17 percent

* J. A. Becker, in private communication, has indicated that his field emission studies show that there may be a small field emission minimum in the vicinity of the (210) direction.

of the metal of the wire. The shingle structure, however, has been found to occur on wires heated only on a.c. Nevertheless, it was believed that this type of structure could be eliminated, or at least greatly reduced by a careful examination and selection of the crystal to be used.

A. PRODUCTION OF SINGLE CRYSTALS AND STRUCTURE OBSERVED BEFORE PROLONGED HEAT TREATMENT.

With this purpose in mind, a program of single crystal production was instituted. Wires to be recrystallized were first polished (9) to remove die-marks and to produce a uniform circular cross-section. The recrystallization process itself was carried out in what is commonly called an electron projection tube (10) after the method of Robinson (2). A typical projection tube is shown in figure 1a. The tube consists of a fluorescent coating on the inside wall of a cylindrical pyrex tube coaxial with the filament, which filament is held taut by a tungsten helical spring of proper design (11). A nickel collector electrode serves by secondary emission to maintain the phosphor at an appropriate applied anode potential. Under a sufficiently strong radial field the thermal electrons travel in straight lines radially to the screen. The illumination of any part of the screen is proportional to the emission density of the portion of the filament having the same cylindrical coordinates of azimuth and distance along the wire axis, and hence gives a qualitative measure of the emission pattern from the whole wire, magnified in the azimuth coordinate through the electron projection properties of the tube by the ratio of the envelope radius to wire

radius, or approximately 600 with the diameters used. The projection tube, then, offers a means of following the recrystallization process, and subsequently permits a careful examination of orientation, length, and degree of perfection of single crystals produced.

Six wires, each five-mils in diameter and approximately 14 inches long, were carried through the recrystallization process. Of the six, four were of G. E. #218 wire, dated 1939, each of which produced crystals several centimeters in length. The remaining two were of Callite type 200H, dated 1940, neither of which produced crystals of more than millimeter length under the Robinson method of recrystallization. One G. E. wire was recrystallized at 1980°K., three at about 2100°K. The first seed crystal appeared in the 1980°K. run after about $1\frac{1}{2}$ hours; it proceeded to extend until it filled the entire 14 inch wire with one relatively imperfect crystal. The 2100°K. runs each produced several crystals averaging three or four centimeters in length. The latter temperature was considered more suitable to the purpose of producing a number of crystals of satisfactory length for the selection process. In the case of each recrystallized wire the nature of the crystals was noted both visually and photographically, and cathetometer measurements were made to fix the positions of crystal sections showing an emission pattern free from flaws.

Then the wires were removed from the projection tubes, and each selected section was examined carefully for structure visible under a light microscope of 100 power magnification. In the case of each wire it was possible to resolve shingle structure associated with the (110) direction, even in the case of wires subjected to only mild heat

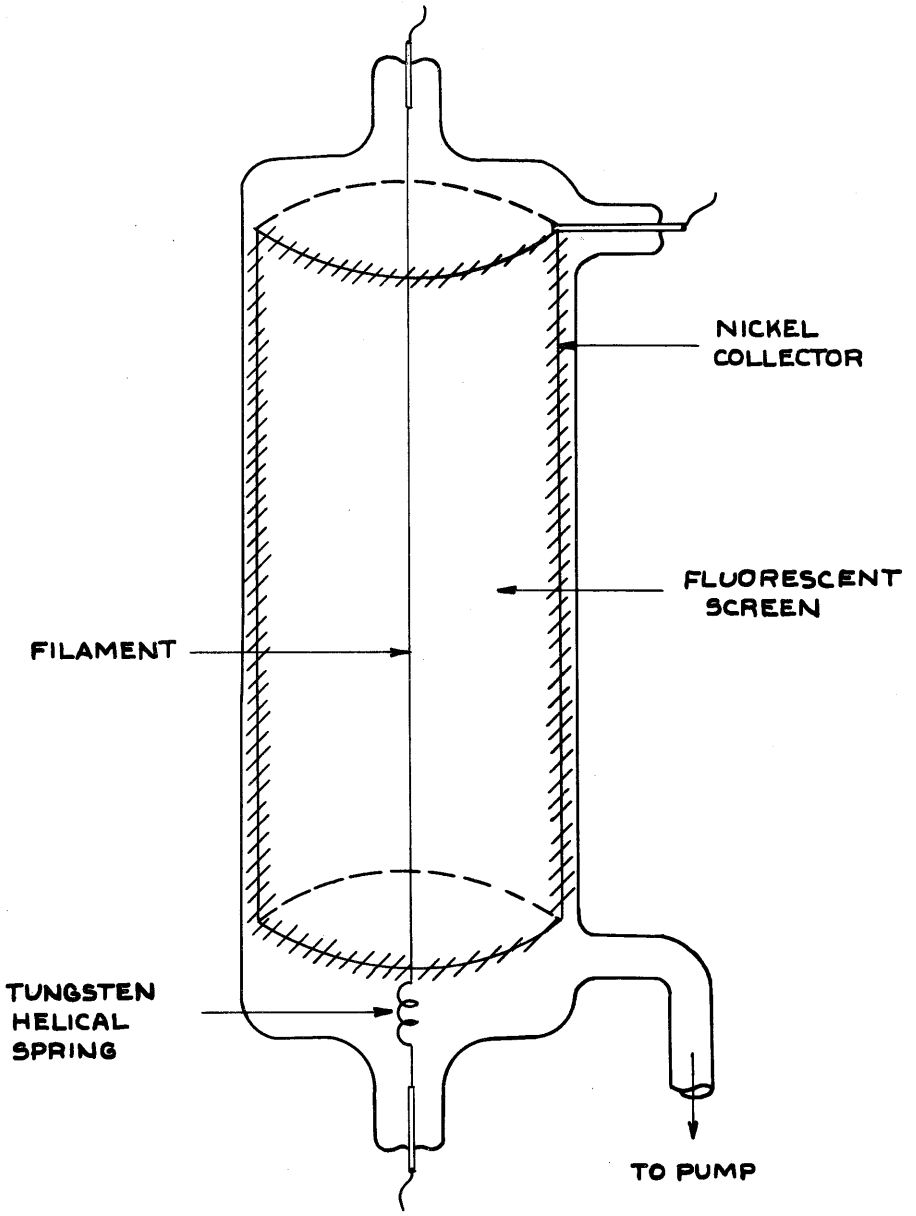

Fig. 1a. Cylindrical electron projection tube.

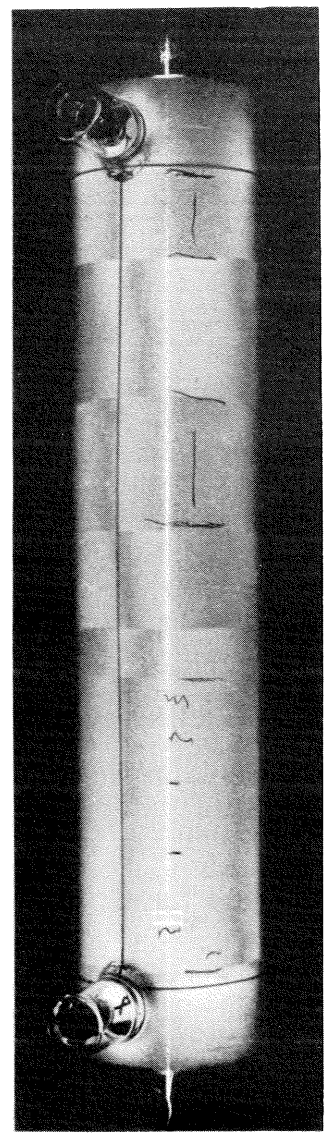

Fig. 1b. Projection tube pattern of wire containing single crystal section used for quantitative thermionic measurements. The white marks set off the single crystal section. The dark marks are crayon lines on the tube for identification purposes.

treatment. The 1980°K. run is of particular interest. The total heat treatment given the wire before removal for examination under microscope amounted to 22 hours at 1980°K. plus 20 minutes at 2280°K. According to the Jones and Langmuir tables (12) this treatment should produce an average reduction in diameter by evaporation of about 3×10^{-8}cm, far below the resolution of an optical microscope. Not only was the shingle structure observed on the two surfaces normal to the (110) directions, but this structure was superimposed upon what appeared to be a plateau, or flat surface, on the crystal. Even when the shingling was particularly faint, one could make out two lines parallel to the wire axis and separated by a few degrees of azimuth which have come to be interpreted as edges of a plateau in the light of more pronounced structure and other evidence to be presented. In addition to the plateau and the shingle structure, crystal boundaries and small surface crystal "lakes" were visible in the 1980°K. wire. All recrystallized wires showed all of these effects before prolonged heating; however, the 1980°K. wire was subjected to the least rigorous heat treatment before examination by microscope.

As indicated above, the shingle structure observed in recrystallized wires before prolonged heat treatment varied both in form and in visibility. In the case of the 1980°K. crystal for example, all of the shingles observed on one of the (110) surfaces were oriented with apexes pointed to the right; all of those observed on the diametrically opposite (110) surface were oppositely oriented with apexes pointed to the left. The shingling is probably a result of the failure of the crystal face diagonal to be aligned precisely along the wire axis. The orientation

of the apexes of the shingles then indicates the direction of "dip" of the true crystal planes with respect to the wire surface. If a true cylinder cut from a perfect crystal is considered, one would expect to find opposite directions of dip on the diametrically opposite surfaces. Actually this was usually but not always found to be the case for crystals examined. In some few instances the apex orientation was the same on both sides of the wire at the same point along the axis. There is, however, insufficient evidence to preclude the possibility of the crystal being imperfect in this case; perhaps the two (110) surfaces are actually located on two different crystals of almost identical orientation in the wire but with a longitudinal boundary between them. Such a boundary would be more difficult to resolve under the microscope than one between crystals of considerably different orientations. No examination of this phenomenon was made after prolonged heat treatment; heat treatment would have accentuated such a boundary, making it more easily seen.* In a few cases a (110) surface was found with right-oriented shingles on one side of a region showing very little or no shingling and with left-oriented shingles on the other side. A slight bend in the wire before crystallization could produce this effect; Johnson reported a similar type of crystal growth in helices of tungsten (5). In some isolated cases (110) surfaces were found with little or no shingling in evidence over several millimeters of length along the axis of the wire. Such a section should

---

* Back reflection Laue X-ray photographs of Nichols' tungsten crystals, discussed in reference 7, but not published, show sets of closely overlapping spots rather than sharp single spots, indicating several orientations differing by a degree or so in direction.

have a more nearly perfect orientation of face diagonal along the wire axis. Both from the point of obtaining a shingle-free (110) surface and in having precise (hhk) directions exhibited normal to the wire axis, such a section would show promise for quantitative thermionic measurements. After inspection of the qualitative thermionic emission pattern from each of the four G. E. wires, followed by microscopic examination of the surfaces, a single wire was selected for further investigation. The wire selected had been recrystallized at 2090°K. The projection tube pattern of this wire is shown in figure 1b.

B. FURTHER TREATMENT OF RECRYSTALLIZED WIRE

It has been pointed out that even crystal sections showing a minimum of shingle structure when examined before prolonged heat treatment are not entirely free from visible markings (e.g. the plateau edges can almost always be made out). In order to determine the effect of moderate heat treatment upon size and shape of the surface structure, the selected wire was re-inserted in a projection tube and subjected to the temperature schedule of table I.

Table I. Heat treatment of recrystallized wire.

Temperature °K.	Time
2610°	4 hours
2720°	30 minutes
2820°	10 minutes
2915°	2 minutes

Although after this treatment the surface of the wire appeared in general to be almost entirely free from any markings which could be resolved under the optical microscope, the size and appearance of the plateau and

shingle structure did not appear to be materially altered. Hence it was felt that there was some possibility that the structure had been produced during the recrystallization process, and if once removed, might not return under subsequent heat treatment. The wire was therefore again polished, this time using only the finest grade of abrasive due to the more rapid polishing rate of single crystals, and operating the polishing machine at a low rate of speed to prevent twisting, bending, or fracture of the recrystallized wire. After polishing sufficient to remove all traces of previous markings, accompanied by a reduction of diameter of about one percent, the wire was again placed in a projection tube. After the heat treatment of table II,

Table II. Heat treatment of recrystallized wire after second polishing.

Temperature ^{o}K.	Time
2760^{o}	340 minutes
2990^{o}	10 minutes

it was again examined under the microscope. This relatively severe heat treatment (sufficient to evaporate about two percent of the diameter)* was found to have restored the plateau and shingle structure to much the same condition as observed before polishing the recrystallized wire.

From the wire in this condition a single crystal section showing a

---

* As measured by micrometer. From the Jones-Langmuir tables (12) one computes a reduction three times as large. In general the evaporation computed by the Jones-Langmuir tables was greater than that observed by diameter measurement. A complete set of diameter values and evaporation data is given for the wire in Appendix I.

minimum of shingling and lake structure along with a flawless qualitative pattern was selected for quantitative thermionic measurements. The section chosen is marked on the photograph of the projection tube pattern of the wire, figure 1b. A determination of the diameter was also made at this time by weighing short pieces cut from each end of the sample to be used. Further heat treatment administered to the single crystal was dictated by outgassing and clean-up procedures; details will be found in Appendix I.

C. SURFACE STRUCTURE OBSERVED ON WIRE SUBJECTED TO PROLONGED HEAT TREATMENT

Early in the heat treatment schedule after selection of the crystal section for quantitative thermionic measurements the opportunity presented itself for further observation of surface structure under somewhat more favorable circumstances than previously encountered. Previous observation had been made of 14 inch lengths of wire mounted on the polishing machine over which the microscope was suspended. Between the first and second runs in the emission measuring tube the $3\frac{1}{2}$ inch section of wire was removed together with its rotatable mount and placed in a jig suitably fixed under the microscope. By now the wire had suffered less than 0.5% additional reduction in diameter by evaporation, making the total reduction in diameter about 2.5% from its value at the conclusion of the last polishing. At this time, in addition to the plateaus previously observed on the surface in the (110) directions, plateaus could be resolved in each of the (001) and (112) directions. These plateaus could be observed only by use of grazing incident light and under most careful adjustment of the microscope. The section of the wire chosen for

thermionic emission study was given particular attention. Although no shingling had been evident on the (110) surfaces at the time of choice of this section, under these favorable conditions very faint shingling structure could be made out. No shingling could be resolved at this time in any of the other directions; however, the difficulty under which the plateaus themselves were observed could easily account for failure to find shingle structure superimposed upon those plateaus.

After completion of the thermionic measurements (see Part II) the single crystal was removed from the measuring tube and once more examined for evidence of surface structure. At this point the diameter of the wire had been reduced through evaporation by 3.5 to 4 percent from its value immediately after the final polishing.

C.1. Photomicrographic Evidence of Plateau Structure.

Photomicrographs were taken of the plateaus found on the single crystal used for thermionic measurements. In each case the illumination was at grazing incidence obtained by adjusting the direct-dark field slide of the Zeiss Epi condenser microscope to a spot midway between the two usual positions. This type of illumination was found necessary in many cases to provide sufficient contrast to make out the structure at all. All photomicrographs show only the top of the wire; the magnification as the pictures are printed is about two hundred fold. An Eastman stage calibrated scale was photographed under the same conditions as the pictures, from which the dimensions of the structure have been obtained. The estimated error in dimensions quoted is probably no greater than 20 percent, some difficulty arising in achieving

and recognizing a correct focus.

Figure 2a is taken looking directly down on the (110) surface, at 180° azimuth, of the section of the single crystal used for thermionic measurements. The plateau is about 0.01 mm in width or about 11 degrees in azimuth. Faint shingling with apexes directed toward the right can easily be detected on the photographic negative. The photomicrograph of the opposite (110) surface at 0° azimuth shows oppositely directed shingling of about the same degree on a plateau of about the same size.

Figure 2b is of the 235° (112) plateau. This plateau is about 7 degrees wide. No shingling could be detected on the original negative. The diametrically opposite (112) surface at 55° also showed no resolvable shingling, but very faint shingles could be made out on the photographic negative of the 125° (112) plateau. The mate opposite to the 125° plateau could not readily be observed due to the structure of the supporting mount. All of the (112) surfaces photographed appeared to be of the same size.

Figure 2c shows the 90° (001) surface. The plateau seen here is also about 7 degrees wide. Shingling with apexes directed toward the right can be seen on the negative. Under close scrutiny of the photomicrograph, one can make out a periodic diagonal scoring of the surface laying it out in a pattern of diamonds. This scoring, found only in the vicinity of the (001) surface, resembles the markings left by the polishing machine, even to having the proper angle with the axis. Although one would not expect any polish marks to survive heat treatment sufficient to evaporate 3.5 percent of the wire diameter, it must be concluded that the vicinity of the (001) surface retained sufficient markings to permit

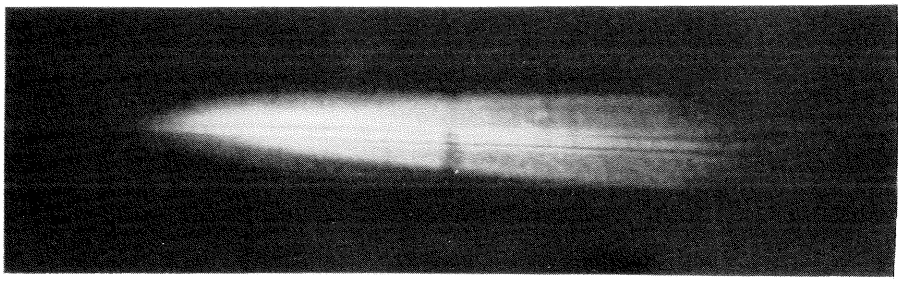

(a) 180° (110) plateau

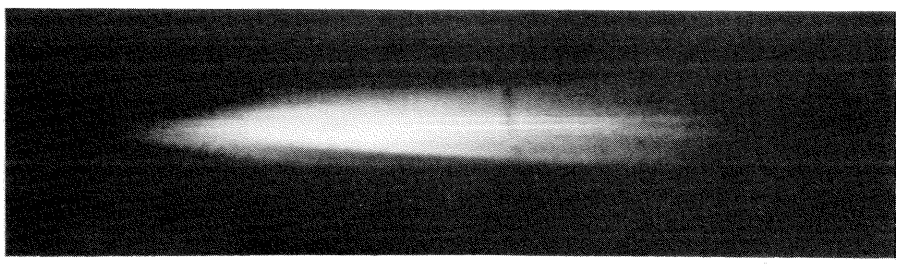

(b) 235° (112) plateau

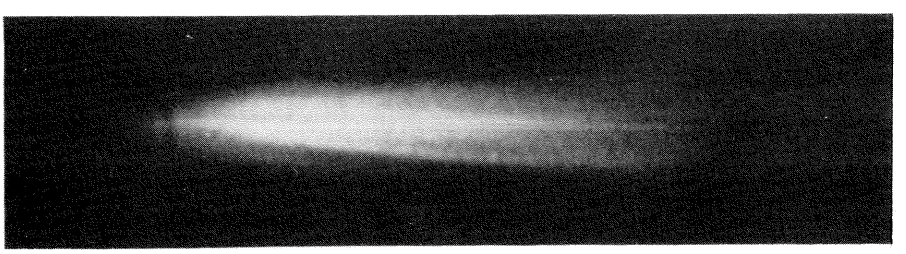

(c) 90° (001) plateau

Fig. 2. Photomicrographs of single crystal showing plateau structure.

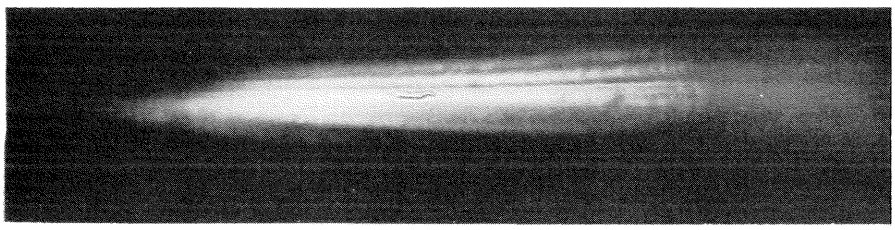

Fig. 3. Photomicrograph 15° off a (110) direction, indicating plane nature of plateau.

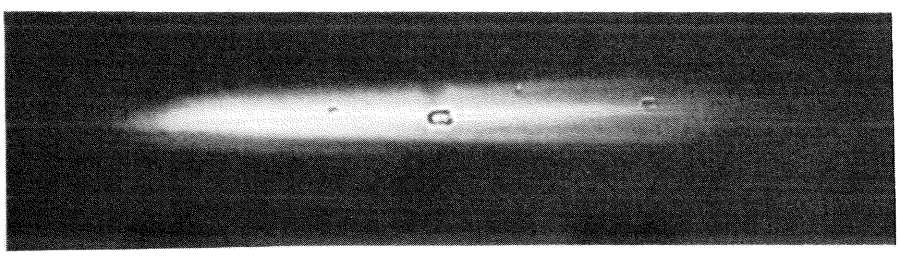

Fig. 4. Photomicrograph of surface crystal "lake" situated directly on a (112) direction.

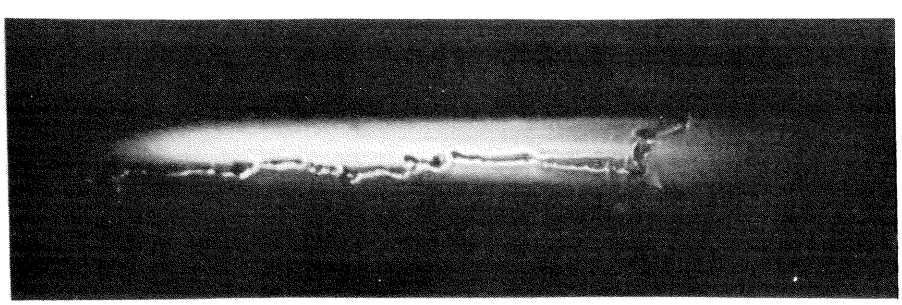

Fig. 5. Photomicrograph of a typical grain boundary between two crystals.

their observation. The 270° (001) surface was not readily available for observation due to the structure of the supporting mount.

The remaining photomicrographs were taken elsewhere on the wire than the crystal section used for quantitative measurements. Figure 3 is taken about 15° from directly down on a (110) surface. Of particular interest is the region to the left of the "plateau" where the illumination intersects the surface of the wire. This photograph has been interpreted as indicating the existence of a truly flat surface normal to the (110) direction. Shingling is present on the (110) surface, apexes pointed to the left. In the center of the picture is found a not too prominent surface crystal "lake" imbedded in the single crystal. Figure 4 illustrates a prominent surface crystal lake situated directly on a (112) plateau. The lake is approximately 0.01 x 0.015 mm in size. Three other smaller lakes can also be seen in the photograph. Figure 5 shows a typical grain boundary as found in prewar G.E. 218 wire after prolonged heat treatment. Note the longitudinal nature of the boundary. In some cases boundaries have been observed to run along the length of the wire for two or three centimeters before closing on themselves. After heat treatment sufficient to evaporate a few percent of the wire diameter, the grain boundaries cut deeply into the surface of the wire. In the case of the one shown in figure 5 sharp detail could be focussed over a vertical range of about .015 mm (15% of the wire diameter).

C.2. Emission Evidence of Plateau Structure.

Additional evidence of the existence of plateaus on the surfaces normal to the (110), (112), and (001) directions is to be found in polar

plots of thermionic emission vs. azimuth around the wire, the emission being measured at constant filament temperature. It has been known that these three directions yield minimas of thermionic emission (4, 7), and studies of field emission from points of the order of 10^{-5} cm radius have indicated the existence of regions of measurable extension in the vicinity of these directions over which field emission was essentially constant (13, 14, 15). Figures 18abc of Part II are polar plots of thermionic emission from the chosen single crystal. The measuring tube had a slit of 2.3° in azimuthal resolution; other details of the thermionic emission measurements will be found in Part II of this paper. The coordinates of the polar plots of figure 18 are $\log_{10}$ of the current and azimuth in degrees. To obtain the values of plateau width tabulated in Table III, 2.3° has been added to the width over which the thermionic emission is essentially constant, as measured on figure 18b. Values of plateau width obtained by photomicrograph are also tabulated for comparison. The agreement is well within the experimental error of the photomicrographic measurement.

Table III. Plateau widths.

Direction of Plateau	Width from Photomicrograph	Width from Polar Plot of Emission
180° (110)	11°	Results invalid; see Part II
55° (112)	7°	6.8°
125° (112)	7°	6.3°
235° (112)	7°	6.3°
90° (001)	7°	7.8°

C.3. Interferometer Measurements of Wire Diameter.

At the same time that the photomicrographs were made, a precision measurement of wire diameter was taken. Although the primary purpose of the diameter measurement was to establish a temperature scale in terms of heating current, it was possible to obtain thereby a measure of diameter of the wire vs. azimuth. For this purpose the wire was left in the rotatable mount from the measuring tube, which was placed in the jig to permit various diameters to be measured; azimuthal orientation was simultaneously noted for each diameter. For the diameter measurement the simple optical wedge interferometer was used. Two rectangular optical flats placed in contact at one end were separated by the wire at the other end so as to form a small dihedral angle whose measurement in radians is the wire diameter divided by the length of the optical flats. This arrangement was illuminated by normally incident mercury green light, and using a travelling microscope, a count was made of the total number of fringes between the wire and the point of contact of the optical flats. The true point of contact was ascertained by illumination with white light. The axial length of the wire section supporting the upper optical flat amounted to about one millimeter. It should be stated that since the crystal section measured was located at the center of a wire $3\frac{1}{2}$ inches long, some slight twisting of the wire might have occurred if the optical flats came to rest in such a way as to impose a torque on the wire; care was exercised not to exert twisting forces on the wire due to lowering of the optical flat thereon. The precision of the angular measurement connected with diameter determination was about 4 degrees. Both thermal expansion effects and compression of the wire due to weight of the optical flat were negligible.

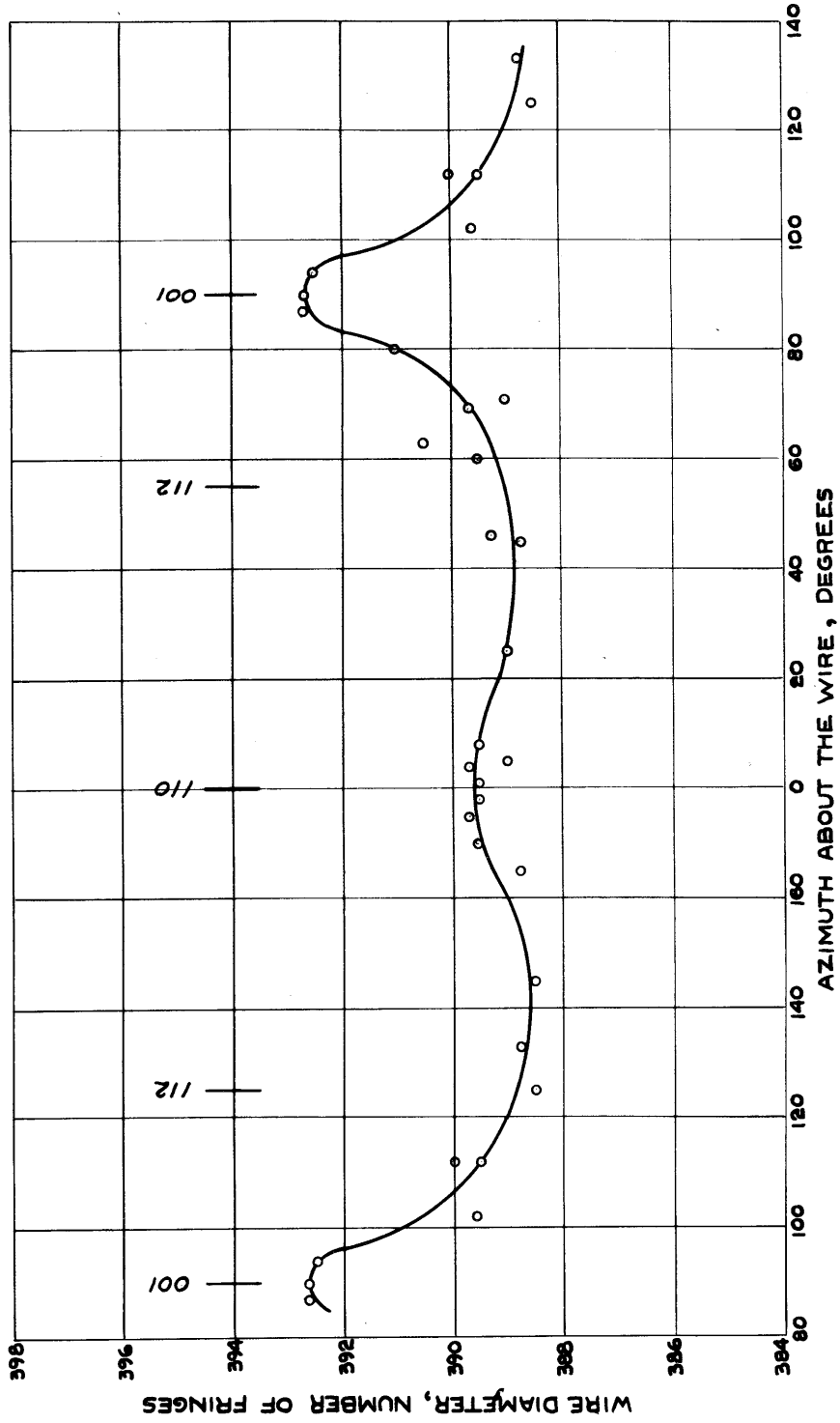

Fig. 6. Wire diameter as a function of angle around the wire.
A simple wedge interferometer was used with mercury green light.

Figure 6 shows the results of several such diameter determinations made on the selected single crystal, each point having been verified by at least one recount. Two conclusions may be drawn from the plot: (a) the average diameter of the wire, obtained by graphical integration, is 389.5 fringes, or $(\frac{1}{2} \times 5.461 \times 10^{-5}) \times (389.5) = 0.010636$ cm, probably accurate to better than 0.2 percent, (b) the plotted points show upward departure from the average in the vicinity of the (001) direction and probably in the vicinity of the (110) direction. No significant deviation can be seen in the region of the two (112) directions. If one computes the deviation in wire diameter to be expected over an 11 degree flat plateau, one finds that it amounts to 0.5 percent, 0.5×10^{-4} cm, or about two fringes. The deviation over a 7 degree plateau would then amount to about one fringe. These computed values are in qualitative agreement with figure 6; deviations observed, especially in the (001) direction are of this order of magnitude. Structure of this size may also be expected to lie close to the limit of resolution of an optical microscope, explaining the difficulty encountered in visually observing the structure.

D. THE EFFECT OF TEMPERATURE ON PLATEAU WIDTHS

Becker has shown (14) that on field emission points of the order of 3×10^{-5} cm in radius, the steady state size of the (001) and (112) planes increases by almost a factor of two in linear dimension as the temperature is lowered from 2600°K. to 1200°K. He also found that the time necessary to reach a steady state increased as the temperature was lowered: a time of the order of a few seconds or less is required at 2600°K. while at 1200°K. several minutes is necessary. In order

to ascertain whether a similar change in plateau size could be produced on a wire of 0.5×10^{-2} cm radius, the wire containing the selected crystal was subjected to the temperature schedule of table IV while located in the emission measuring tube just prior to final removal for the study of surface structure.

Table IV. Heat treatment to study the effect of temperature on plateau width.

Temperature	Duration of Heating
3030°K.	2 minutes
1230°K.	92 hours

Each heating period was preceded and followed by a rapid emission measurement of the width of the 55 degree (112) and the 90 degree (001) plateaus at the lowest temperature convenient, 1560°K. A reading of the two widths took approximately ten minutes to complete. The three sets of width measurements agreed with each other to 0.1°, and indicate no experimentally observable change in plateau size under the stated limited temperature schedule.

Herring (16) has shown that under certain reasonable assumptions one can relate the times necessary to reach an equilibrium structure in two similar situations to the scale factor of the two configurations. He has shown that if the mechanism of structure development is surface migration, the ratio of times required to reach equilibrium will be the fourth power of the scale factor. If the mechanism is volume diffusion the ratio will be the cube of the scale factor. Since the scale factor between the wire and Becker's field emission point is $(0.5 \times 10^{-2}\text{cm}/3 \times 10^{-5}\text{cm})$ or 1.6×10^{2},* one may expect that equilibrium

---

* By private communication from Herring.

times 6.6×10^8 or 4.1×10^6 times as large as Becker's will be found in the case of the wire, depending upon whether the mechanism is surface migration or volume diffusion. If these ratios are correct and particularly if surface migration is the transporting mechanism, one can hardly make quantitative comparison of equilibrium times at any temperature due to the disparity of the time scales. Certainly these ratios applied to Becker's data cannot lead one to expect perceptible material transport here in finite times at temperatures much lower than, say about 2000°K. As to explaining the failure to observe any change in plateau width due to the 3030°K. treatment of Table IV, it is possible that previous flashes near 3000°K. had been sufficient to establish an equilibrium surface structure, which had not been altered by intervening heat treatment. Referring to Appendix I, Part 5, one finds $28\frac{1}{2}$ minutes at 2785°K. just before the final data were taken. This or prior treatment must have established a plateau width which was unaltered by the temperature treatment during the taking of the final data. The most extensive heating of the wire during the taking of final data occurred during retarding potential runs, when 1990°K. was maintained for 12 hours immediately prior to the test of Table IV. Recalling (Section A) that the freshly recrystallized 1980°K. wire (total treatment: 22 hrs. of 1980°K., 20 min. of 2280°K.) showed definite plateau structure, it is rather difficult to explain why there was no change in plateau width from the "near 3000°K." state during the retarding potential temperature treatment. From the limited data presented here one may conclude that either (a) the structure observed in the 1980°K. wire was not merely due to the 1980°K. treatment, i.e.

it may have been a result of the recrystallization process or it may have been due to the 20 min. at 2280°K., or (b) the structure obtained by heating at 1990°K. is indistinguishable by the plateau width test from the "near 3000°K." structure. Although one might not expect to find changes in size as large as the 2:1 effect observed by Becker at lower temperatures, the measuring tube provides a tool capable of detecting changes of only a few percent.

If limited to wires as large as 0.005 cm in radius, further investigations at temperatures in the 2000°K. to 3000°K. range would be interesting. Alternatively, work with wires of considerably smaller radius, if practicable, would permit the use of lower temperatures. It is also possible that in place of the measuring tube the use of an aluminized projection tube would simplify such experiments. Previous thermionic emission projection tube work has been done without opaque backing of the fluorescent coating. Under such conditions the visible radiation from the hot wire has made difficult the observation of emission in the vicinity of the minima.

E. CONCLUSIONS TO PART I

There is convincing evidence, both from photomicrographs and from plots of thermionic emission vs. crystallographic direction, that surface structure is present on a single crystal of tungsten heated sufficiently by alternating current in a good vacuum to evaporate 3.5 to 4 percent of its diameter. This structure consists of what appear to be "plateaus" normal to each of the (110), (001), and (112) directions of a cylindrical crystal with face diagonal along the axis of the cylindrical

wire. The (110) plateau extends over about 11 degrees in azimuth on the surface of the 0.01 cm wire, the (001) plateau over 7 degrees, the (112) plateau over 6 degrees. Superimposed upon the plateau can usually be seen a "shingle" structure which is more pronounced in some cases than others and which is usually oriented in opposite directions on the plateaus 180 degrees apart on the wire. This shingle structure probably results from the failure of the face diagonal to be aligned precisely along the wire axis.

Both the plateau structure and shingling were visually observed in the (110) direction of a wire given only mild heat treatment: 22 hours at 1980°K. and 20 minutes at 2280°K. This heat treatment produced a reduction in diameter due to evaporation of about 3×10^{-8} cm.

Johnson (5) found no structure on tungsten crystals given a.c. heat treatment in vacuum sufficient to evaporate 17 percent of the wire diameter; from the known resolution of his observations, he concluded that there was no structure greater than a few thousand atom diameters in size on the crystals he studied. The structure observed here is probably about 5×10^{-5} cm in size, no larger than the upper bound set by Johnson. Johnson did, however, report that flat surfaces appeared to develop in the (001) and (110) directions of crystals heated in lamp gas (86% argon + 14% nitrogen), or in pure argon. He found that the (001) surfaces were larger than the (110) surfaces, whereas the reverse was observed in the present investigation. However, it is reasonable that the surface structure to be found on a crystal in equilibrium with its vapor, as is approximately the case for a wire heated in a gas, would be different from that obtained by heating the wire in vacuum. In the latter case the mechanism of structure formation

must be one or more of the following: uncompensated evaporation, surface migration, or volume diffusion. The structure observed on the 1980°K. wire indicates that at least some of the material transport is accomplished by means other than evaporation.

A brief and inadequate heat treatment schedule failed to produce any change in plateau size as a function of temperature.

PART II. THERMIONIC DATA FROM A SINGLE CRYSTAL OF TUNGSTEN.

A. DESCRIPTION OF EQUIPMENT.

The tube used to make the quantitative thermionic measurements was originally designed and constructed by R. B. Nelson. This tube was first used to study crystallographic dependence of thermionic emission from single crystals of tungsten by M. H. Nichols (7), he having rebuilt the tube to incorporate certain refinements. The tube was again rebuilt, with further modifications, for the purpose of making the present measurements. Although the tube has been described Nichols (7), in view of the modifications incorporated, and for the sake of completeness, a general description follows.

A.1. General Description of Measuring Tube.

The metallic parts of the tube are all of tantalum with the exception of one molybdenum flat spring, a helical filament spring of tungsten, and stem leads of tungsten. The envelope is of pyrex with nonex stems and a nonex ion gauge side bulb. Figure 7 is a schematic diagram and figures 8a,b are photographs of the metallic parts of the measuring tube in its final form. A sufficiently high voltage is applied between the single crystal filament A and anode B to cause the thermal electrons from the filament to proceed radially in straight lines to the anode B. Those electrons whose trajectories are in line with the slit system SS' pass through to the collector D and are measured. As will be seen from Schottky plots discussed in Sec. C, an applied anode-filament voltage of about 750 volts is required for

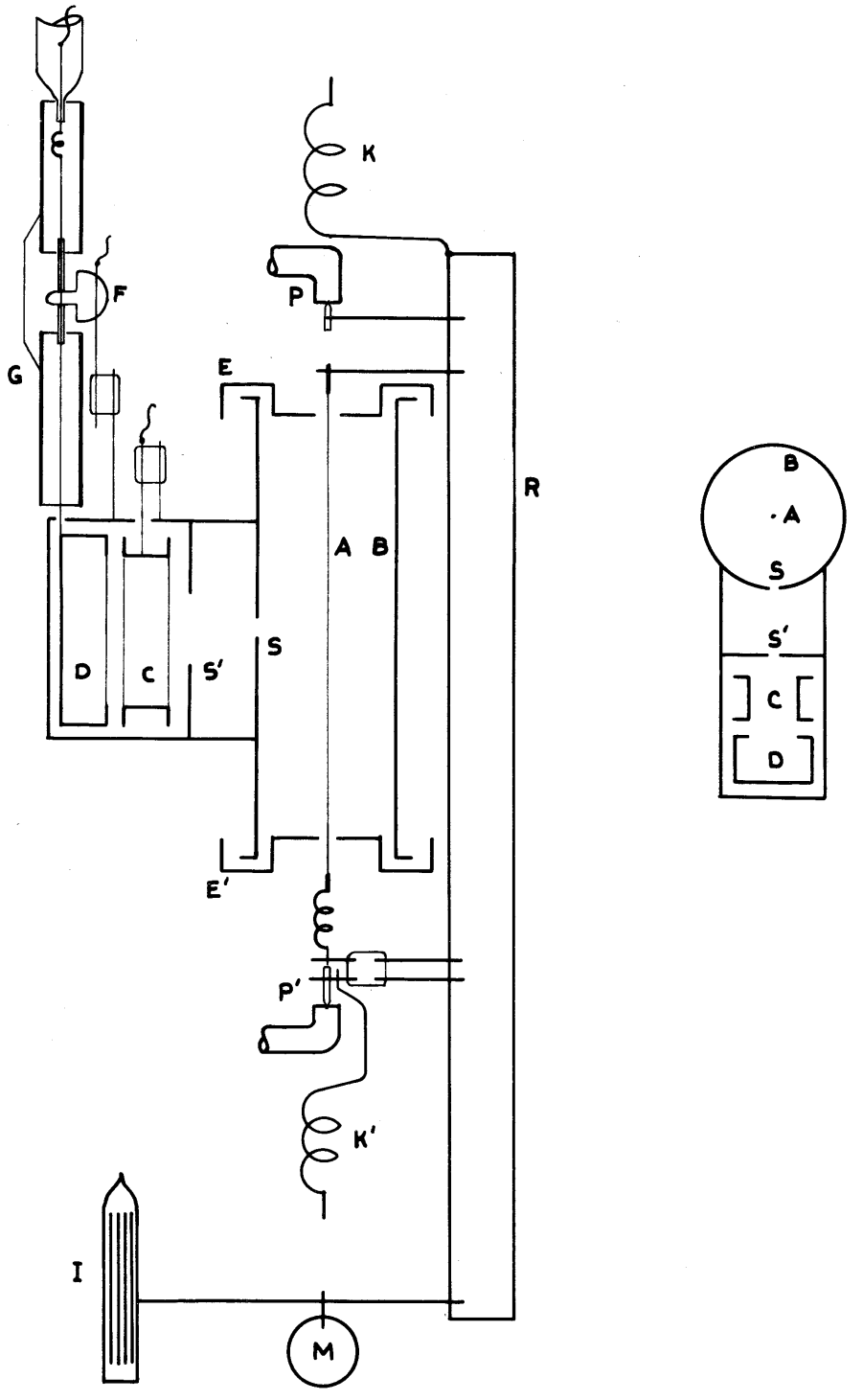

Fig. 7. Cross-section and top view of tube used to measure the thermionic constants for different crystal directions. The crystal wire A is mounted in the rotor R so that it can be rotated in front of the slit S cut in the cylindrical anode B.

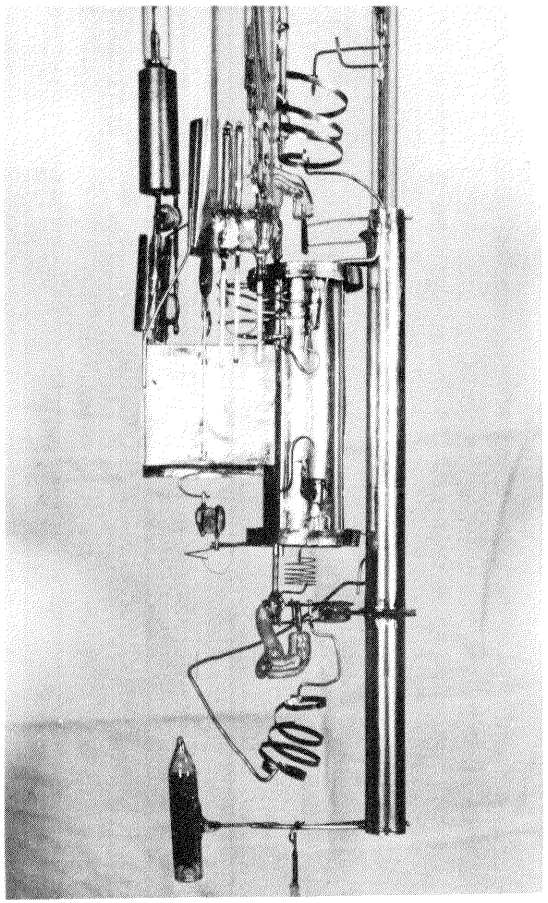

(a)

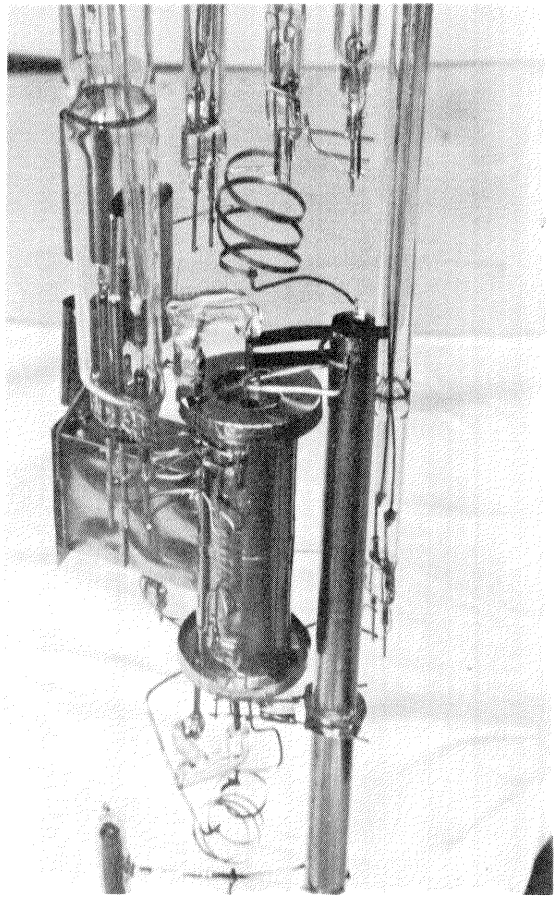

(b)

Fig. 8. Photographs of tube used to measure the thermionic constants for the different crystal directions. Various elements can be identified by comparison with fig. 7.

satisfactory projection properties. The upper operating potential difference is limited by field emission difficulties to about 2800 volts when other electrodes have their normal values. A negative potential of 540 volts relative to the anode B on secondary suppressor electrode C was found to eliminate slow secondaries from the slits SS' and to keep slow secondaries from leaving the collector D. The end-guards EE' were both operated at negative $22\frac{1}{2}$ volts with respect to the filament to prevent escape of stray electrons from the ends of the filament-anode region. The end-guards also serve to shield the collector lead and its vicinity from the one to three kilovolt x-rays generated at the anode B. With the installation of the end-guards, the principal modification of the tube, the guard rings G were found to be unnecessary. However, they were operated at positive 180 volts with respect to the anode, a potential previously found to be most effective in preventing stray electrons from reaching the collector lead. The collector D was operated at the anode potential for all measurements except those in connection with retarding potentials.

The single crystal wire A, figure 7, is supported by the rotor frame R, being held taut by a helical spring of 0.015" tungsten (11). The rotor frame is supported at the points PP' by tungsten pivots in pyrex bearings. The pivot at P is supported by a flat molybdenum spring to maintain the accurate centering of the axis of rotation in the plane of the slit system. The rotor can be rotated about PP' from outside the tube by causing an electromagnet to attract the laminated soft iron rod I which is sealed in a pyrex capsule, thus bringing the different crystal directions of the single crystal in A into alignment with the

slit system SS'. The mirror M permits the measurement of the azimuth through which the crystal has been rotated. The tantalum spirals KK' serve to conduct heating current through the wire and yet permit free rotation of the rotor R. The glass insulator F supporting the collector is of special design (17) and the tungsten rod which in turn supports the insulator can be maintained at any desired potential. Normally the rod is held at the same potential as the collector to prevent leakage through the insulator.

The whole metallic system is suspended from a single tungsten-to-nonex press; all the remaining leads, of which there are eight, are flexible, thus permitting the glass envelope to change its shape freely, as it does to a certain extent during the baking process, without throwing any of the parts out of alignment. The slit S used by Nichols was replaced by one slightly narrower to increase the resolution, and considerably shorter, to accommodate the single crystal chosen. The dimensions of the slit S used are: 0.514 mm x 3.40 mm. The collimating slit S', 1.90 mm x 12.7 mm, does not serve to limit the beam. Since the diameter of the anode B is 2.54 cm, slit S provides an azimuthal resolution of 2.3°, compared with Nichols' value of 2.9°. The cross section of the slit is 3.1 times as small as that used by him. The anode B is constructed with a removable section, directly opposite the slit S, running the full length of the anode to permit insertion of the crystal wire A. Two tantalum strips serving as doors are held by grooves provided on either edge of the opening, one strip being inserted from the top and one from the bottom. It was found that if the tantalum doors were cut from heavier metal than that from which the anode was constructed,

little trouble arose from poor electrical contact and excessive heating when the anode was outgassed by R.F. induction.

The end-guards EE' also were constructed with openings to permit insertion of the crystal wire A. The openings in this case were closed after insertion of the wire by additional pieces of tantalum spotwelded in place. The end-guards were constructed in the shape shown in figures 7 and 8 to offer as complete shielding against stray electrons and x-rays as possible, to conform to the previous design of the tube, and to form a structure mechanically strong enough to prevent sagging while held at yellow heat for long periods of time. The attempt was also made to maintain as large spacings from both anode and filament as possible without materially altering the construction of the tube. Each end-guard is mounted on two nonex insulators, one of which is situated between the anode B and the path of the rotor backbone, as can be seen in figure 8.

The rotor frame R is constructed on a half inch cylindrical backbone of tantalum. This gives a light, strong structure which is easy to outgas by R.F. induction. The capsule containing the laminated iron rod I was evacuated by fore-pump; the iron was glowed by induction to a red heat for several minutes before the capsule was sealed off. Laminating the iron rod prevents its becoming excessively hot during the outgassing of the other metal parts of the tube by induction, while evacuation prevents large stress on the glass capsule which may be softened by the outgassing heat treatment.

A.2. Evacuation and Mounting of the Tube.

The tube was evacuated by a mercury-vapor diffusion pump, backed by

a mercury-vapor jet pump, and trapped by liquid nitrogen during the final stages of outgassing. The measuring tube was sealed off from the pumps and a getter was flashed before any measurements were taken. The tube was subjected to the evacuation schedule a total of five times before the investigation was completed:

(a) Initial evacuation without ion gauge. Poor vacuum.

(b) Evacuation with ion gauge. Ion gauge stem was leaky.

(c) Evacuation without flashing getter for purpose of leak testing.

(d) Satisfactory evacuation with ion gauge, barium pellet getter, unmodified tube, i.e. without end-guards, EE'.

(e) Satisfactory evacuation with ion gauge, tantalum getter, modified tube, i.e. with end-guards, EE', installed.

Since each of the five evacuations followed approximately the same schedule, only the last one will be described. The last evacuation was accompanied by installation of the parts in a new envelope. The new blank was conducted through a full-scale evacuation schedule with all stems, getter bulb, and a Westinghouse type WL 5966 anti-x-ray ion gauge (18) in place, but with no metal parts assembled within the main envelope. The purpose of the preliminary evacuation was to check the new envelope for leaks. After sealing the blank off, the ion gauge filament was continuously heated, but pressure readings were taken only periodically, to avoid the known pumping action of an electron discharge (19). Since the only metal parts in the blank were those few associated with the ion gauge, it was felt that a pressure vs. time characteristic of the sealed off envelope would give a reasonable

estimate of the leakage rate into the envelope. After initial transitory fluctuations principally due to seal off and gettering action of the grid of the ion gauge, the pressure rose at a steady rate of approximately $\frac{1}{2} \times 10^{-9}$ mm of mercury per hour. No change in this rate was experienced when fore-vacuum was applied to the outside of all stems of the blank. This rate is in good agreement with the expected rate of rise due to diffusion of helium through the pyrex envelope as predicted by the work of Urry (20) and of others (21); agreement is also good with experimental rates of rise determined in this laboratory from different ion gauges sealed off alone or with various getters. One can conclude that any other leak in the envelope was small compared to the helium diffusion rate through the pyrex walls.

After the preliminary test of the envelope, the metallic parts of the tube, including the end-guards EE', were assembled therein. Two tantalum getters were formed, each of 5 inches of 0.005" wire wound into a 1.5 mm helix about $1\frac{1}{2}$ inches long, and placed in the getter side bulb. The evacuation schedule of two cycles of alternate baking and R.F. induction heating is described in detail in Appendix II. Each stage of the outgassing process was continued until a "sticking" pressure, of about 10^{-7} mm of mercury or better, was indicated by the McCleod gauge. Of particular interest is the fact that considerable gas was released when the rotor was first moved in the evacuated tube. It cannot be ascertained whether this gas was released from the pivot bearings or from associated glass or metal structure, but it is probable that failure to rid the system of such gas was at least partly responsible for the poor vacuum encountered in evacuation (a). All of the remaining

four evacuation schedules included a rotor "exercise" to eliminate this source of gas before seal-off. Also, it was found that a tantalum getter of the type described was apparently more satisfactory than the barium pellet getter previously used. If the tantalum getter is properly outgassed, the amount of gas released in the final stages of processing, when the getter is flashed, can be reduced by several orders of magnitude from that accompanying the flash of the barium pellet getter. A lower ultimate pressure, as indicated by the continuously pumping ion gauge was thereby achieved.

It was found that the ultimate pressure in the sealed-off tube was a function of, among other things, the temperature of the ion gauge bulb walls. The lower the temperature of the ion gauge walls, the lower the ultimate pressure to which the ion gauge would pump, all other factors being equal. Obviously the ultimate pressure depends upon an equilibrium between ion gauge pumping rate and total leak rate, where the principal factors in the leak rate are diffusion of helium through the glass walls and release of gas from the various parts of the tube. The total ultimate pressure as indicated by the ion gauge was about 1.5×10^{-9} mm of mercury under normal operating conditions, for the entire period during which final measurements were taken. This pressure, however, is the total pressure in the tube, probably consisting almost entirely of helium partial pressure, the partial pressure of "active" gasses being much smaller, as indicated by the failure to detect any change in low temperature thermionic emission after many days of allowing the crystal to remain at room temperature. "Emission decay" tests of 7 days and 27 days, at the outset and at the conclusion respectively of the thermionic

measurements, showed no detectable change in emission in the (112) direction as measured at 1585°K. The emission in each case was compared with that from the surface just flashed clean by raising it to 2800°K. for a few seconds.

The photograph of figure 9 shows the tube mounted for use. In order to keep the tube free from mechanical vibrations, it was suspended from the top by a single wire (22). Fastened to the bottom of the tube was a set of fins, immersed in S.A.E. 30 oil to damp out oscillations. The legs of the supporting table were placed on one inch sponge rubber. No difficulties were experienced at any time from mechanical disturbances. The portions of the tube above the mirror M and iron rod I were enclosed by a copper shielding jacket. Complete enclosure was found to be unnecessary.

A.3. Measurement of Azimuthal Orientation of Crystal.

Attached to the rotor R of figure 7 is a mirror M, an unsilvered plane of glass, provided for the measurement of azimuth through which the crystal wire has been rotated. For the angle measurement a galvanometer lamp with an external vertical slit, and a cylindrical celluloid protractor were used as shown in figure 9. The protractor is marked at 10 degree intervals and provided with a movable 10 degree section further divided into 2 degree intervals. Provision is made for (a) placing the protractor coaxially with the crystal wire, (b) directing the lamp beam through the axis of the crystal wire, (c) establishing a reference point with respect to the wire orientation, and (d) measuring azimuth from this reference point. The protractor is placed coaxially

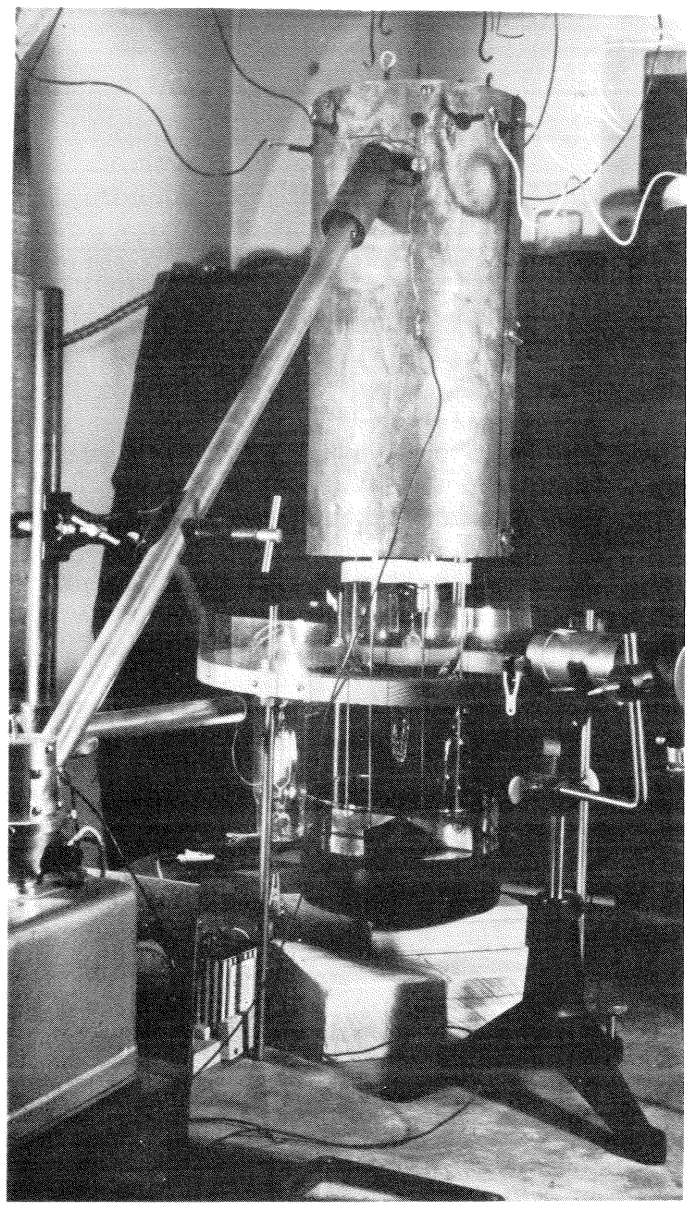

Fig. 9. Photograph of measuring tube mounted for use showing the getter and ion gauge side-bulbs, the copper jacket surrounding the tube, the oil damping bath, and the lamp and celluloid protractor used to measure the angle through which the crystal is rotated.

with the crystal wire by aligning the lower pivot point P' with two orthogonal diameters of the protractor. The lamp beam is directed through the axis of the crystal wire by noting that the initial passage and the unreflected passage through the protractor are on a diameter. The internal limit of travel of the rotor, imposed by the presence of the pivot support and collector housing, is used to establish a reference point on the protractor. The azimuth is then determined by averaging the angle of first passage of the beam through the protractor with the angle of reflected passage through the protractor. The absolute precision of the azimuth determination is about 1 degree, but relative precision over small intervals of azimuth is about 0.3 degrees.

A.4. Measurement of Temperature of Crystal.

For the temperature measurement, use is made of the Forsythe-Watson temperature scale for tungsten (23). Forsythe and Watson have tabulated total emissivity and resistivity of tungsten as a function of temperature in the range from room temperature to 3000°K. Knowing the diameter precisely, one can then obtain the temperature in terms of the heating current through the crystal wire. Use of the current rather than voltage, power, or resistance, is preferable in this case because it avoids necessity for correcting for the cooling effects of the wire supports, as long as the end effects do not extend to the center of the crystal wire. The measurement of the root mean square of the alternating current used is accomplished by comparison with a direct current with the same heating effect.*

* In order to avoid the "d.c. etch," as discussed in Part I, alternating current exclusively was used to heat the tungsten crystal. A simple calculation shows that for the 0.005" wire used, heating by means of 60 cycle current will produce at a mean temperature of 2000°K., a

The circuitry involved will be described in the next section. The current measurement can be made to better than 0.2 percent, which corresponds to 2 degrees on the temperature scale.

The best measurement of the diameter, 0.010636 cm ± 0.00002 cm, was accomplished by use of the optical wedge interferometer as described in Part I.C. This measurement was made after taking the thermionic data, immediately after the wire had been removed from the measuring tube. Due to the extensive heat treatment of the wire, sufficient to evaporate 3.5 to 4.0 percent of its diameter during the course of the whole investigation, this final diameter value is not correct for all temperature determinations. However, the final and best values of the thermionic constants were taken just before the wire was removed from the measuring tube. At the conclusion of these thermionic measurements, the wire was flashed at 3030°K. for two minutes to check the reproducibility of the data just taken. According to the Jones and Langmuir tables (12), this flash produced evaporation sufficient to reduce the diameter by 0.000027 cm., an amount about equal to the uncertainty in the original measurement. The diameter used for final and best values of the thermionic constants is then 0.010662 cm± 0.00002 cm. The uncertainty in diameter represents an uncertainty in temperature of about 3 degrees Kelvin. The total uncertainty in temperature then amounts to about 4 degrees Kelvin, not including effects due to possible difference in emissivity or

---

peak to peak 120 cycle temperature fluctuation of 8°K. In order to reduce this fluctuation for thermionic measurements, a 400 cycle current source was used. Peak to peak fluctuation with the alternating current in this case amounts to less than 1.5°K. at 2000°K. For smaller mean temperatures, the fluctuation will of course be smaller, both in absolute value and percentage-wise.

resistivity of the tungsten from that used by Forsythe and Watson, nor including the uncertainty in their temperature scale.

As to the diameter values used during other parts of the investigation, various methods were employed for their determination. The only other set of thermionic data reported in detail, the pre-end-guard data, utilizes a diameter obtained by a correction of 0.6 percent from 0.010662 cm with evaporation data; refer to Appendix I for details of this correction. A determination by weighing measured lengths of wire cut from either end of the piece used in the measuring tube was made when the single crystal was transferred from projection tube to measuring tube. The diameter of the polished wire before recrystallization, as well as the diameters before and after repolishing, was obtained by micrometer. All values, each with method used to obtain it, are tabulated in Appendix I.

Because the crystal wire is only 8.2 cm long, cooling of the center of the wire below the temperature of an infinite wire carrying the same heating current sets the lower temperature at which measurements can be relied upon. From Richardson plots (Sec. C) it was found experimentally that this cooling became important at about 1350°K. At this temperature the emission gave evidence that the temperature of the crystal segment was about 0.4 percent lower than that calculated for an infinite wire. Calculations based on the tables given by Langmuir, MacLane, and Blodgett in reference 24, considering cooling only to the nearest support, at 3.73 cm from the slit, predict that at 1350°K. the effect should be about 0.1 percent. In view of the approximations involved in the end-loss calculations, the agreement is considered satisfactory.

A.5. Electrical Circuits.

The complete schematic for measurement of the thermionic data is shown in figure 10. Except for the collected current, all variable currents and voltages were measured by the Type K Leeds and Northrup potentiometer.

A.5.a. Electrometer Circuit.

Collector currents over the range from 10^{-6} amp. to 10^{-13} amp. were measured by use of an Applied Physics Corporation Vibrating Reed Electrometer (25), in conjunction with seven resistors. Six Victoreen resistors, covering the range from 10 megohm to 10^{6} megohm in decade steps were used with a precision wire-wound one megohm resistor, all mounted in a shielded, desiccated electrometer box, with polystyrene insulation and gold switching contacts. Due to the feedback circuit of the Vibrating Reed Electrometer, the instrument maintains the input terminal essentially at ground potential, measuring the voltage on the lower end of the resistor necessary to achieve this condition. The maximum departure of the input terminal from ground, i.e. the maximum error signal, is about one millivolt with full scale meter deflection on the highest meter range, 1000 millivolts. The entire set of resistors was calibrated every time a Richardson plot was taken, this being easily and accurately accomplished by use of near full scale readings on the 1000 mv. and 100 mv. ranges of the electrometer meter. The Victoreen resistors proved remarkably stable, showing little drift over periods of several weeks. Specifications for the resistors claim a

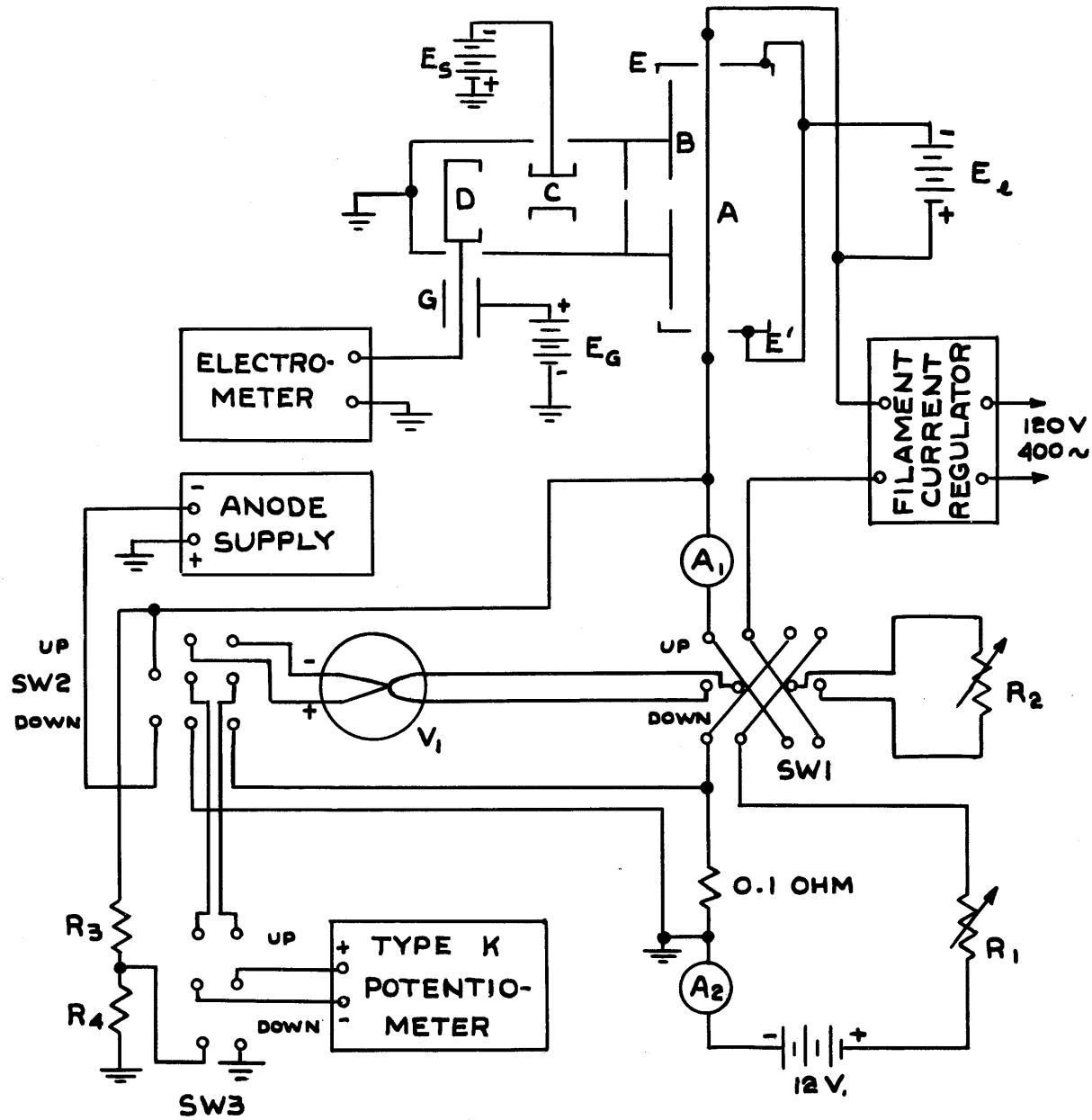

Fig. 10. Circuit schematic for thermionic measurements.

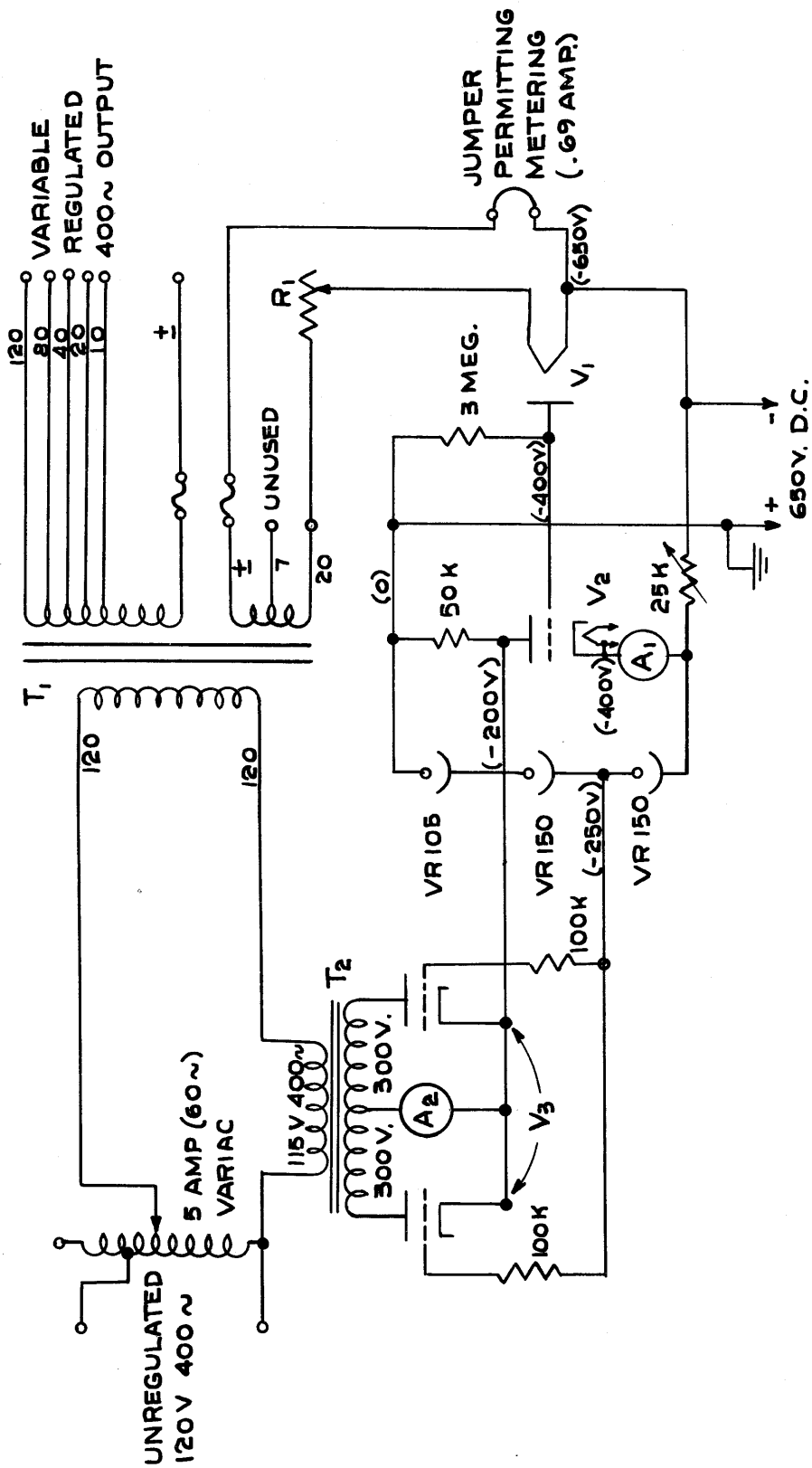

Fig. 11. Circuit for filament current regulator. Typical operating voltages shown in parentheses.

T_1 - Special 400~, 360va transformer, each winding insulated for 10 kv
V_1 - Special diode described in text
V_2 - Type 6SN7 tube
V_3 - Type 6AS7 tube
R_1 - Special 14Ω fine current control
A_1 - 5 ma DC meter, operated about 4 ma
A_2 - 500ma DC meter, 250ma max. per 6AS7

voltage coefficient of less than 0.02 percent over the range of voltage used. The meter provided with the Vibrating Reed Electrometer was calibrated by use of the potentiometer and found to yield better than the one percent precision desired, on all ranges. Provision had been made to use the charging rate of a capacitor for measurement of the smallest currents, but the resistor drop arrangement proved to be satisfactory for currents as small as 10^{-13} amp. Measurement of lower currents was not ordinarily necessary, due to the lower limit on temperature, imposed by end losses.

A.5.b. Filament Current Measuring Circuit.

The measurement of the root mean square of the alternating current used to heat the crystal wire was accomplished by comparison with a direct current of the same heating effect. Referring to figure 10, with SW1 in the "up" position, the alternating heating current passes through the heater filament of V_1. After equilibrium is reached, the thermal e.m.f. generated by a constantin-copper thermocouple junction welded to the center of the heater filament is measured by the potentiometer. SW1 is then thrown to the "down" position, replacing the alternating current by a direct current furnished by the 12 volt storage battery. This direct current is adjusted by R_1 to produce the same thermal e.m.f. as before; the value of the direct current is then measured across the standard 0.1 ohm. It is apparent that the true heating effect of the alternating current is measured, regardless of waveform, which is in fact considerably distorted by the filament current regulator.

The tube V_1 was constructed with a $5\frac{1}{2}$ inch filament of 0.003" tungsten. At the center of the filament there is a small nickel tab, to which the junction of 0.003" copper and 0.004" constantin is welded. The tube contains approximately 1 cm pressure of hydrogen to permit thermal equilibrium to be reached more rapidly. The copper and constantin leads are joined to nickel wires in two small tubes projecting from V_1 for convenient immersion in a constant temperature bath. A water bath was found to be sufficient for the short time equilibrium necessary for the current measurement. At the highest currents measured, about 1.2 amp., equilibrium conditions were achieved in about five minutes.

Ammeters A_1 and A_2 are provided to permit pre-adjustment of the comparison direct current to approximately its final value in order to achieve stability in the D.C. circuit and to prevent excessive drift in V_1 when the switch-over takes place. A dummy load, R_2, is inserted in the circuit not connected to V_1 to maintain the same heating conditions as those under which the measurements are made. R_2 is adjustable over the range of impedance of V_1.

Ammeter A_1, a Weston model 435 dynamometer ammeter with 1 amp. and 2 amp. full scale ranges is accurately calibrated with every measurement of current. It was found that this meter reproduced its own readings to the precision with which they could be read, i.e. 0.2 percent of full scale at full scale, but about 0.4 percent of full scale at half scale due to the non-linear scale. Measurements of filament current not requiring the utmost in precision (those in connection with Schottky plots and retarding potential plots) were made by applying the proper correction to the meter readings of A_1.

A.5.c. Filament Current Regulator.

In view of unavoidable output fluctuations of the 400 cycle motor-generator filament power source, a filament current regulator was required. A thermionic regulator of the type first used by Ridenour and Lampson (26) was designed, to provide constant filament currents for periods long enough to permit accurate measurements of the temperature. The regulator, see figure 11, reduces a 25 percent input voltage variation to about 0.1 percent output current change under normal operating conditions. In essence the circuit consists of a temperature limited diode V_1, heated by an auxiliary secondary of transformer T_1, which converts a small change in filament current into a large plate voltage signal. This signal controls a variable impedance in series with the primary of T_1 in such a way as to maintain a constant voltage output from T_1.

V_1, the temperature limited diode, was constructed of a 6 cm filament of 0.003" tungsten, enclosed by an anode 2 cm in diameter. The use of 0.003" wire in V_1, compared to the 0.005" wire for the tungsten crystal, gives the regulator filament less than half the heat capacity of the crystal filament and ensures the relatively more rapid response of the regulator to input fluctuations. One stage of D.C. amplification is provided in the 6SN7 which serves to control the grids of a 6AS7 full wave load on the secondary of T_2. R_1, a rheostat with 40 individual point contacts, was hand wound with a taper appropriate to permit uniform variation of output voltages from T_1 over a range of 2 to 1 to bridge the gaps between successive output taps. A General Radio 5 amp. Variac (60 cycle model) is used to adjust the T_1 primary voltage to bring V_1 to its operating point under widely varying external loading

conditions. Indication of operation within the range of regulation is provided by metering the 6SN7 cathode current (A_1), while loading of the 6AS7 is metered by A_2. Additional loading can be permitted by adding another 6AS7 in parallel with the one shown. Since both secondaries of T_1 operate into low resistance loads, extreme care was found to be necessary in circuit wiring to either secondary. Unsatisfactory operation was found to result from oxidized contacts of R_1, from fluctuating resistance of fuses operated near full rating, and even from standard knife switches in some cases.

A.5.d. D.C. Power Sources.

Four direct current power sources are required according to the schematic, figure 10. They maintain, with respect to the anode B, the potentials of (a) the crystal wire A, (b) the secondard suppressor C, (c) the end-guards EE', and (d) the guard ring G.

The anode-cathode supply consists of a standard full-wave rectifier using two Raytheon RKR-72 tubes, filtered by a capacitor-inductance filter of three 2.5 mfd. condensers and two 16 hy. chokes. Controlled by a Variac, the output is adjustable from zero to 5 kilovolts. Although a Sola regulating transformer was used, line fluctuations were sufficient to warrant the use of a 1005 volt VR tube regulator in conjunction with all Richardson plot data. The output of the supply is fused by a three inch length of platinum Wollaston wire with etched diameter 0.0002".

Due to the proximity of the secondary suppressor electrode C to the collector D and the resultant capacitive coupling between the elements, it was found necessary to use an extremely well filtered and regulated

supply for E_s. A 540 volt battery, made up of $67\frac{1}{2}$ volt units was used for all thermionic data.

The end-guards EE' were held by battery at $22\frac{1}{2}$ volts negative with respect to the crystal wire.

The guard ring G was battery operated at 180 volts positive with respect to the anode (and collector).

B. OPERATING CHARACTERISTICS AND ANOMALOUS BEHAVIOUR OF TUBE.

Preliminary to actual use of the tube, a complete set of operating characteristics was taken to evaluate the effectiveness of, and correct operating point for, each of the auxiliary electrodes. Two forms of anomalous behaviour, not previously reported by Nichols in his earlier work with the same tube, were discovered by their influence on the form of the operating characteristics. The first of these effects will be called the x-ray photoelectric effect; the other, the secondary emission effect. There are two reasons why these spurious effects were more noticeable in the present investigation: (a) Nichols' slit S was three times as large in cross-section as the present one, giving three times as large a ratio of signal to extraneous effect if the latter does not depend upon slit size. This is precisely the case for the first spurious effect. (b) All operating characteristics were run with the crystal oriented so as to yield a minimum of measured thermionic current, i.e. a maximum of spurious effect compared to signal. The orientation used by Nichols is not known, but from the nature of his characteristics and the order of magnitude of his collected currents, it is doubted that it was the direction of minimum emission (7, 27). In the following, the various

electrode characteristics will be presented; anomalous behaviour will be discussed as evidence for its presence is disclosed.

B.1. Guard Ring Characteristic and the X-Ray Photoelectric Effect.

Assuming for the moment that other electrodes have been fixed at appropriate voltages, the proper potential of the guard ring G required to shield the collector lead from stray electrons escaping from the open end of anode B can be determined by finding the dependence of collector current I_c upon the guard ring potential E_g. Initial measurements were made without the presence of the end-guards EE', the unmodified condition of the tube as previously used by Nichols. Plots of I_c vs. E_g when the crystal is oriented to give emission from a (111) direction appear in figure 12a. The (111) direction yields one of the maxima of emission and the curves of fig. 12a are quite similar to those obtained by Nichols. Fig. 12b shows curves taken in the (110) direction, the direction of lowest emission. Both fig. 12a and fig. 12b show an increase of collector current in the negative vicinity of the zero guard ring potential. This is undoubtedly an increase due to collection of stray electrons in the vicinity of the guard ring, the potential being most favorable for directing such electrons to the collector lead. There are two distinguishing features of fig. 12b: (a) The current collected in the most negative guard ring region, although independent of E_g, shows a much greater dependence on anode-cathode voltage E_p than does the current collected in the positive guard ring region. (b) There appears to be a linear dependence of I_c on E_g for positive E_g.

It is claimed that the first feature is due to photoelectric emission from the guard ring, produced by x-rays of one to three kilovolts from the anode B, and collected by the collector lead due to the favorable field between it and the guard ring. This is optically possible, since without end-guards EE' a considerable area on the inside of the cylindrical guard ring can be "seen" by a substantial anode area. The reverse phenomenon, photoelectric emission from the collector lead when E_g is positive, is not likely to be so pronounced due to the much smaller surface area of the collector lead. The anode potential dependence of I_c observed for E_g positive is very nearly in agreement with that predicted by the Schottky mirror image theory, whereas the dependence observed with E_g negative is much greater than expected. This is true even for the plots of fig. 12a, although the differentiation is much smaller in degree.* One cannot satisfactorily account for the first feature of fig. 12b by other mechanisms than x-ray photoelectric emission. The efficiency of photoelectric emission production should increase rapidly with the energy of x-rays in the one to three kilovolt range as observed, whereas a photoelectric effect caused by black body radiation from the luminous filament should have no anode potential dependence. Secondary emission effects are not likely since the curves do not show any change when E_g is made more negative than the filament, a condition which should preclude the arrival of <u>any</u> electrons, stray primaries or secondaries produced by them, in the vicinity of the guard ring. A test with the filament cold indicated no field emission difficulties.

---

* It will be seen in Sec. B.3 that the anode potential dependence of the collector current in the (110) direction is also anomalously influenced by the "secondary emission effect."

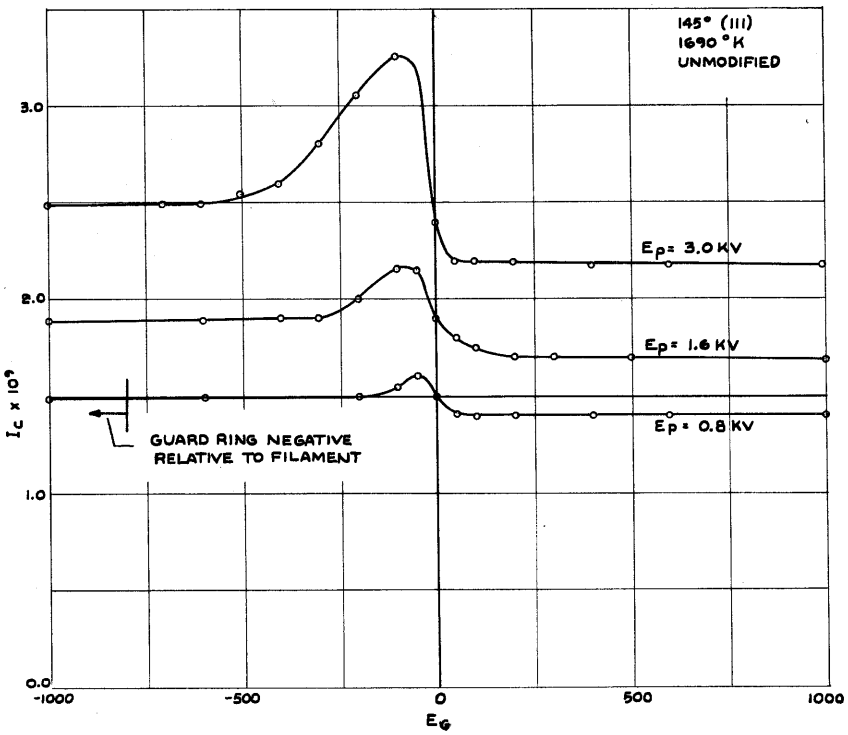

(a) (111) direction. No pronounced anomalous behaviour is evident.

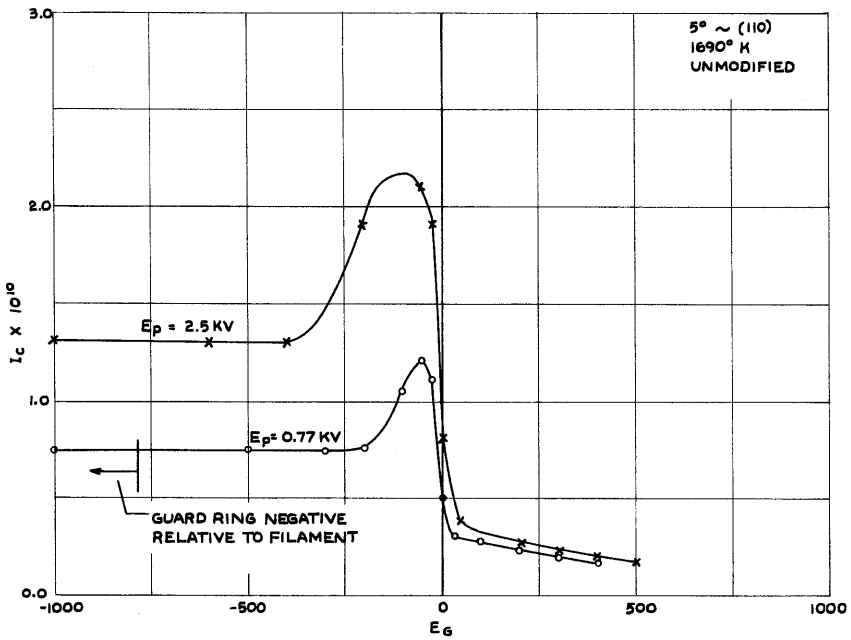

Fig. 12. Guard-ring characteristics of the unmodified measuring tube (without end-guards). These are plots of collector current I_c vs. guard-ring potential E_g relative to collector.

(b) (110) direction. Both forms of the anomalous "x-ray photoelectric" effect are observed. For negative E_g the spacing of the two curves is too great; for positive E_g the curves slope downward.

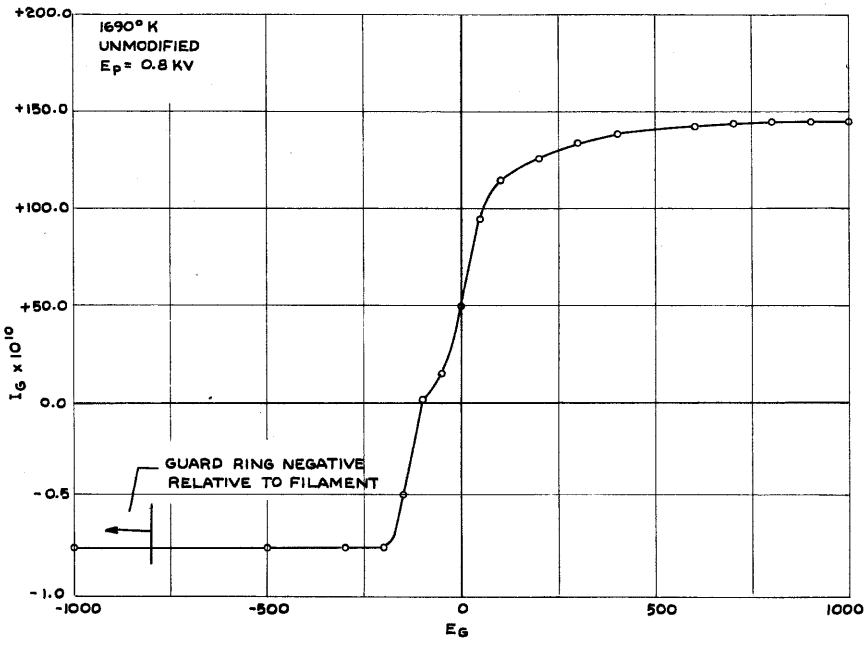

Fig. 13. Guard-ring volt-ampere curve of the unmodified tube (without end-guards).

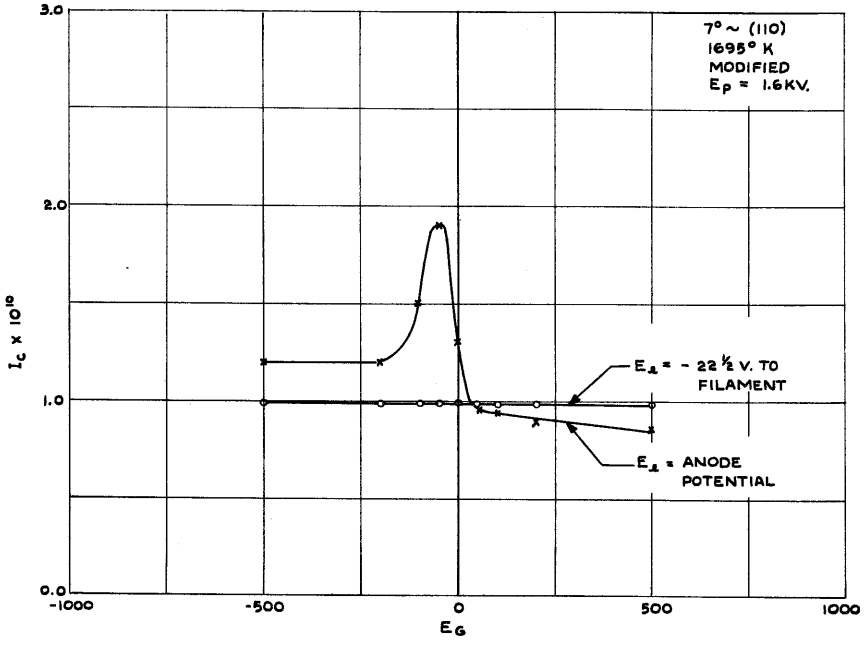

Fig. 14. Guard-ring characteristics, (110) direction, of the modified measuring tube (with end-guards installed). The curve for E_e = -22 1/2 volts shows complete elimination of the x-ray photoelectric effect.

It is claimed that the second feature of fig. 12b, the linear decrease of collected current with increase of positive E_g, is due to electron emission from the glass surface of the insulator that supports the collector, particularly from the wetting glass which provides a thin covering for the collector lead over several millimeters of its length. This emission is most likely secondary emission arising from bombardment of the glass by stray primary electrons escaping from the open end of anode B. There may also be a photoelectric emission arising from the x-ray illumination as discussed in the last paragraph. Since the nearest metallic electrode to this glass is the guard ring itself, the emission serves to charge the surface of the glass to the potential of the guard ring. The conductivity of the pyrex glass then permits a leakage of current through the glass to the tungsten lead. From the slope of the curves of fig. 12b, the resistance of the leak is 5×10^{13} ohms. One obtains the same value of resistance when different ranges of collected current are used, and this value is not inconsistent with what one would expect from the resistivity of pyrex, 10^{14} ohm-cm, and the dimensions of the wetting glass. It is evident that a constant current leak is insignificant, even for the (110) direction for higher temperatures, when the collector current is large compared to the leakage current. Further evidence of dielectric charging is given by the very long times required for reaching equilibrium after changing conditions in the measuring tube, especially if a change in E_g is involved. Here again, the effect is noticed only in the (110) direction where the measured emission is low. Nichols reported a similar time effect in connection with his measurements in the (110) direction (27).

If the explanation of the anomalous behaviour is valid, one can predict the shape of a volt-ampere characteristic for the guard ring. There should be a rather large positive electron current I_g for values of E_g positive enough to attract the stray electrons from the open end of the anode and the photoelectrons released in the vicinity of the guard ring. For values of E_g sufficiently negative, there should be repulsion of stray and photo-electrons; I_c should even go negative, due to x-ray photoemission from the guard ring. Both behaviours are indeed observed in the guard ring volt-ampere characteristic of fig. 13. In addition, there is no change in the guard ring current when the guard ring is made more negative than the filament. In reading fig. 13, note the discontinuous change in scale of the ordinate at the origin. The stray current collected for E_g positive is about 200 times as large in magnitude as the photo-electric current released when E_g is negative. Also note that the latter current is of the same order of magnitude as the collector current of fig. 12b.

The choice of a completely satisfactory operating point on the curves of fig. 12b is of course impossible. However, since the slope on the E_g positive side is significant only for low temperatures and the (110) direction, and since the photoelectric current is appreciable only for negative E_g, a value of 180 volts positive was chosen for the unmodified tube as used to obtain the "pre-end-guard" data.

In view of the importance of obtaining reliable emission data from the (110) surface, it was considered worthwhile to eliminate the effects of x-rays and stray electrons by modification of the tube. For this purpose the end-guards EE' were installed as described in Sec. A.1.

Their behaviour was perfectly satisfactory, as demonstrated by the $E_e = -22\frac{1}{2}$ volt guard ring characteristic of the modified tube, fig. 14. Although the guard ring is now unnecessary, the previously established operating point, 180 volts positive, was used. With correct operation of the end-guards, dielectric charging no longer appeared to occur, in view of the absence of all time effects in reaching equilibrium electrometer readings.

It should be mentioned that a preliminary measure to eliminate the x-ray photoelectric effect by insertion of a grounded tantalum shield between the open end of the anode and the guard ring failed to eliminate time effects. This suggests that the glass surface charging is at least partly due to bombardment by stray electrons. The volt-ampere characteristic of the guard ring, fig. 13, indicates that there is sufficient stray current available. Further evidence will be discussed in connection with the end-guard characteristic in the next section.

B.2. End-Guard Characteristic.

It has been seen (fig. 14) that with the end-guards negative $22\frac{1}{2}$ volts with respect to the filament, the guard ring characteristic is a constant to within one percent, indicating no radiation in the vicinity of the collector lead. No change is observed for any moderately negative end-guard potential E_e, and even operation with E_e equal to the filament potential gives the same curve. If E_e is set equal to the anode potential, the shape of the guard ring curve shows that some stray electrons escape the end-guards and reach the guard ring region. Under this condition of operation the sloping characteristic and the time

constant phenomenon reappear when E_g is positive (see fig. 14). This shows that some of the surface charging previously observed is definitely due to the stray electrons. Although it seems plausible that the charging is due to direct bombardment of the glass by the stray electrons, it is conceivable that the stray electrons create x-rays which in turn bombard the glass. Operation of E_e negative with respect to the crystal filament, however, both eliminates stray emission and intercepts x-rays from the anode.

In order to ascertain the degree of distortion of the field at the slit due to the presence of the end-guards, a set of measurements was made with the two guards, E and E', at different potentials. To avoid stray electron and time constant effects, a direction of maximum emission from the crystal was used, a (116) direction. Operating the crystal at 1750°K., no change in collected current was observed when either end-guard was held at the usual potential, $22\frac{1}{2}$ volts negative, while the other was varied from anode potential to filament potential. The anode-filament potential was 1005 volts.

B.3. Secondary Suppressor Characteristic and the Secondary Emission Effect.

The correct operating point for the secondary suppressor electrode C is determined by taking a curve of collector current I_c vs. suppressor voltage E_s. Once again the behaviour is as expected if any but the crystal direction of lowest emission is used. In fig. 15a, a suppressor characteristic for the next to lowest emission direction, the (112), is given. If the suppressor is sufficiently negative, all the slow secon-

daries liberated at the collector or at the slits are returned or repulsed and there is no change in collected current as E_s becomes more negative. When E_s is positive, the collector current is reduced to a negative value; in this case secondary electrons released from the collector proceed to the positive suppressor. That the current becomes negative shows that the ratio of secondaries to incident primaries is greater than unity. Fig. 15a is similar to the suppressor characteristic obtained by Nichols (27).

On the other hand, if a suppressor characteristic is taken with the crystal oriented to give emission from the (110) direction, a curve of the form of those of fig. 15b is obtained. It is asserted that this behaviour is due to collection through the slit system of secondary electrons emitted at the anode B, secondaries coming from anode regions upon which the impinging emission density is much greater than the emission density in the direction of the slits. This is electron-optically possible, due to the imperfect resolution of the slit system SS'. Since S' is three times as wide as S, electrons proceeding at an angle up to about 6 or 7 degrees with the radial direction can penetrate the slits to reach the collector. Moreover, the vertical resolution is very poor indeed, due to the length of slit S and emphasized by the excessive length of S' (see description of equipment, Sec. A.1). Depending upon their energies, locations when emitted, and angle of emission, some secondaries starting inward towards the crystal wire will be re-directed towards slit S with small enough deviation from the radial direction to permit passage through to the collector. A typical electron path is shown in fig. 16. The trajectory was calculated by a graphical stream

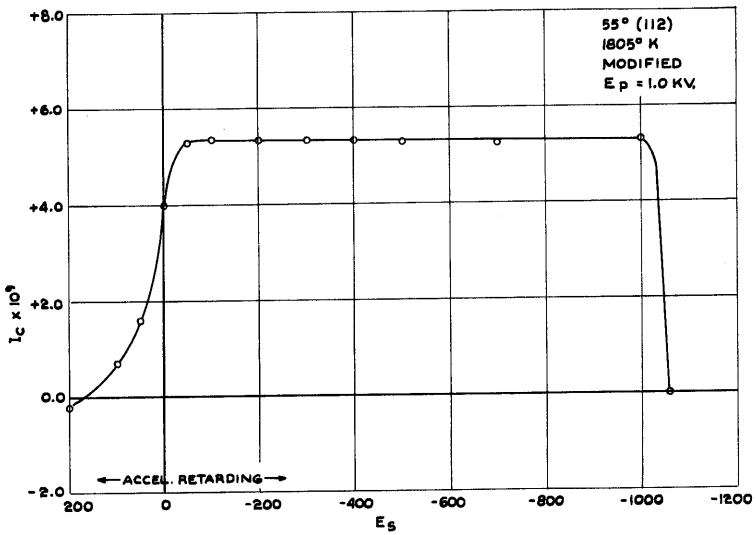

(a)

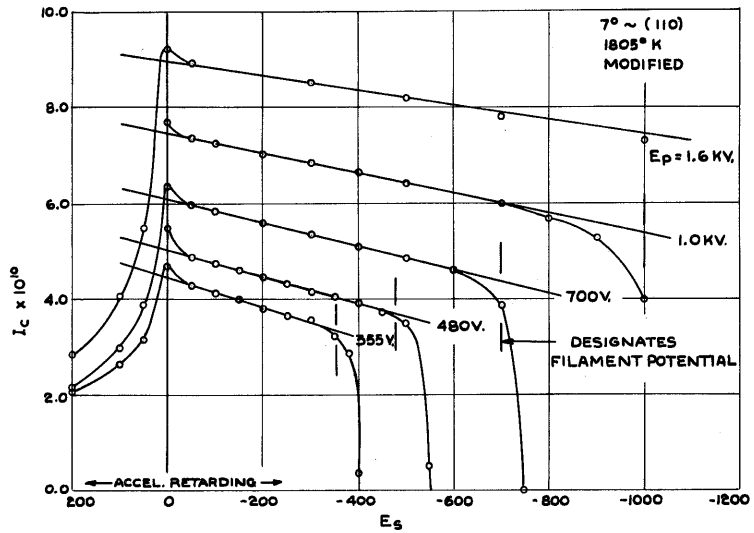

(b)

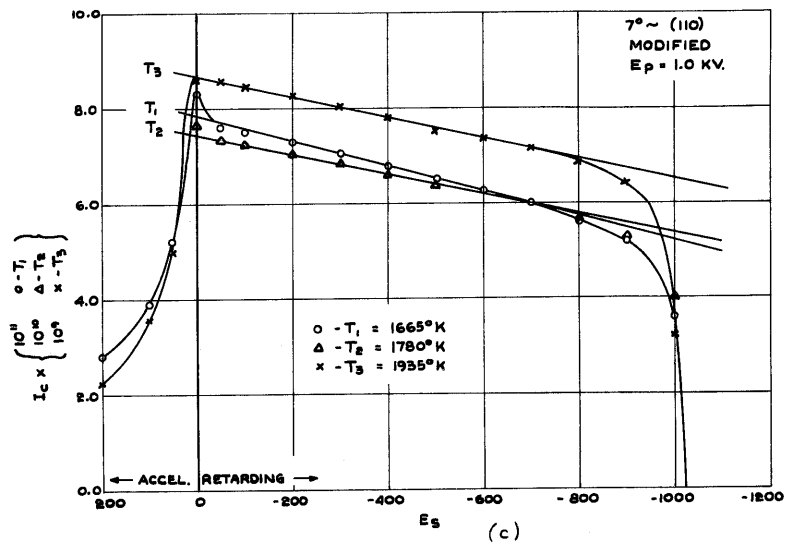

(c)

Fig. 15. Suppressor characteristics of the final (modified) measuring tube, showing the secondary emission anomalous behaviour in the (110) direction.

(a) (112) direction. No anomalous behaviour evident in this, the second lowest emitting direction.
(b) (110) direction. Characteristics for different anode-cathode potentials. Secondary emission trouble produces sloping characteristics with steeper slope at lower anode voltages.
(c) (110) direction. Characteristics for three temperatures. The spurious secondary emission effect is larger, relative to the total current, at lower temperatures.

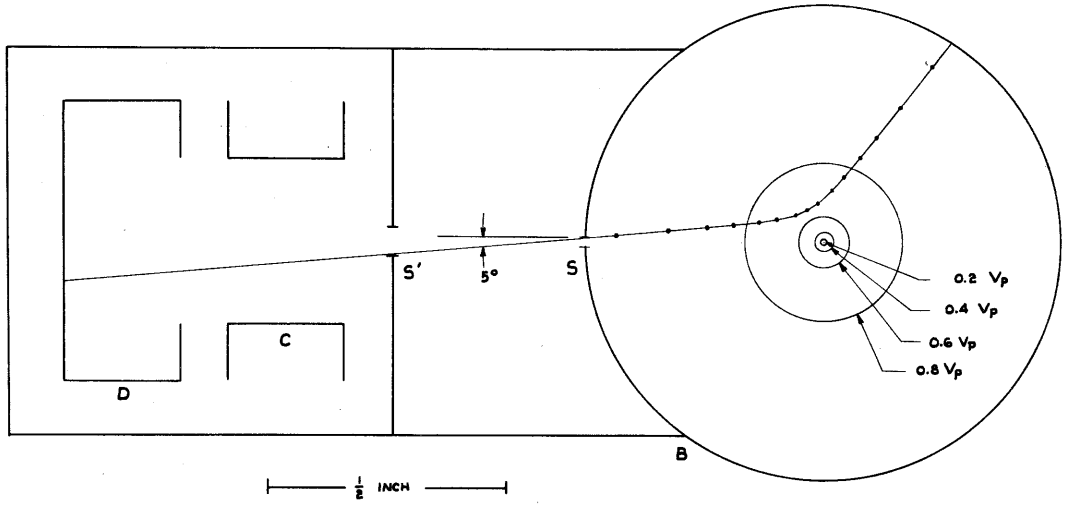

Fig. 16. Graphically computed path of a secondary electron emitted from anode so as to enter slits SS' to be collected at D. The electron is emitted with one-half primary energy at 5° to the radial direction.

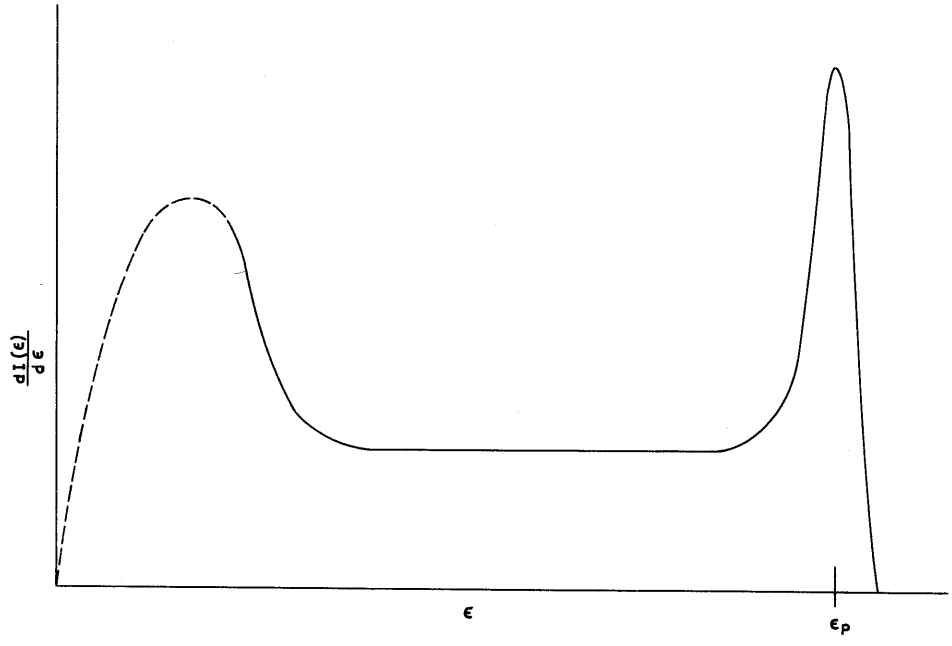

Fig. 17. Qualitative form of energy distribution of spurious plus true (110) current, from the shape of the suppressor characteristics of fig. 15.

plotting method for an electron leaving the anode at 5° from the normal, with one-half of the primary electron energy. This electron originated at 120° in azimuth, measured from the slit. More energetic 5° secondaries can come from anode regions of larger azimuth, while less energetic secondaries must come from nearer anode regions.

There is considerable evidence that this explanation is the correct one. Since radiation in the vicinity of the collector lead has been eliminated by the end-guards one must conclude that the behaviour is not external to the collector housing. The normal nature of suppressor characteristics in all other directions would indicate that the suppressor electrode is performing satisfactorily. One must conclude then that a spurious current is passing through the slits from the cathode-anode region. The suppressor characteristic is, in reality, an integrated energy distribution curve of the collected current, since the suppressor electrode serves to establish a potential barrier across the path from the slits. From the nature of the curves of fig. 15b, one would conclude that the energy distribution of the collected current is qualitatively of the form shown in fig. 17. But this is the type of energy distribution reported for secondary emission (28, 29, 30). The relatively large low energy peak, the almost constant distribution over moderate energies, and a very sharp peak at the full primary energy, are all characteristic. Indeed, if it were not for the full energy peak of the secondary energy distribution, arising from elastically scattered primaries, it would be a relatively simple matter to obtain a good approximation to the magnitude of the "true" (110) current by merely extrapolating the suppressor curve to eliminate all electrons having suffered energy loss. But since the

elastic "secondaries" are indistinguishable from "true" (110) current, such a subtraction would only incompletely eliminate the spurious effect.

Further evidence as to the nature of the spurious current is provided in its anode voltage and filament temperature dependence. If the magnitude of the effect is measured by the energy density of the medium energy secondary electrons, it is proportional to the slope of the suppressor characteristic. It has already been found that an x-ray photoelectric effect has a monotonic increasing dependence upon anode voltage, but it is known, at least in the case of low energy secondary emission, that there is a maximum in the efficiency of secondary production as a function of primary energy; according to Koller (31), this maximum occurs at 600 volts for tantalum. Since the slope is greater for the 600 volt suppressor characteristic than for higher voltage characteristics (fig. 15b), secondary emission must be the preponderant effect. Fig. 15c shows suppressor characteristics taken at three temperatures yielding collector currents in the approximate ratios 1 : 10 : 100. It can be seen from the slopes of the three curves that, relatively speaking, the spurious effect becomes more pronounced as the temperature is lowered. This would be expected since the surfaces producing most of the primary emission responsible for the secondary emission are of lower work function than the (110) surface.

Elimination of the secondary emission effect was not undertaken, due to shortage of time, and uncertainty as to the degree of suppression required to yield meaningful data in the (110) direction. A reduction by a factor of six might be accomplished by replacement of the second slit S' by one of the same optical size as the first slit S. This, of course,

would require very careful alignment of the slit and wire system. A further improvement might be realized by coating the anode with lamp-black to reduce the secondary emission, if such a technique proved practical. More far-reaching modifications involving magnetic or electrostatic focussing, insertion of a mesh anode, surrounded by a second anode operated at a lower potential, etc., are apparent. It might be practical to monitor the spurious current through a pair of slits deliberately misaligned with the filament in order to arrive at a subtractive correction. The technique of correction used to obtain (110) data with the tube as described will be discussed in Section C.

For directions other than the (110) a battery potential of minus 540 volts with respect to the anode was applied to the suppressor.

B.4. Collector Characteristic.

The collector was varied over several hundred volts both negative and positive with respect to the anode. As long as the collector was positive both with respect to the filament and with respect to the suppressor, there was no dependence of collector current upon collector potential.

C. THERMIONIC CONSTANTS AS A FUNCTION OF CRYSTALLOGRAPHIC DIRECTION

Two complete sets of thermionic data were taken: (a) the final data, using the modified tube to eliminate the x-ray photoelectric emission trouble but not free from the secondary emission difficulty, and (b) the pre-end-guard data, taken with the unmodified tube and subject to both forms of anomalous behaviour. The final data are unaffected by the

secondary emission trouble except for measurements taken in the vicinity of the (110) crystal direction, where corrections have been applied to the data as will be described. The pre-end-guard data are taken with the tube basically as used by Nichols; the results show good agreement with those he obtained. The effects of the x-ray photoelectric emission are also significant only for directions of minimum emission, particularly for the (110) direction. Thermionic constants derived from both sets of data will be tabulated, and illustrative curves will be given for comparison when there is significant difference between the two runs.

At the conclusion of the final data run, the wire was flashed two minutes at 3030°K. to check reproducibility of the data. In no crystal direction did emission after the flash differ by more than five percent from the pre-flash final data.

C.1. Polar Plots of Emission vs. Azimuth about the Wire.

In figures 18a, b, and c the dependence of emission upon crystallographic direction is given for three crystal temperatures. The patterns show the symmetry of a body centered cubic crystal with face diagonal along the wire axis, and are identical in form with those obtained by Nichols (7). The assignment of crystal directions is in agreement with his and with the results of Martin (4), both of which were corroborated by an x-ray determination of directions. There are clearly minima of emission along the (110), (112), and (001) directions, and a maximum occurs in the (111) direction. Following the suggestion of Nichols (7), the other maximum will be designated (116), although it is not likely

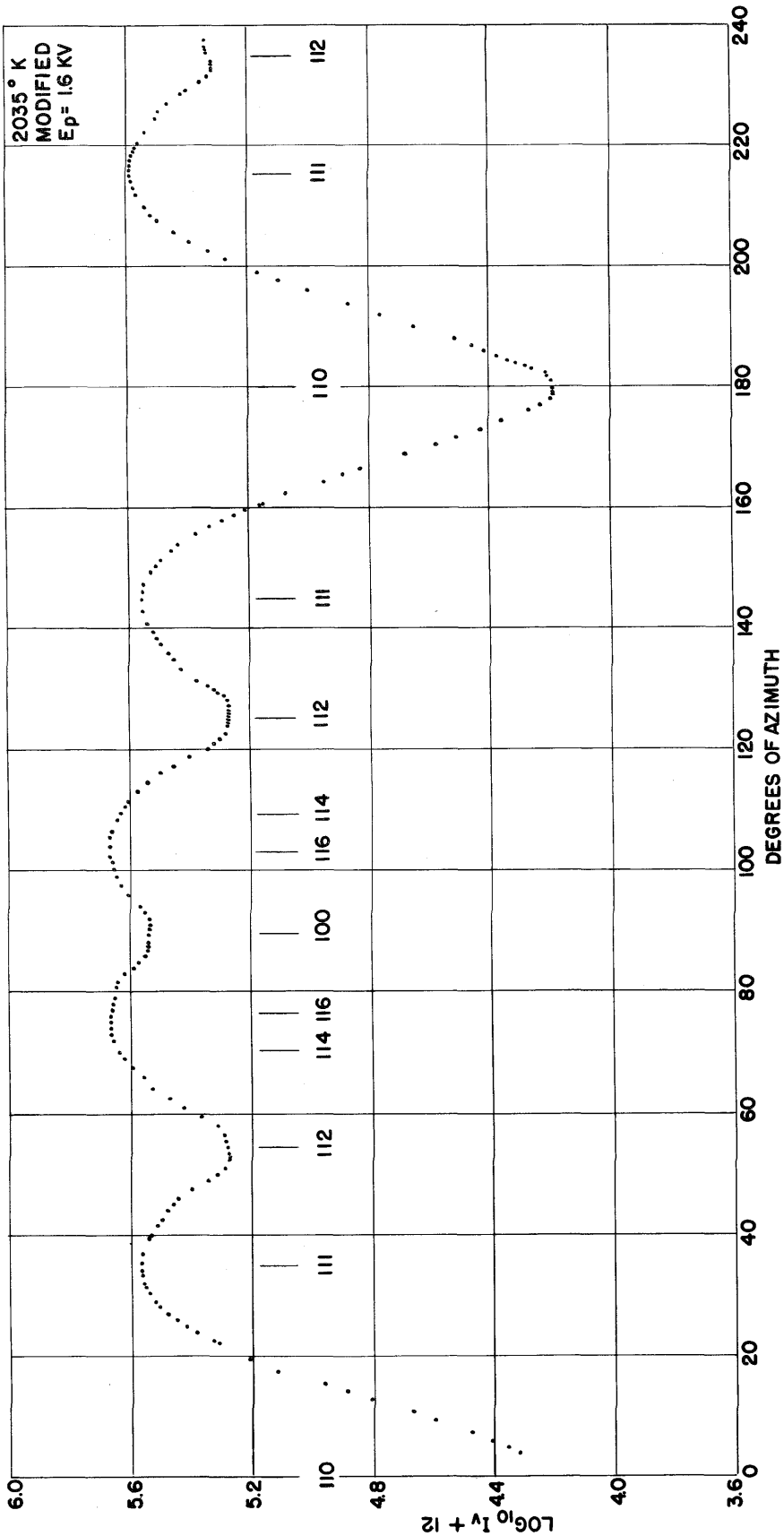

Fig. 18a. Emission vs. azimuth at 2035°K.
Surface gradient, 5.5 x 10^4 volts/cm.

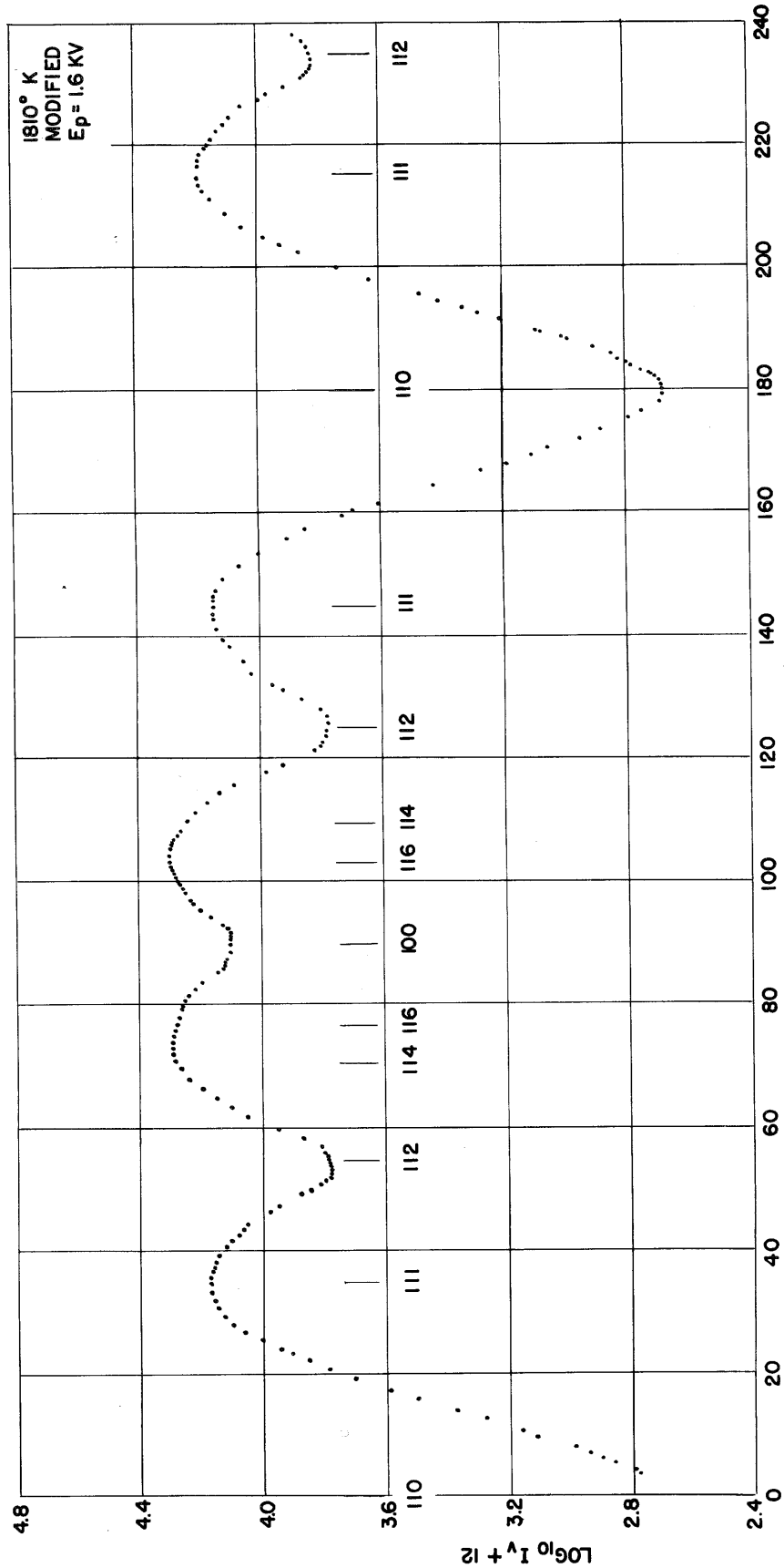

Fig. 18b. Emission vs. azimuth at 1810°K.
Surface gradient, 5.5 x 10^4 volts/cm.

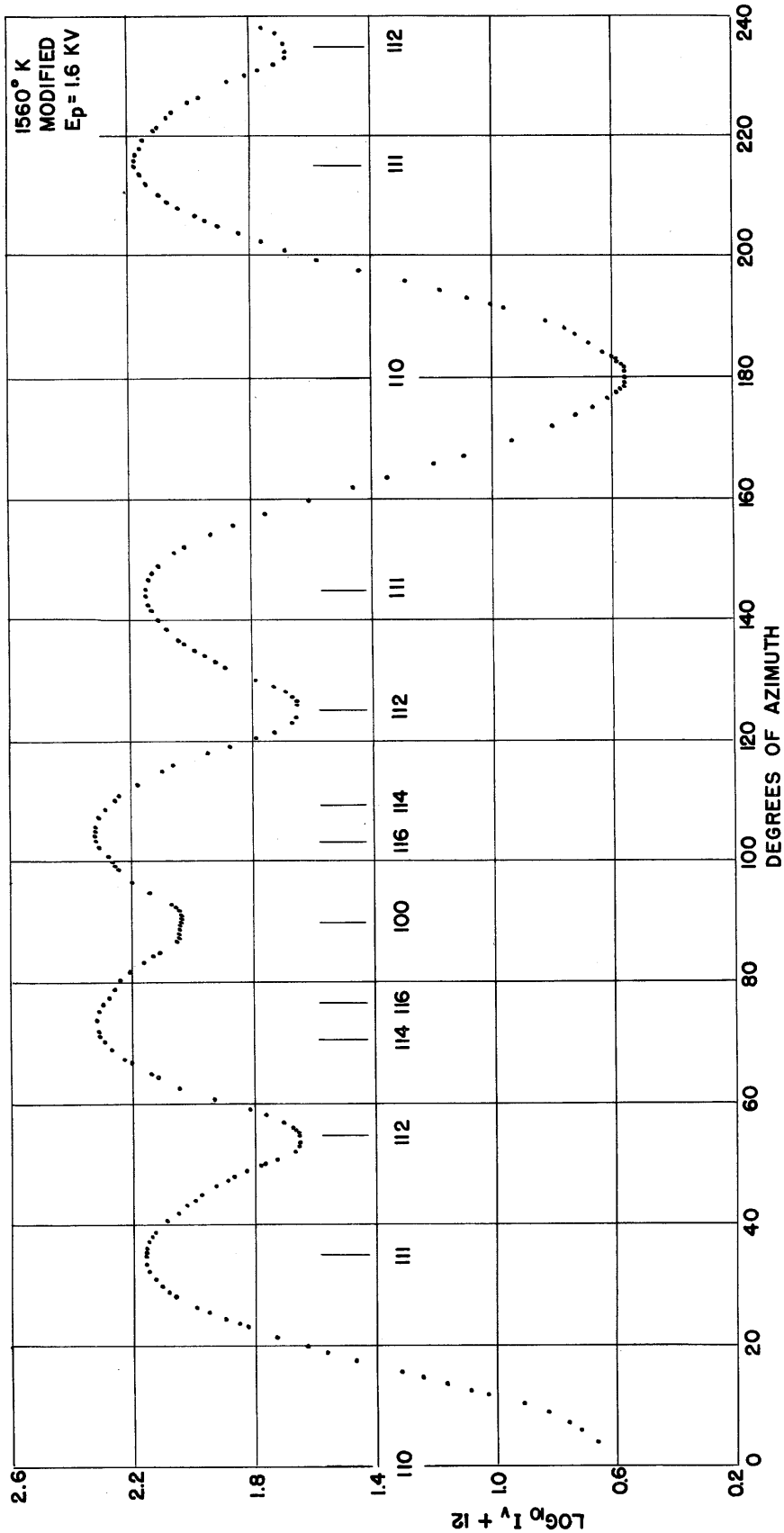

Fig. 18c. Emission vs. azimuth at 1560°K.
Surface gradient, 5.5 x 10^4 volts/cm.

characteristic of a particular set of Miller indices. One will recall that only directions having Miller indices of the form (hhk) are displayed by a cylindrical crystal having a face diagonal along the wire axis; the only elementary directions are those of the form (11k).

The distinguishing feature of the polar plots as compared with those obtained by Nichols, is the appearance of definite "flats" of emission in the various directions of minimum emission. This phenomenon suggests the existence of "plateaus" on the surface of the crystal normal to the (110), (112), and (001) directions, as discussed in Part I. That these flats did not appear on Nichols' polar plots is probably due to the fact that his measurements were made on a wire which had been subjected to only a mild heat treatment after re-polishing before the data were taken. It is likely that this heat treatment was not sufficient to produce plateaus which could be resolved by his slit system, which had a resolution of about 3 degrees. The data of fig. 18 were taken in the final tube, after heat treatment sufficient to evaporate $3\frac{1}{2}$ to 4 percent of the wire diameter (see Appendix for detailed history). The existence of the plateaus was apparent on all previous runs, but there was heat treatment sufficient to evaporate about 2 percent of the wire diameter before the first one was taken. The difference between the final data and the pre-end-guard data is not significant as pertains to the polar plots and only the final data are displayed in fig. 18.

It should be noted that the data for the vicinity of the (110) directions are not reliable, due to the secondary emission effect. Qualitatively speaking, currents lower than those observed in the (112) direction are likely to be in error. For this reason it is also not

certain that the width of the (110) plateau, as derived from fig. 18, is accurate.

C.2. Schottky Plots: Dependence of Emission on Anode-Filament Potential.

In addition to the use of the Schottky plot in reducing high field emission data to zero field values, the shape of the Schottky plot may give information as to the patch nature of the emitting surface (8). Finally, from the periodic deviations from the Schottky line, information can be derived concerning reflection effects. Schottky plots were taken for each crystal direction corresponding to a maximum or a minimum. The pre-end-guard data did not differ significantly from the final data with the exception of those for the (110) direction. In that case, the pre-end-guard data were difficult to obtain, due to the very long times involved in reaching equilibrium electrometer readings. As explained in Sec. B, this was due to glass surface charging effects. The final tube plots for the (111), (112), (116), (001), and (110) directions are presented here; the (110) data will be discussed separately later.

C.2.a. Schottky Coefficients for Reduction of Currents to Zero Field Values.

Except for the periodic effect, the data follow the well known law derived from the Schottky mirror image theory:

$$\log_{10} i_V = \log_{10} i_o + SV^{1/2}/T \qquad (C.1)$$

where i_V is the high field emission current, i_o the zero field value, V the anode-filament potential in volts, T the temperature in degrees

Kelvin. Assuming that the filament is perfectly round and smooth, one derives from the Schottky theory and the electrostatics of the cylindrical configuration used here the theoretical value for S:

$$S = 1.905 \frac{1}{\sqrt{r \log_e R/r}} \qquad (C.2)$$

where r is the radius of the single crystal wire and R the radius of the anode, both in cm. The theoretical value of S using the wire radius for the final data is 11.2. Fig. 19 is a typical plot, showing the voltage dependence of emission for the 90° (001) direction at 1930°K. and 1650°K. The two sets of data are superimposed to show the agreement in slope. Fig. 20 shows one Schottky plot for each class of directions measured. In general, Schottky plots were taken at two temperatures for each direction. Agreement of slope between the two was within 5 percent. Due to the effect of the periodic Schottky deviation and the limited range of voltages over which the tube could be used, the precision of the slope cannot be expected to be better than 5 percent. The average value of the empirically determined Schottky slope, S, is tabulated for each direction in table V.

C.2.b. Information Regarding Patchy Nature of Surfaces.

Schottky plots for all directions except the (110), for which meaningful data are not available, can be seen (fig. 20) to show no deviation (other than periodic) from the Schottky line for voltages higher than 750, which corresponds to a field gradient of 26,000 volts/cm. At this point the Schottky plots for the (112) directions begin to deviate

Table V. Schottky slopes, S, for different directions

Direction	Schottky slope S	
	Pre-guard tube	Final tube
35° 111	11.9	12.8
145° 111	12.0	12.8
215° 111	10.6	12.3
55° 112	12.9	12.8
125° 112	12.5	13.2
235° 112	10.8	11.5
75° 116	12.2	12.8
105° 116	12.0	12.3
90° 001	12.4	12.7
180° 110*	10.4*	9.1*
Theoretical	11.1	11.2

* For comparison only; value of S for (110) direction obtained in usual way is erroneous. See Sec. C.4.

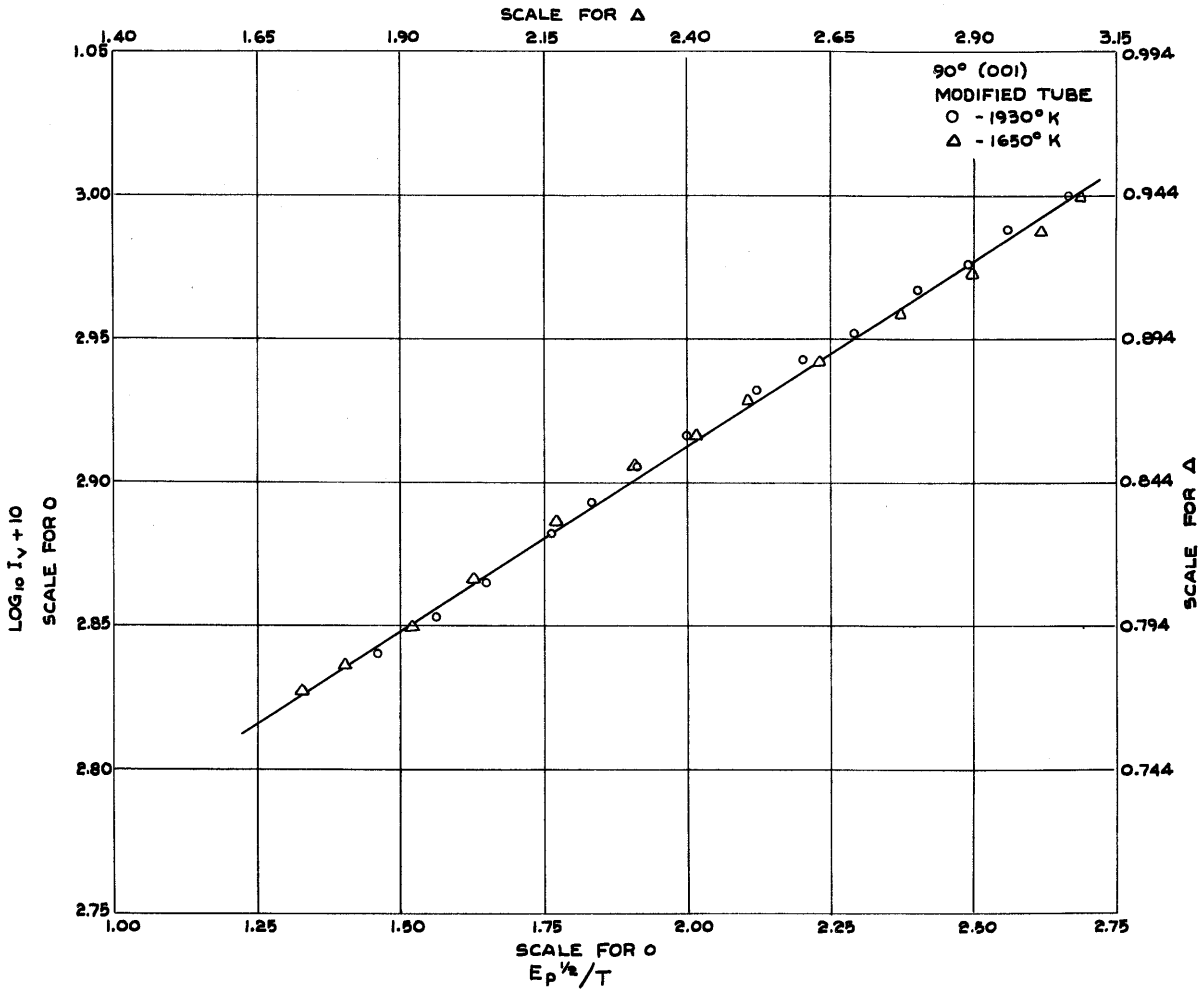

Fig. 19. Schottky plot for the 90° (001) direction.
o data at 1930°K., Δ data at 1650°K.

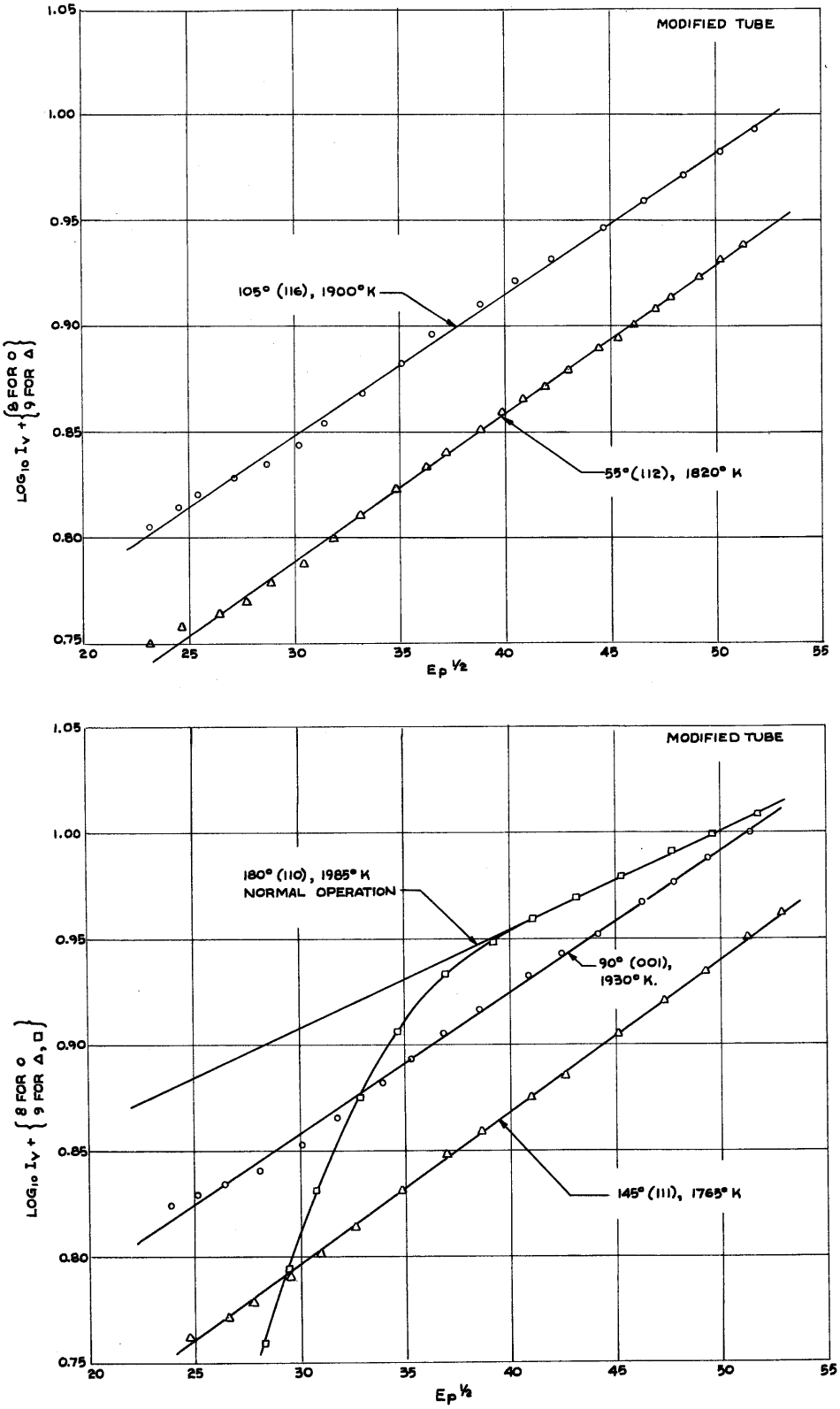

Fig. 20. Schottky plots, one each for the (111), (112), (116), (001), and (110) directions. The (110) plot is discussed in Sec. C.4.

upward, clearly indicating failure of the projection properties of the tube due to thermal velocities (see Appendix III). Deviation occurs only at even lower potentials for the high emission directions, e.g. the (116), as might be expected in view of the broad nature of the peaks of the emission vs. azimuth plots, fig. 18. The thermal velocities, which introduce an effective loss of resolution in projection would not disturb a broad peak as readily as they would affect the narrow minimum to be found in the (112) direction. Tangential fields, due to either small-scale or large-scale patchiness cannot produce an upward departure from the Schottky line. Small-scale patchiness results in a downward transition to the anomalous Schottky region, as discussed in reference 8. On the other hand, the tangential fields obtained on a perfect cylinder cut from a single crystal would be directed from the high work function surfaces to the low work function surfaces. Therefore any departure in the (112) direction due to large-scale patch fields would be downward, as electrons are drawn tangentially away from the (112) direction. It is worth while, however, to consider the tangential fields one may expect on a perfect cylinder cut from a single crystal. An estimate of the large-scale patch fields resulting from the occurence of different crystal directions around the cylinder can be had in $\delta\phi/\delta y$, where $\delta\phi$ is the difference in work function and δy is the separation of the two directions. Taking adjacent (112) and (116) directions and using the contact potential, 0.17 volts, between the two directions as obtained in Sec. D, we find an average tangential field of the order of 0.17 volts/0.17 x 10^{-2} cm, or 100 volts/cm. Since the shape of the plots of emission vs. azimuth (fig. 18) would indicate a much steeper than average gradient near the (112) direction, but a smaller

than average gradient near the (116) direction, this figure should be corrected upward for the (112) direction, downward for the (116). Near the (112) direction the patch field would then be several hundred volts/cm, enough to produce deviation from the Schottky line not far below 26,000 volts/cm (see Appendix III). If this is the case, the Schottky plot shows no significant patchiness of smaller dimensions than the spacing of the different crystal directions.

C.2.c. Evidence of Periodic Schottky Deviations.

Superimposed upon the Schottky lines for the directions under consideration is seen evidence of the periodic Schottky deviation (32,33,34,35). Indeed, the fact that the voltage range of the tube is so limited as to include only about one cycle of this deviation makes it difficult to assign a correct slope to the Schottky line, since one cannot clearly choose a reference line for a periodic deviation on the basis of only one cycle of the fluctuation. No attempt was made to improve the anode voltage stability to make detailed study of this effect practical. It is felt that a relatively simple modification of the tube to provide the function of the end-guards without so great a limitation due to field emission, together with improved anode supply regulation, would permit investigation of the periodic Schottky effect from different directions on a single crystal.

C.3. Richardson Plots: Dependence of Emission on Temperature.

The apparent emission constants for a uniform surface are defined and discussed by Herring and Nichols (8). Briefly, the "apparent work function" of an emitting surface is obtained by measuring the

emission at various temperatures, extrapolating the emission at each temperature to zero field by an empirically determined Schottky coefficient, and plotting the resulting log (j_o/T^2) against $(1/T)$. The apparent work function ϕ^* is a measure of the slope of this Richardson plot:

$$\phi^* = - \frac{k}{e} \frac{d \ln(j_o/T^2)}{d (1/T)} \qquad (C.3)$$

Since the extrapolated zero-field emission from a uniform surface will obey the Richardson-Laue-Dushman equation:

$$j_o = A (1 - \bar{r}) T^2 \exp (-e\phi/kT) \qquad (C.4)$$

it follows that:

$$\phi^* = \phi - T \frac{d\phi}{dT} - \frac{kT^2}{e(1 - \bar{r})} \frac{d\bar{r}}{dT} \qquad (C.5)$$

where j_o is the zero-field emission density in amp./cm^2 of the cathode surface, $\bar{r}$ is the average reflection coefficient, A is a universal constant equal to 120 amp/cm^2/deg^2, and ϕ is the "true work function" of the surface. The "apparent emission constant," A^*, is defined similarly in terms of the intercept of the Richardson plot of the zero-field currents:

$$\log A^* = \text{value of } \log(j_o/T^2) \text{ extrapolated linearly to } 1/T = 0 \qquad (C.6)$$

For a uniform surface this gives:

$$A^* = A\,(1 - \bar{r})\,\exp\left[-\frac{e}{k}\frac{d\phi}{dT} - \frac{T}{(1-\bar{r})}\frac{d\bar{r}}{dT}\right] \quad (C.7)$$

If one considers a surface made up of patches of different emitting properties, equation (C.4) must be replaced by:

$$j_o = AT^2 \sum_i f_i(1 - \bar{r}_i)\,\exp(-e\phi_i/kT) \quad (C.8)$$

where f_i is the fraction of the surface, assumed independent of temperature, occupied by the ith type of patch. In analogy with eqs. (C.3) and (C.5), the apparent work function ϕ^{**} for the patchy surface is given by:

$$\phi^{**} = -\frac{k}{e}\frac{d\,\ln(j_o/T^2)}{d(1/T)} \quad (C.9)$$

$$= \sum_i w_i\phi_i^* \quad (C.10)$$

where w_i is the fraction of the total zero field emission from the ith type of patch and ϕ_i^* is the zero field apparent work function of the ith type of patch. The apparent emission constant A^{**} for a patchy surface is defined in the same manner as was A^* by eq. (C.6). For further discussion of the apparent thermionic constants, refer to Herring and Nichols, reference 8.

Richardson plots were made for each of the (111), (112), (116), (001), and (110) directions. The data for the (110) direction will be discussed in the following section. There is some reason to believe that the data for the remaining directions may be characteristic of uniform surfaces and free from patch effects. Evidence in addition to that

provided by Schottky curves and observation under an optical microscope will be submitted in connection with contact potential measurements in Sec. D. However, because patchiness of the surfaces cannot be absolutely denied, the apparent thermionic constants will be doubly starred.

Richardson plot data both from the final tube and from the unmodified tube (without end-guards) will be given. Fig. 21 is a composite Richardson plot of the final tube emission from the different directions. In fig. 22 final plots are shown for certain directions with pre-end-guard data superimposed to illustrate the result of elimination of the x-ray photoelectric effect. Complete results for both tubes are tabulated in table VI, along with the values obtained by Nichols, as given in reference 8.

Differences between the pre-end-guard data and those of Nichols' can be due to: (a) differences in emission from the two crystals, or (b) differences in the contribution of spurious current from either of the anomalous effects.

Difference between the final data and the pre-end-guard data is a measure of the x-ray photoelectric effect. For all except the (110) data, the spurious current contribution is seen to be small.* There was virtually no effect on the data from high emission surfaces; the low emission Richardson plots were somewhat reduced in slope and intercept by elimination of the effect. It will be recalled that normal operation of the unmodified tube with the guard ring 180 volts positive left the reduced anomalous effect of x-ray photoelectric emission from the

---

* The location of the pre-end-guard Richardson lines above the final lines is probably due to error in the temperature scale used for the pre-end-guard data. See Appendix I for details of evaporation calculation by which the pre-guard diameter was obtained from the more precise final value.

Table VI. Thermionic constants for the different crystal directions. Both final and pre-end-guard values are tabulated. Nichols' results, reference 6, are given for comparison. The precision of ϕ^{**} is about 0.5 percent, that of A^{**} about 10 percent.

DIRECTION	FINAL		PRE-END-GUARD		NICHOLS'	
	ϕ^{**}	A^{**}	ϕ^{**}	A^{**}	ϕ^{**}	A^{**}
35° (111)	4.39	54	4.38	55		
145° (111)	4.37	47	4.36	49	4.39	35
215° (111)	4.38	54	4.39	65		
55° (112)	4.65	118	4.68	163		
125° (112)	4.64	110	4.68	150	4.69	125
235° (112)	4.65	133	4.66¢	153¢		
75° (116)	4.29	40	4.31	48	4.39	53
105° (116)	4.29	40	4.30	46		
90° (001)	4.52	105	4.52	119	4.56	117
180° (110)#	4.58#	8.0#	4.66#	11.8#	4.68#	15#

¢ Unreliable data due to deterioration of vacuum over long interval between remainder of pre-end-guard tube data and this measurement.

Anomalous behaviour invalidates (110) data obtained under normal operating conditions. True (110) current smaller than these figures indicate. See Sec. C.4.

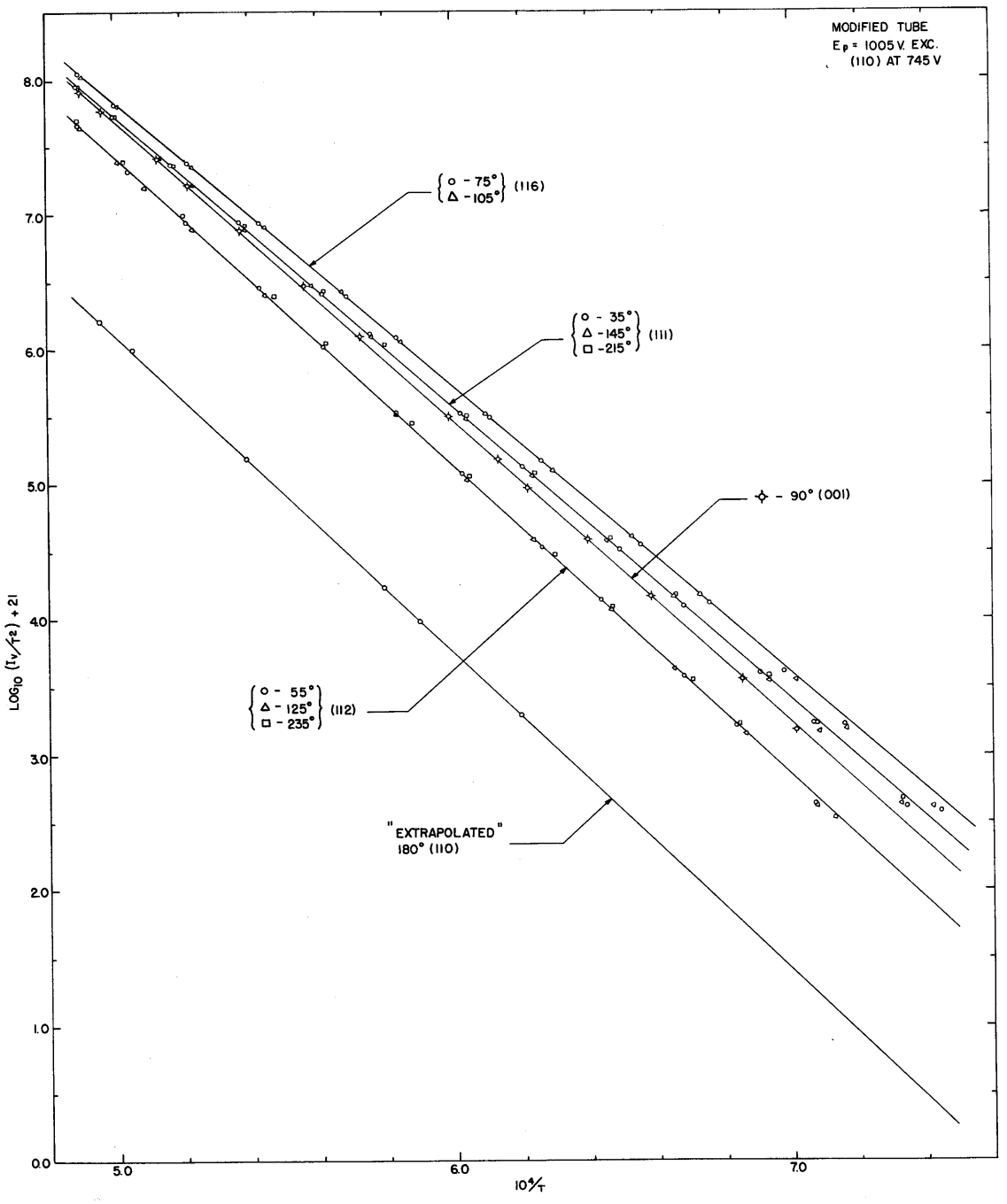

Fig. 21. Richardson plots for the different directions using final data from the modified measuring tube. The "extrapolated" (110) plot, partially corrected for anomalous tube behaviour (secondary emission effect), is a conservative upper limit on the "true" (110) emission.

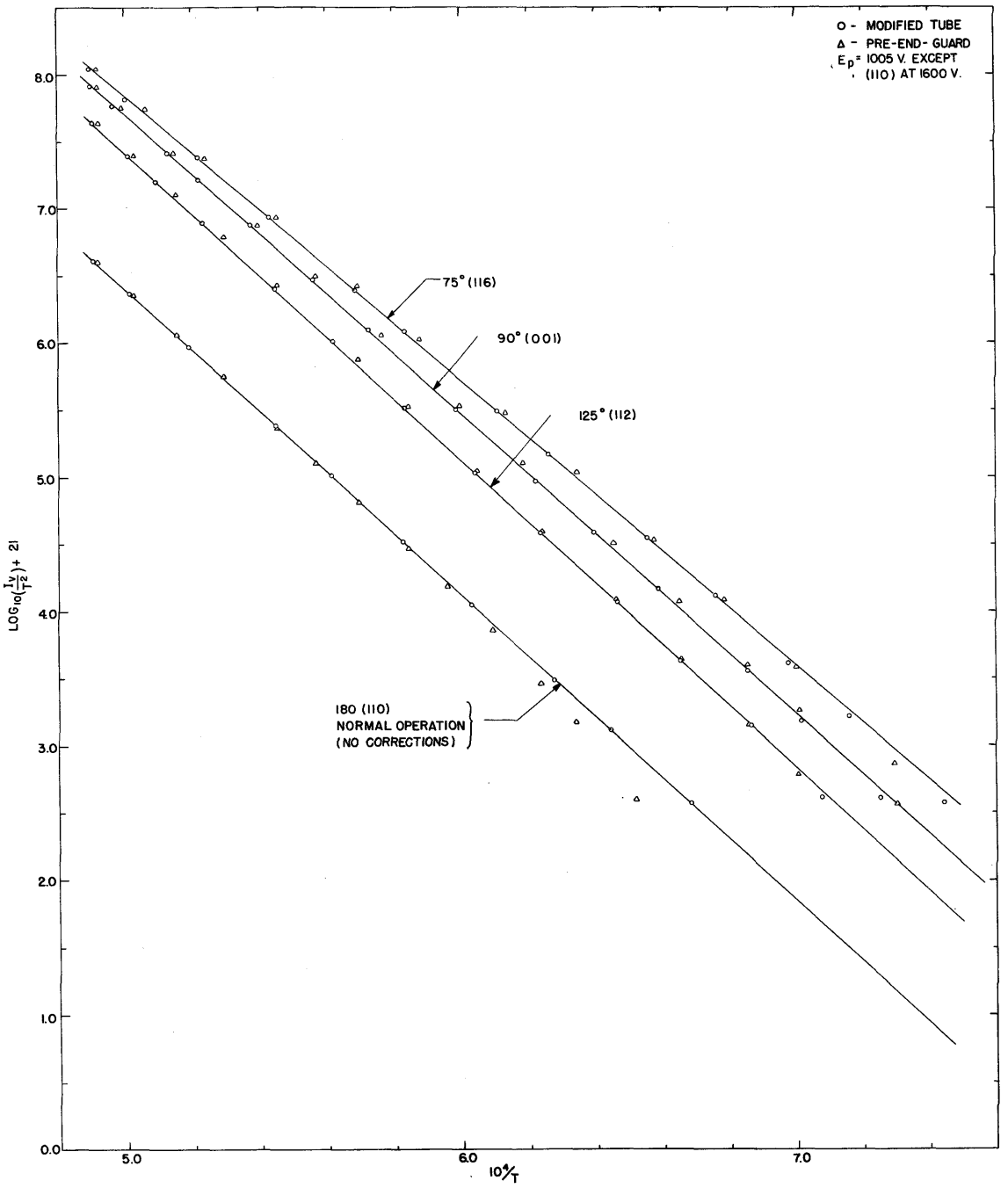

Fig. 22. Comparison of Richardson plots of pre-end-guard data Δ with corresponding plots of final data o. The Richardson lines are drawn for the final data.

collector lead itself, which should produce just the change observed. Since the x-ray production depends upon an average emission to the anode, it will be proportional to an average work function emission. For a low-emission surface (e.g. the (112)) the work function is higher than the average; hence the spurious contribution of the x-ray photoelectric effect should be more important at lower temperatures. Since the effect subtracts current from the electrometer reading, this means that the slope of the low emission Richardson line will be increased in magnitude by the presence of the spurious effect. Such was found to be the case (fig. 22).

Since it has been seen that the x-ray photoelectric effect produced only small changes in the thermionic constants, and since evidence was presented in Sec. B that the secondary emission effect was negligible in these directions, it is reasonable then to compare data with those obtained by Nichols. In general, the precision limits for the values of the apparent thermionic constants overlap (0.5 percent for work function, 10 percent for emission constant). However, the (116) surfaces as measured in this investigation, have a work function about 0.09 volts lower than obtained by Nichols. It is quite likely that the differences observed are due to the difference in heat treatment of the crystal before measurements were made. Although the treatment Nichols gave his crystal was quite sufficient to produce data characteristic of pure tungsten, as indicated by reproducibility through all temperature cycles, the treatment given in this case was sufficient to produce considerable evaporation, as already indicated. It is likely that this heat treatment was responsible for the appearance of the "plateaus" in the directions

of minimum emission, and it is probable that the surface obtained in the (116) direction was sufficiently different from that of Nichols' to account for the difference in constants. On the other hand, the effect, if any, of the d.c. etch on Nichols' crystal apparently did not extend to the (111) surface, in view of the agreement of the constants for that direction.

All Richardson lines show downward departure for temperatures below about 1400°K. This is due to reduction in temperature by conduction to the ends of the wire (see Sec. A.4). Slight systematic departure from a straight line is also observed for high temperatures. Careful check of the current measuring apparatus, current dependence of the standard resistor, etc., leaves uncertainty in the temperature scale as a possible source of this deviation.*

C.4. Data for the (110) Surface.

Nichols has interpreted his results as indicating that his (110) surface was a patchy surface. Evidence presented was: the break in the Schottky plot for the (110) surface at a surface gradient of about 5×10^4 volts/cm, the very low A^{**} value of 15, and the evidence of shingling on the (110) surface as observed by microscope. It is contended here that although a patchy surface cannot be completely ruled out on the basis of the present information, the two forms of anomalous behaviour of the tube will act so as to produce both the break in the

* Temperature dependence of ϕ^{**} can produce curvature of the Richardson line (see eqs. C.10 and C.5). It will be recalled, however, that a linear temperature dependence of ϕ for a uniform surface will not produce a curvature.

Schottky plot and the low value of A^{**}, as well as to obscure information regarding the true emission from the (110) surface.

If data are taken in the same way as they were for other surfaces, without regard for the secondary emission effect, the results are in good agreement with those obtained by Nichols. Both the final tube and the pre-end-guard tube yield Schottky plots with slightly lower than average slope and with definite departure from the Schottky line at about the same surface gradient as observed by Nichols. The Schottky plot so obtained by the final tube is plotted along with the valid Schottky plots for other directions in fig. 20. The pre-end-guard thermionic constants, $\phi^{**} = 4.66$, $A^{**} = 12$, obtained by normal operation of the tube are in good agreement with those of Nichols', $\phi^{**} = 4.68$, $A^{**} = 15$. It will be recalled that the crystal used was selected with the purpose of eliminating the shingle structure on the (110) surface. Although the shingling was not in fact completely removed, the degree of shingling was greatly reduced from that encountered by Nichols. If the shingling were related to the patchiness of the (110) surface, one would expect higher ϕ^{**} and A^{**} from the present measurements, rather than the slightly lower values obtained. When the x-ray photoelectric effect was eliminated in the final tube, the constants were affected in the same way as were those of the other minimum surfaces, but to a larger degree: $\phi^{**} = 4.59$, $A^{**} = 8.0$.

If, as has been suggested, the peculiar shape of the suppressor characteristic is due to secondary emission coming through the slit system, the collector current for the (110) surface is actually the sum of the "true" (110) current plus an undetermined amount of spurious secondary emission current. Certainly we can, in view of the linear

nature of the suppressor characteristic, make a valid extrapolation to the filament potential on the curve to eliminate a good fraction of that spurious current. If this is done for a number of temperatures, data for an "extrapolated" Richardson plot, fig. 23, are obtained, with "extrapolated" thermionic constants, $\phi^{**} = 4.72$, and $A^{**} = 9.7$. That these constants are both higher than the previous uncorrected values, would indicate that the spurious effect is of a low work function nature. But unfortunately the extrapolation technique does not eliminate all of the spurious current; there still remains that part of the secondary emission which has suffered no energy loss, that composed of elastically scattered secondaries, which is indistinguishable from "true" (110) current. At this point we can only definitely state that the true (110) current has emission constants higher than $\phi^{**} = 4.72$, $A = 9.7$.

An estimate of the correct value of the (110) constants can be made under two assumptions: (a) that all of the secondary emission current has the same effective work function, and (b) that, as has already been found for the similar (112) and (001) surfaces, the apparent emission constant of the (110) surface may be expected to have a value near 120. Under the first assumption one can arrive at the effective work function of the remaining full-energy spurious current, while the second permits the measurement of the amount of the spurious current present. In order to obtain the effective work function of the spurious current it is necessary to have a measure of a part of it. This can be accomplished by measuring that part of the current which has suffered energy loss, i.e. the difference between the left and right extrapolations of the suppressor characteristic. If this difference is taken

for each of a set of suppressor characteristics at different temperatures, one obtains data for the pure spurious current Richardson plot of fig. 23. The effective work function of this plot is 4.42 volts. Knowing the effective work function of the spurious current, there remains but to subtract enough of it to leave a Richardson plot with apparent emission constant of 120. This was done by a method of successive approximations; the apparent work function of the "true" (110) Richardson line so obtained is 5.26 volts.

As to the validity of the first assumption, it is not unreasonable that the electron-optics of the secondary emission effect might be such as to cause the elastic secondaries to have a different effective work function from those which have a reduced energy. In other words, the areas of the anode contributing to the spurious current which reaches and enters the slits might vary with the energy of the secondaries. If these areas are furnished primary current by filament patches of different work functions, the effective work function of the secondary emission might depend upon the energy of the secondary electrons. However, the curve of fig. 16 and the discussion of Section B.3 indicate that for energies as large as one-half the primary energy, secondary electrons are admitted from a sufficiently large percentage of the anode area to ensure an averaging effect. The linearity of the suppressor characteristics always observed then would deny that there is any energy dependence. Further, the remarkable agreement between the effective work function, 4.42 volts, and the average work function of doped polycrystalline tungsten, 4.45 volts, as recently published by Nichols (3), suggests that the secondary emission as obtained here is

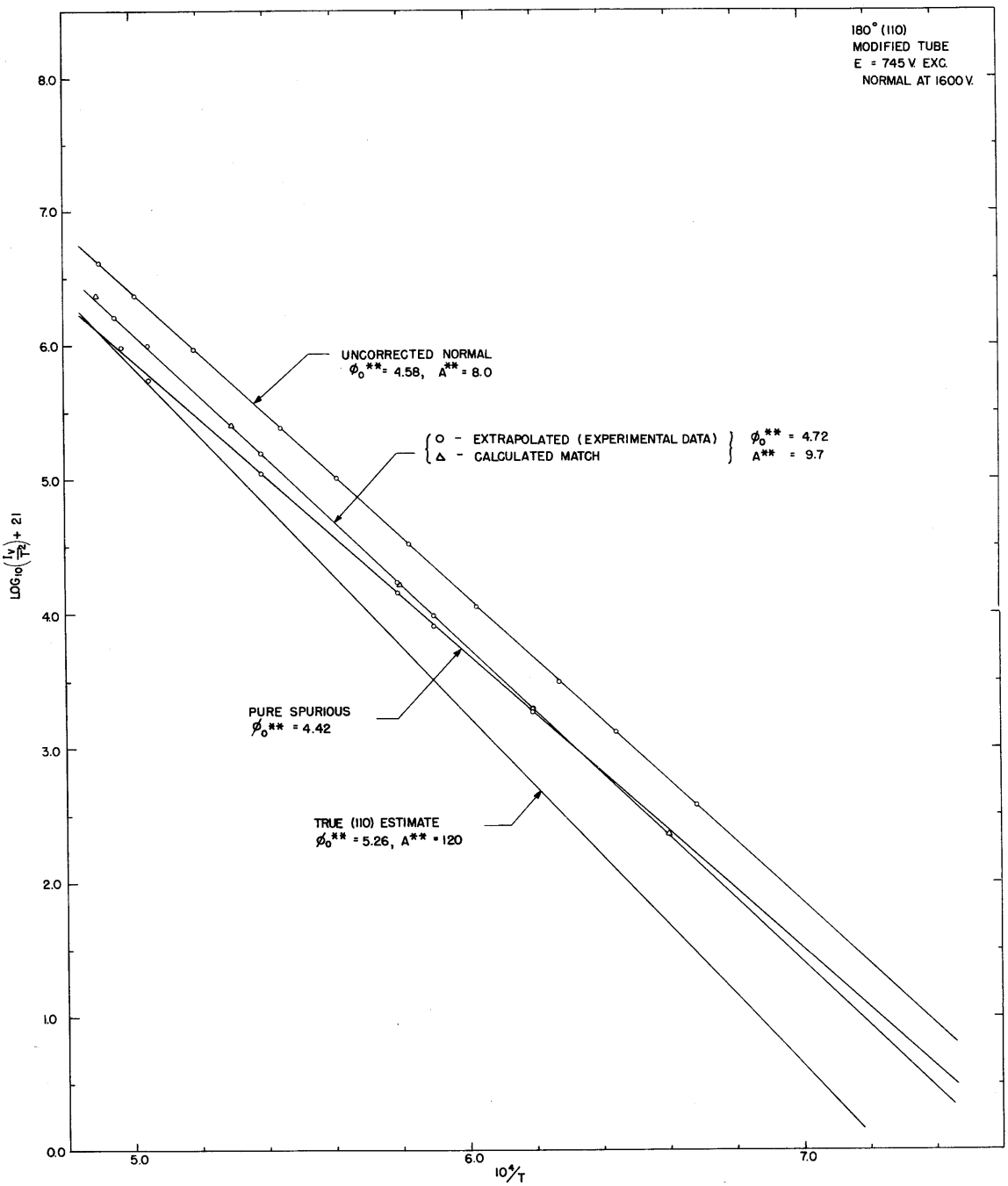

Fig. 23. Final tube Richardson plots for the (110) direction. Data plotted are the: (1) Uncorrected normal, taken as for other directions without correction for secondary emission effect; (2) Extrapolated, giving a conservative upper limit for the "true" (110) current; (3) Pure spurious, representative of the spurious secondary current alone; (4) Estimate of the true (110) current (see Sec. C.4).

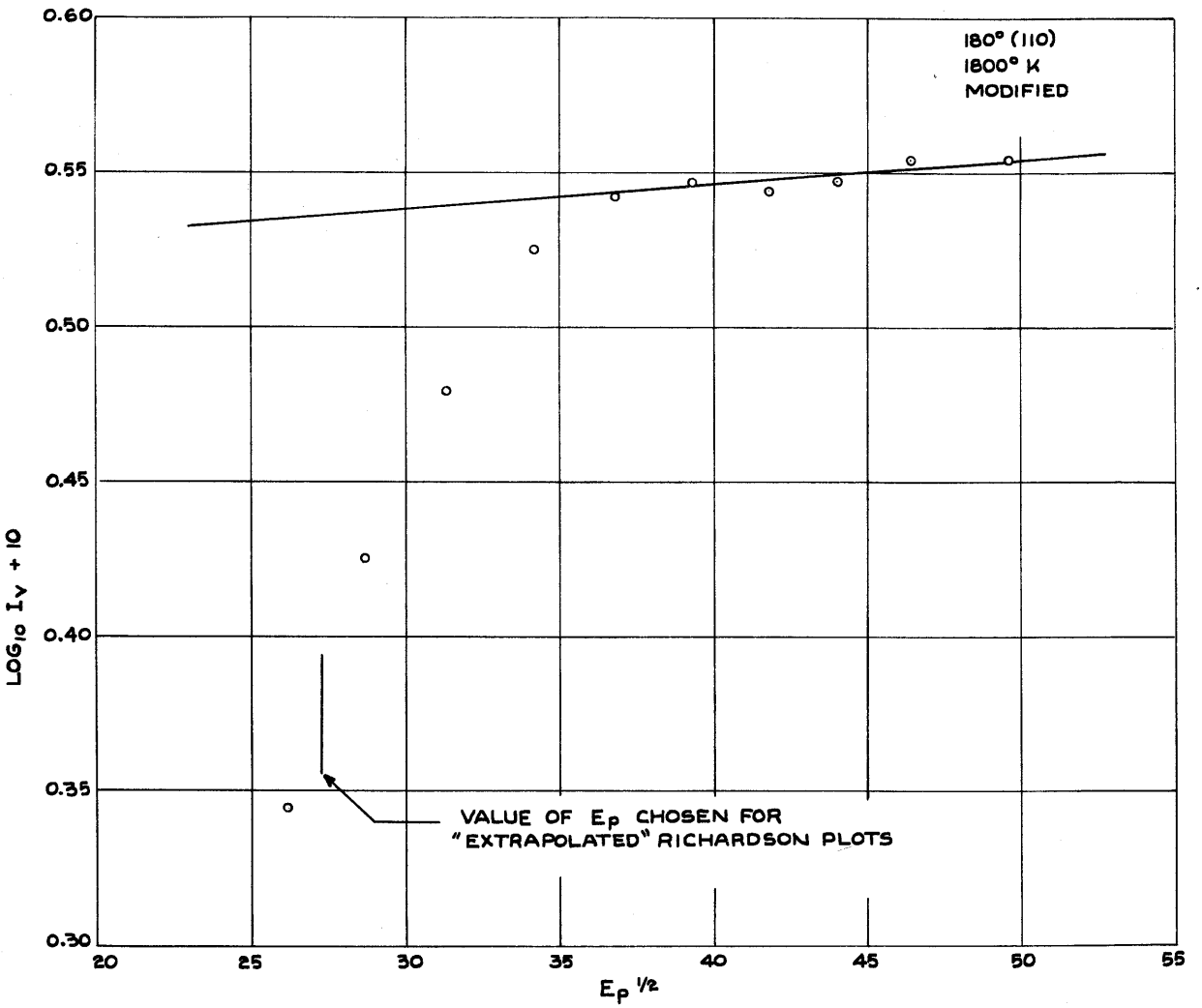

Fig. 24. "Schottky plot" of extrapolated data for the (110) direction.

dependent upon a high field average over all of the crystal. If this is the case for the whole range of energies, certainly the same holds true for the full energy component. As regards the second assumption, although it is not impossible that the surface is patchy in nature, it is held unlikely that such is the case. There is no longer any distinction between the (110) and the (112) or (001) surfaces; all have been observed to have both a plateau form and faint superimposed shingling, neither of which produced any departure from $A^{**} = 120$ for the latter two types of surface.*

One more consequence of this explanation, curvature of the Richardson line, should be considered. If the current measured for the (110) direction is really the sum of the true (110) current of work function say 5.26 volts, and a spurious current of work function about 4.42 volts, the Richardson line should be curved concave upward (8). Neither the uncorrected Richardson plots nor the "extrapolated" plot show appreciable curvature. In fact, the pre-end-guard uncorrected Richardson line has an excessive downward droop for low temperatures. The downward droop is easily explained; it is merely the consequence of the glass insulator charging and leakage encountered in pre-end-guard operation as discussed in Sec. B.1. A similar downward droop was reported by Nichols on one of his (110) directions (27). The failure to observe concave upward curvature in the final tube plot lies in the small magnitude of the effect. To illustrate the curvature to be anticipated,

---

* It should be noted that an A^{**} value of 120 does not conclusively demonstrate that a surface is not patchy. A balanced contribution of patchiness and work function temperature dependence could "accidentally" produce the value near 120.

several points were calculated for the combination of straight 5.26 volt and 4.42 volt Richardson lines prescribed to add to the "extrapolated" (110) current. The points are plotted as triangles, Δ, along with the experimental extrapolated curve in fig. 23. Calculations were based on a perfect match at $10^4/T$ of 5.3 and 6.2. It is seen that the curvature produces only very small deviation from the straight line in the range of temperature for which data are available.*

Due to the dependence of the secondary emission process upon primary energy, no data significant in the usual sense could be obtained from a Schottky plot by extrapolation procedures. It was found that the voltage dependence of the full-energy spurious contribution to the extrapolated current outweighed that of the "true" (110) current. The "Schottky plot" obtained by extrapolating suppressor characteristics taken at several anode-filament voltages is given in fig. 24. The plot shares the rapid downward trend at low voltages which marked the original un-extrapolated Schottky curves, but for higher voltages it becomes almost constant, implying that there the decline of full-energy secondary current approximately equals the Schottky rise of the true (110) current. Of the two extreme operating conditions suggested by the Schottky plot to give the most favorable ratio of true to spurious current, it was decided to use the low anode-filament voltage. 745 volts was chosen as the lowest voltage regulated potential for which the projection properties of the tube were satisfactory as indicated by Schottky plots for the other directions, and all "extrapolated" (110) Richardson data

---

* Actually, if one were to expect the same small systematic high temperature droop as observed for the other directions, the curvature may account for the (110) values found precisely on the Richardson line.

were derived from suppressor curves taken with this anode voltage. Since no meaningful Schottky slope was available, the theoretical value of 11.2 was used to correct the extrapolated data to zero field values.

To summarize the various apparent thermionic constants with the conditions under which they were obtained, see table VII.

Table VII. Summary of (110) thermionic constants

Description	ϕ^{**}	A^{**}
Nichols (7)	4.68	15
Pre-end-guard, normal operation	4.66	12
Final tube, normal operation	4.58	8.0
Final tube, "extrapolated"	4.72	9.7
Pure spurious current, effective slope	4.42	
Estimate by subtraction of spurious current to give $A^{**} = 120$	5.26	120

D. CONTACT POTENTIALS FROM RETARDING POTENTIAL DATA

In view of the relative ease with which the tube and circuit already described could be modified to permit the taking of retarding potential data from the same measuring tube, it was decided to check the results obtained for the (110), (111), (112), (116), and (001) surfaces by contact potential measurements among them. Although the electron-optics did not prove to be ideal for retarding potential measurements, the results indicate that the data are probably significant.

D.1. Modified Electrical Circuit for Retarding Potentials.

The circuit schematic for the retarding potential measurements is given in fig. 25. The principal change is the operation of the filament at only a few volts from ground (collector potential) putting the anode

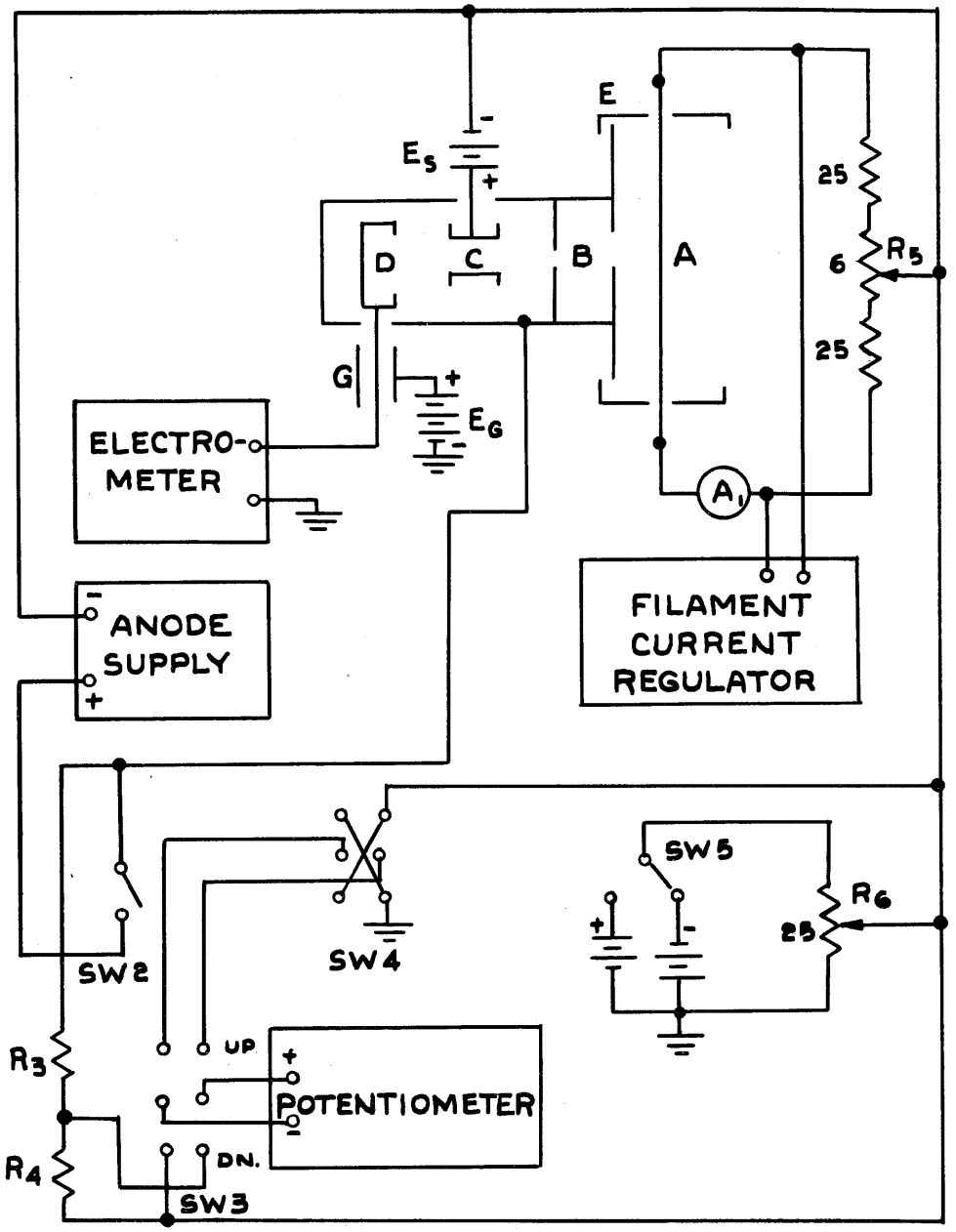

Fig. 25. Modified circuit schematic for retarding potential measurements.

1005 volts positive with respect to ground. The setting of the 25 ohm helipot R_6 and the position of SW5 determine the filament-collector potential, which can be measured by the Type K Potentiometer. Due to the a.c. heating of the crystal wire a balanced return was used to minimize the alternating voltage superimposed upon the filament-collector potential. With the heating current used and proper adjustment of the balancing resistor R_5, the maximum potential deviation of either end of the crystal segment from the potential of the center of the segment amounted to 0.13 volts. For the data to be presented the secondary suppressor electrode C was operated 3 volts positive with respect to the filament. The end-guards EE' were operated $22\frac{1}{2}$ volts negative with respect to the filament, as before. The filament current was measured by the calibrated ammeter A_1. For other details of the circuit, refer to the unmodified schematic, fig. 10.

D.2. Operating Conditions for Retarding Potential Plots.

For a uniform plane cathode in the absence of space charge, the retarding potential characteristic would have an abrupt change in slope at the filament-anode potential corresponding to zero field between the electrodes. In the case of cylindrical geometry, it is well known that the retarding potential curve approaches the same slope asymptotically but is rounded off in the vicinity of the breakpoint, making the discontinuity in slope more difficult to observe. The situation to be found in the use of the thermionic measuring tube for retarding potential data is more complicated. As has been indicated in the previous paragraph, the projection properties of the tube are maintained by drawing current

under high field conditions; the retarding field is then imposed between the slits SS' and the collector D. Hence both the accelerating and the subsequent retarding potential fields are curved, the latter in a rather complex fashion, making a situation difficult to analyze analytically but certainly not "plane parallel" in nature. A retarding potential curve taken under what are believed to be optimum conditions with also a minimum of rounding due to other causes is that for the 55° (112) surface, shown in fig. 26.

As might be expected, there is no completely satisfactory operating point for the suppressor electrode C. The value used, 3 volts positive with respect to the filament, gave a maximum of collected current when operating well saturated; the actual value of the collected current amounted to only 60 percent of the total slit current as obtained from Richardson plot data, the remainder being lost due to either defocussing or secondary emission.* However, selected runs with the suppressor electrode: (a) 3 volts positive with respect to the filament, (b) at the collector potential, and (c) minus $1\frac{1}{2}$ volts with respect to the collector, gave exactly the same contact potential results, indicating that although the suppressor potential may considerably influence the fraction of slit current arriving at the collector, its influence on contact potential measurement is small.

All retarding potential data were taken at 1990°K.

D.3. Retarding Potential Data.

Retarding potential curves can give two kinds of information: (a) From comparison of the break-points of retarding potential curves

* The secondary emission at these energies should be very small.

taken in two different crystal directions one can obtain the contact potential between the wire surfaces in those two directions. (b) From the shape of the retarding potential curve one can obtain information about the patch nature of the surface. Patchiness produces a breaking away from the corner of the ideal retarding potential curve, see Sections II.6, II.11, and figure 18 of reference 8. Unfortunately the departure from plane parallel geometry discussed above also causes a rounding off of the corner, making the observation of patch effects more difficult. The retarding potential for the 55° (112) direction, for which there is some evidence of a uniform nature, is given in fig. 26. In addition to the visual evidence and evidence from polar plot, Shottky plot, and Richardson data, this retarding potential curve shows the least rounding near the breakpoint, of all the retarding potential curves taken, although its shape is only slightly different from most of the others. In view of the shape of the curve obtained, it is clear that the alternating voltage superimposed upon the filament-collector potential does not make a large contribution to the rounding. A discussion of the contribution of patchiness to the rounding will be given in Section D.4.b.

It should be pointed out that, as opposed to the general case of a retarding potential curve, there will be no anomalous Schottky region separating low field and high field saturation currents in the curves taken with this measuring tube. This results from the fact that the emission is drawn from the filament under high field conditions before the retarding field is applied. Hence the only saturation value observed will be the high field saturation, if indeed the cathode is patchy.

The temperature calculated from the slope of the 55° (112) curve, fig. 26, is 2090°K. as compared with the measured value 1990°K. from the Forsythe-Watson temperature scale. As can be seen from fig. 26, the curve is very nearly linear for the more retarded potentials.

Heinze and Wagener (36, 8) have analyzed the retarding potential method for a patchy cathode in some detail. Briefly, the method involves taking the location of the retarding potential breakpoint as the intersection of the tangent to the retarding potential curve and the tangent to the saturated emission curve. Following the notation of Herring and Nichols (8) and neglecting reflection effects, the intersection point is given by:

$$V = \tilde{\phi} - \phi_A \qquad (D.1)$$

where ϕ_A is the work function of the assumed uniform collector* and ϕ is a mean work function for the cathode defined so that:

$$j_o = AT^2 \exp(-e\tilde{\phi}/kT) \qquad (D.2)$$

From eqs. (D.2) and (C.8), again neglecting reflection, we see that:

$$\tilde{\phi} = \frac{kT}{e} \ln\left[\frac{1}{\sum_i f_i \exp(-e\phi_i/kT)}\right] \qquad (D.3)$$

---

* Although the collector is undoubtedly patchy in nature, all measurements are comparative and hence no advantage accrues from attempting to correct ϕ_A since it cancels out in each case.

And in terms of the apparent work function ϕ^{**} (eq. C.9) we have the relation:

$$\phi^{**} = \tilde{\phi} - T \frac{d\tilde{\phi}}{dT} \tag{D.4}$$

If breakpoints are established for two different directions of the single crystal by the intersection of tangents method, one obtains from eq. (D.1) that:

$$V_2 - V_1 = \tilde{\phi}_2 - \tilde{\phi}_1 \tag{D.5}$$

$$= \phi_2^{**} - \phi_1^{**} + T\left(\frac{d\tilde{\phi}_2}{dT} - \frac{d\tilde{\phi}_1}{dT}\right) \tag{D.6}$$

Or, if $\tilde{\phi}_1$ and $\tilde{\phi}_2$ have only a very small difference in temperature dependence:

$$V_2 - V_1 = \phi_2^{**} - \phi_1^{**} \tag{D.7}$$

Hence if $\tilde{\phi}$ has essentially the same temperature dependence for different crystal directions,* one should obtain the same set of work function differences from the contact potential data as are obtained by differencing the Richardson plot apparent work functions.

In view of the similar shapes of the retarding potential curves for the various surfaces, it was decided to accomplish the intersection of tangents method together with the subtraction of the two breakpoints by superimposing one upon the other, matching saturation currents, and sliding horizontally until the best match is achieved for the more

---

* This cannot be justified in the presence of patches, as will be discussed in the next section.

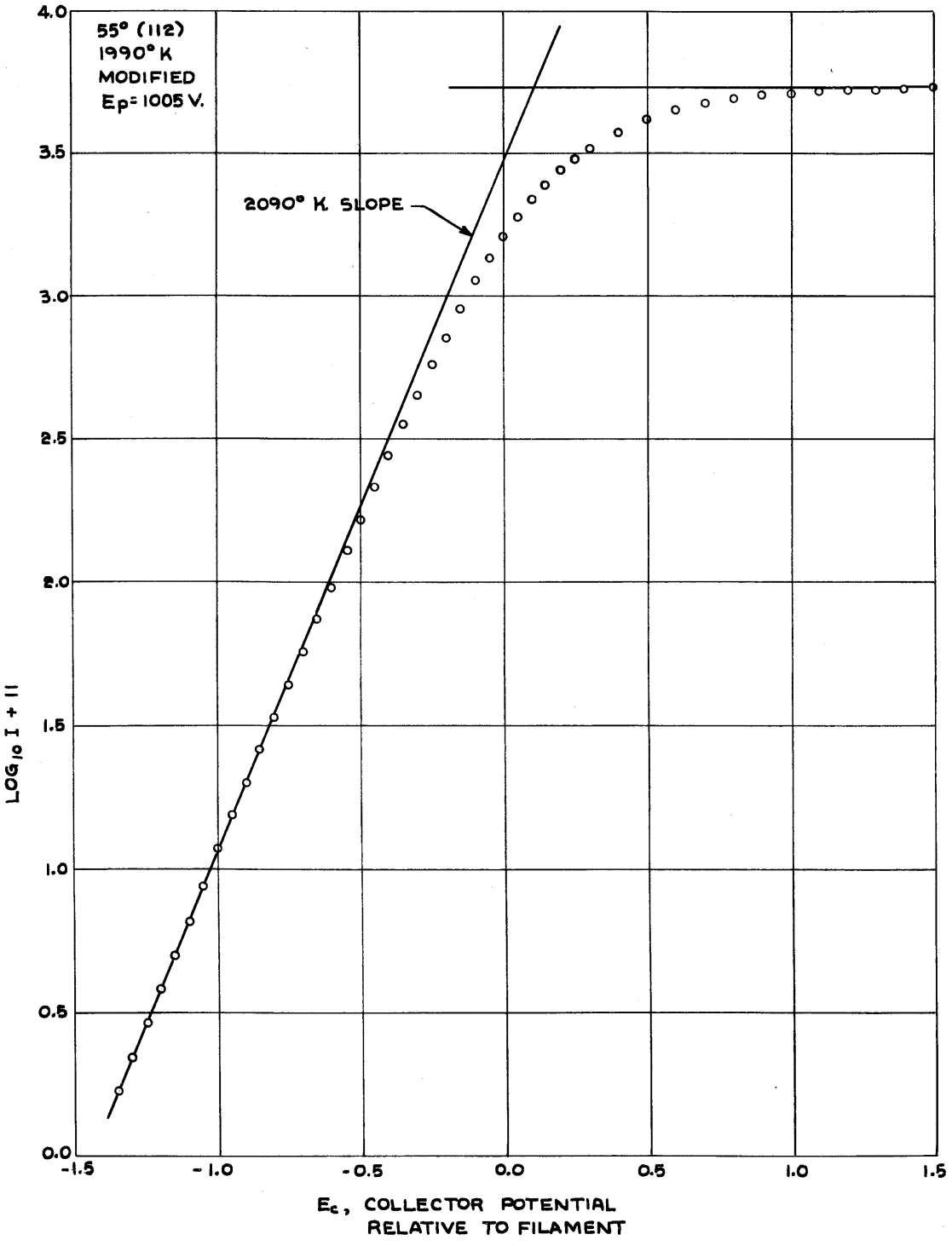

Fig. 26. Retarding potential curve for 55° (112) direction. This curve shows a minimum of rounding and is taken as standard for comparison with those of other directions.

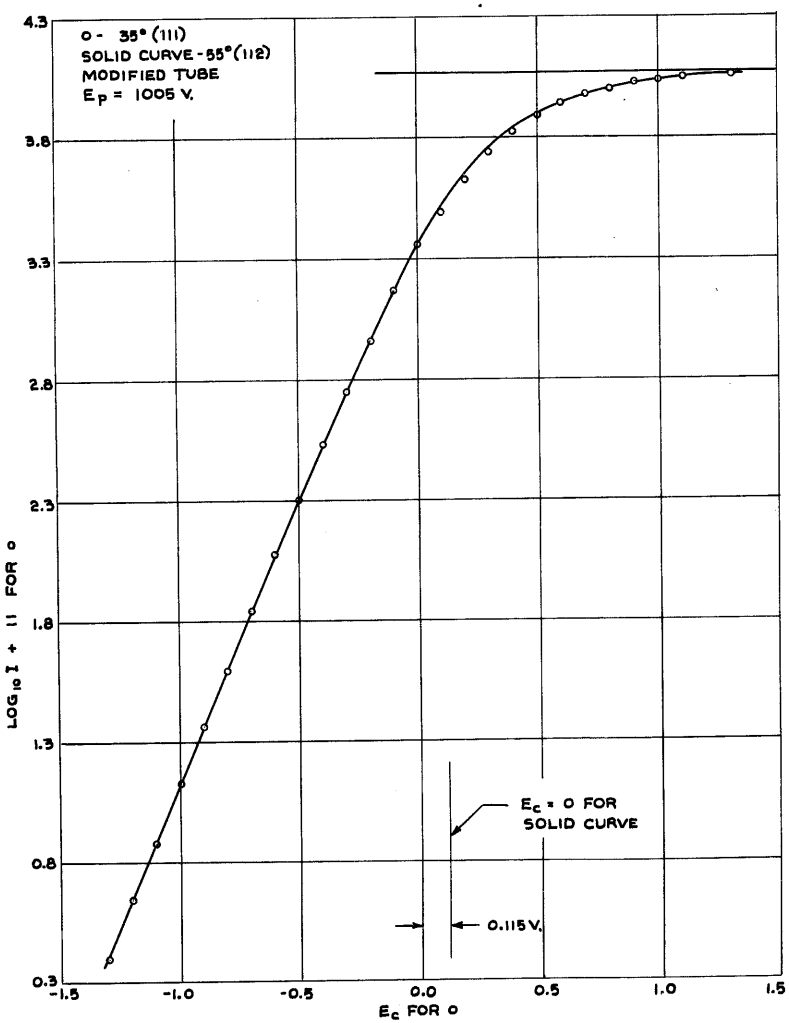

(a)

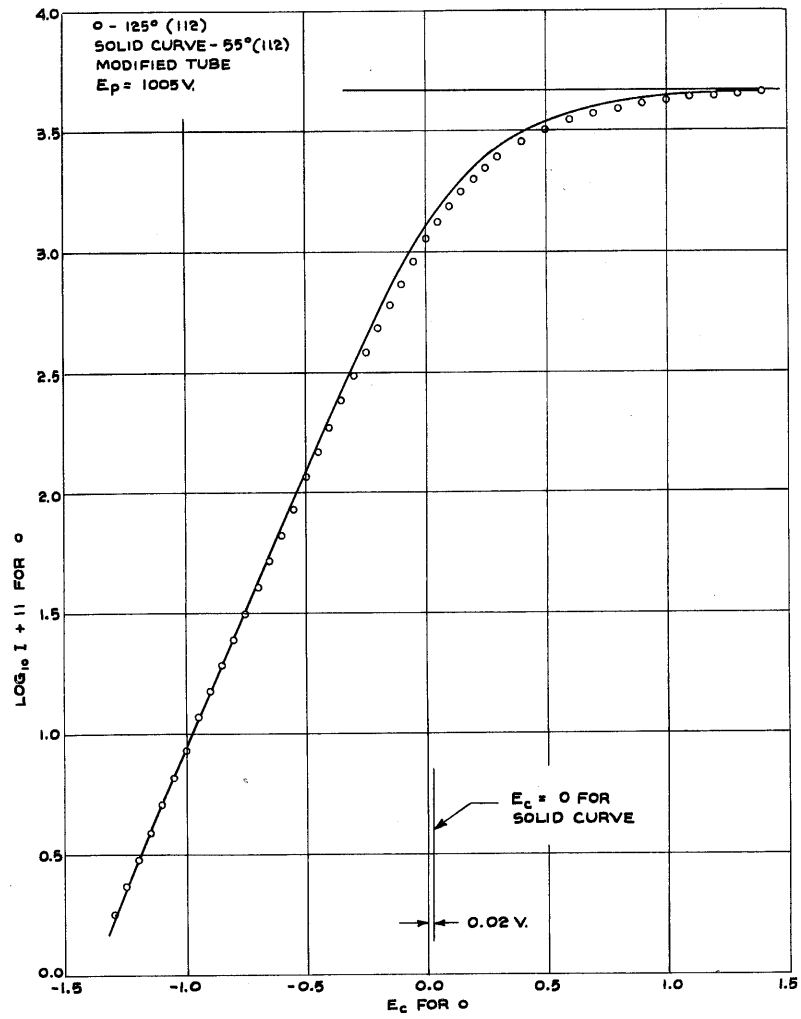

(b)

Fig. 27. Contact potentials between representative surfaces and the standard 55° (112) surface by superposition of retarding potential curves. In each case the curve of fig. 26 is drawn smooth with the data of the superposed surface circled in.

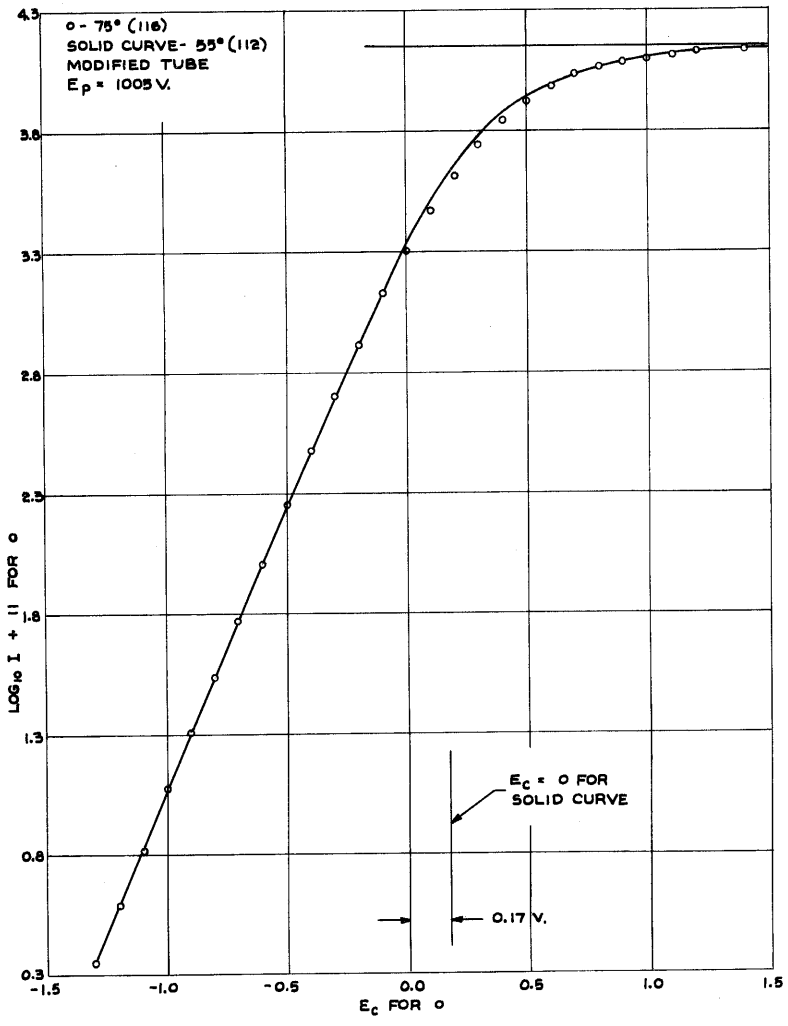

(c)

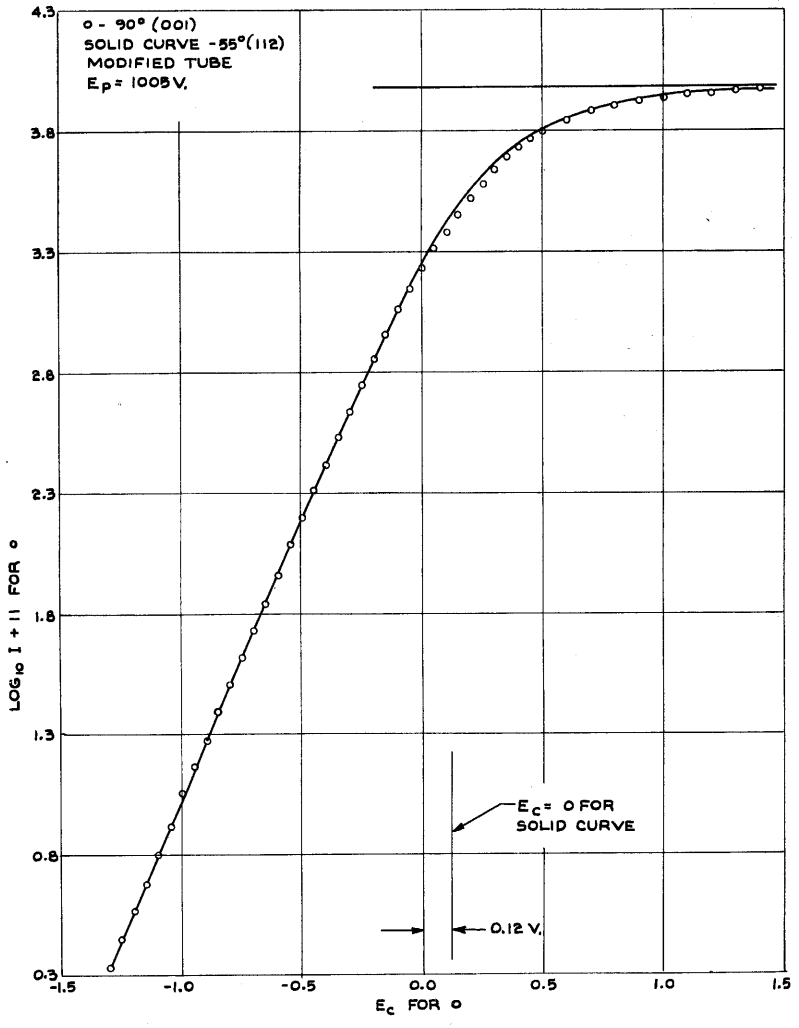

(d)

Fig. 27. (Continued)

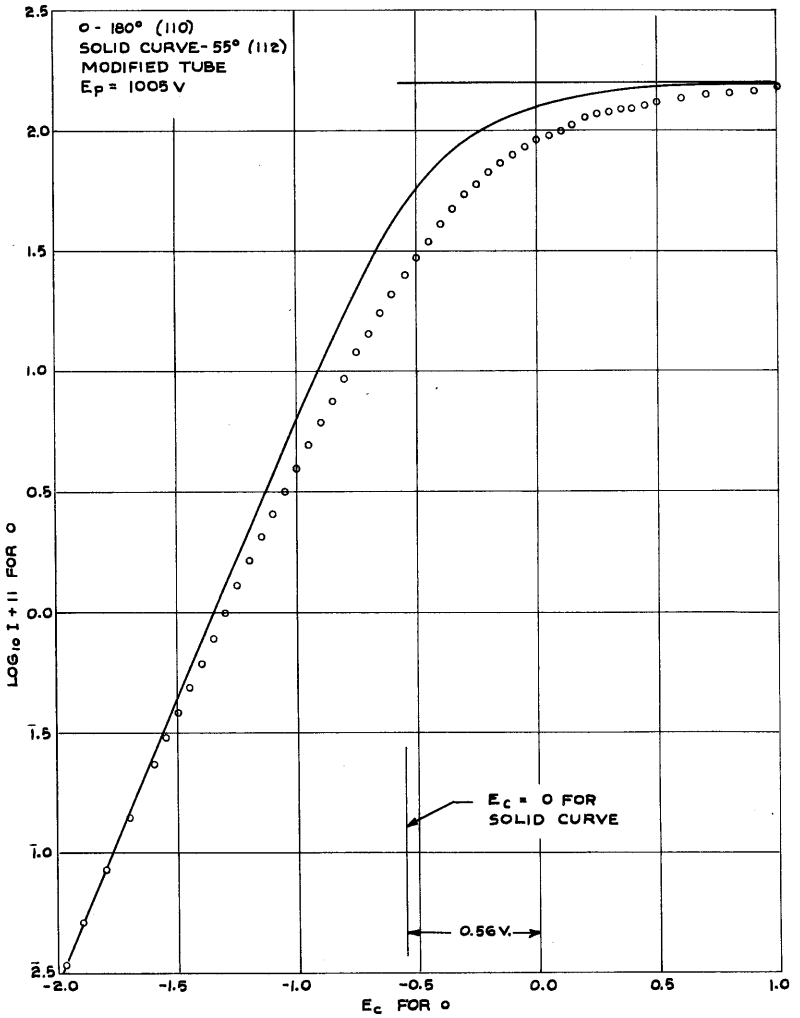

(e)

Fig. 27. (Concluded)

Table VIII. Contact potentials between each direction "x", and the standard 55° (112) direction "s", from retarding potential plots at 1990°K. Corresponding apparent work function differences are also tabulated. Differences in $d\tilde{\phi}/dt$ are then obtained. Assuming uniform surfaces and no temperature dependence for the standard surface, adjusted emission constants A are obtained for all surfaces from their apparent emission constants A**.

DIRECTION	CONTACT POTENTIAL $\tilde{\phi}_s - \tilde{\phi}_x$	$\phi_s^{**} - \phi_x^{**}$	$d\tilde{\phi}_x/dT - d\tilde{\phi}_s/dT$ volts/deg.	A value	
				Apparent	Adjusted
35° (111)	0.115	0.26	$+ 7.3 \times 10^{-5}$	53.6	126
145° (111)	0.13	0.28	7.5	46.5	112
215° (111)	0.13	0.27	7.0	53.8	123
55° (112)	--	--	--	118	
125° (112)	0.02	0.01	--	110	
235° (112)	0.005	0.005	--	133	
75° (116)	0.17	0.35	9.0	39.9	116
105° (116)	0.18	0.36	9.0	39.9	116
90° (001)	0.12	0.13	0.5	105	111
180° (110)	0.56				

retarded region of the curves. The data are all presented in comparison with the 55° (112) surface which is drawn in without points on each figure. The points for the surface under comparison are then circled in, showing the match for the given contact potential and permitting comparison of shapes of the two curves. Comparison is made for one each of the (111), (112), (116), (001), and (110) surfaces in figures 27a to 27e. The contact potential, $\tilde{\phi}_s - \tilde{\phi}_x$, between each surface and the standard 55° (112) surface is tabulated in the second column of table VIII. For comparison, the difference of apparent work function, $\phi^{**}_s - \phi^{**}_x$, between each surface and the standard 55° (112) surface is tabulated in the third column of the table. It should be noted that the work functions involved in the contact potential measurements have not actually been extrapolated to zero field conditions, but each stands lowered by a Schottky term due to the high field condition preceding the retarding field. Since this term is small and constant to one figure at 0.08 volts (see table V), it cancels out from the contact potential measurements.

D.4. Comparison of Contact Potentials with Apparent Work Function Differences; Temperature Dependence of Work Function.

As indicated by eq. (D.6), if there is no significant difference in temperature dependence of $\tilde{\phi}$ among various surfaces of the crystal, one would expect agreement between the contact potentials and the apparent work function differences. Aside from agreement among different surfaces having the same Miller indices, there is agreement in one other

instance, namely between the (112) and the (001) surfaces. Although this does not imply that there is no temperature dependence of $\tilde{\phi}$ for these two surfaces, it does imply that there is little difference in the temperature dependence. It will be recalled that these two surfaces have two other similarities: both have a plateau structure visible under a microscope, and both have apparent emission constants near 120.

Temperature dependence must be responsible for the lack of agreement among all other combinations of surfaces. Indeed, from eq. (D.6) one may compute values of $(d\tilde{\phi}_2/dT - d\tilde{\phi}_1/dT)$. This quantity is tabulated for each surface in comparison with the 55° (112) surface in column four of table VIII. As can be seen from eq. (D.3), in general $\tilde{\phi}$ will be a temperature dependent mean depending primarily upon (a) the temperature dependence of the ϕ_i and (b) the difference in fractional contribution at different temperatures to the total emission by the different work function patches. The latter temperature dependence arises from the mere existence of more than one contributing patch, even though the patches themselves might have no temperature dependence in their ϕ_i. It will be assumed that the f_i are not temperature dependent. Although there is not sufficient experimental information to permit a meaningful analysis of the general case of a patchy surface with temperature dependent ϕ_i, there is reason to believe that the actual case for the tungsten crystal may not be that complicated. The evidence from visual observation, polar emission plot, Schottky plot, and Richardson data, as well as the shape of the retarding potential plot, makes it probable that the (112) and (001) surfaces are uniform and have essentially temperature independent work functions as well (by eq. (C.7),

if they are uniform surfaces, their A** values near 120 indicate little work function temperature dependence).* For the (111) and (116) directions one can plausibly explain the experimental data by either (a) assuming uniform (111) and (116) surfaces with temperature dependent work functions, or (b) assuming patchy (111) and (116) surfaces with temperature independent patch work functions. The (110) direction will not be included in the discussion because of the complicating effects of the secondary emission spurious current associated with the (110) emission.**

D.4.a. Assumption of Uniform Surfaces with Temperature Dependent Work Functions.

To describe the emission, assuming uniform surfaces, one need only replace ϕ^{**} by ϕ^{*} and $\tilde{\phi}$ by ϕ in eqs. (D.1) to (D.7). It is seen (eq. D.5) that the contact potential then gives the difference in actual work functions, while the apparent work function of the uniform surface includes only the temperature independent part if we neglect terms of quadratic

---

* It is conceivable that the right combination of patchiness (to lower A**) and negative work function temperature derivative (to raise A**) would accidentally produce an A** $\cong$ 120.

** Although it has been shown in Sec. C that the collected current in the (110) direction consists of the sum of a "true" (110) current and a spurious current arising from the secondary emission trouble of the measuring tube, a contact potential comparison is given with the 55° (112) direction in fig. 27e. The value obtained for the contact potential, 0.56 volts, would place the work function of the (110) surface at 4.65 + 0.56 = 5.21 volts, in remarkable agreement with the value 5.26 volts estimated apparent work function of Sec. C.4. Since little is known about the exact energy distribution of the secondaries arriving under retarding potential conditions, one should not attach too much significance to this result.

and higher order in T (see eq. D.4 or D.7). In any event, the values of column four, table VIII, then become values of $(d\phi_x/dT - d\phi_s/dT)$. But if $A^{**}_{(112)}$ is assumed to be characteristic of a uniform surface, ϕ_s is temperature independent; hence the values of column four are essentially absolute temperature derivatives of the work functions for the surfaces. Finally, from eq. (C.7) one can obtain an adjusted emission constant A from the known values of $d\phi/dT$ and A^{**}. Adjusted values are tabulated in the last column of table VIII; all lie within experimental error of 120 amp/cm^2/deg^2. So it is seen that in each case the same value of the temperature derivative associated with a surface can account for the disagreement of contact potential and apparent work function difference, and can simultaneously account for the departure of the apparent emission constant from 120.

Since all other contributions to the temperature derivative of ϕ are body functions, the differences in $d\phi/dT$ between different crystal directions must be attributed to a temperature derivative of the double layer. Herring and Nichols (8) estimate that the double layer contribution to $d\phi/dT$ is "probably negative and not more than a fraction of k." The uniform surface hypothesis calls for a double layer contribution of at least 9.0×10^{-5} volts per degree, since differences among the $d\phi/dT$ for different crystal directions are that large. Since $k = 8.6 \times 10^{-5}$ volts per degree, the double layer contribution required is not in too great disagreement with their estimate.

It might be noted that if the (112) surface <u>does</u> have a very small $d\phi/dT$, due to fairly precise cancellation of all contributions (including the relatively large body contributions) to the temperature derivative,

only the double layer derivative can contribute to the net temperature dependence of <u>any patch</u> to be found on a tungsten crystal. This implies that the net temperature dependence of the work function for polycrystalline tungsten must come exclusively from double layer differences. Potter's result (37) for the temperature dependence of the polycrystalline work function, plus 5×10^{-5} volts/deg*, is consistent with the results of table VIII.

It might be mentioned that investigators of field emission from tungsten points (Becker (14), Dyke (15), Müller (13), Nottingham (38)) find values of work function in fairly good agreement with the <u>apparent</u> work functions obtained here. This is not in contradiction with the set of work functions obtained by contact potential measurements under the uniform surface assumption, since measurements of field emission are usually conducted near room temperature. If one assumes the temperature dependence to be linear, ϕ at room temperature will be close to the temperature independent part, or its equivalent in this case, the apparent work function.

D.4.b. Assumption of Patchy Surfaces with Temperature Independent Patch Work Functions.

From eq. (D.3) it can be seen that $\tilde{\phi}$ for a patchy surface is a function of T even if the ϕ_i are temperature independent. In the previous section it was assumed that the surfaces considered were uniform but had temperature dependent work functions which accounted for the

---

* As corrected by Herring, see reference 8.

$d\tilde{\phi}/dT$ and A** experimentally observed to be different from zero and 120 respectively. It was shown that this assumption required the temperature derivative of ϕ due to the double layer to be of the order of k, while the estimate of Herring and Nichols (8) indicates that it is not more than a fraction of k. Hence another plausible explanation can be made on the assumption that any patch to be found on the crystal surface will have a negligible work function temperature dependence. If there is not sufficient evidence to rule out patchiness in the (111) and (116) directions, that patchiness may be responsible for the observed values of $d\tilde{\phi}/dT$ and A** in those directions.

An attempt will be made here to choose patches (each with A* = 120) to explain the experimental data. Due to the indeterminacy of choice among a larger number of patches, only two-patch surfaces will be considered. Although a patchy surface will not likely consist of just two patches, it is felt that the principal features of behaviour will be essentially the same as in the simplified case. It is clear that the choice of patches must satisfy two sets of conditions: the observed apparent emission constants ϕ** and A** must be obtained; and the correct value of $d\tilde{\phi}/dT$ must be given. Herring and Nichols have calculated apparent emission constants for two-patch surfaces in fig. 12 of reference 8. For given values of ϕ** and A** it is seen that a certain latitude in selection of patches is allowed, permitting a choice to give the experimentally observed value of $d\tilde{\phi}/dT$.

To describe the temperature dependence, $d\tilde{\phi}/dT$, of a patchy surface with temperature independent patch work functions, one need only take the derivative of eq. (D.3); arranged for convenience in computation,

this derivative is given by:

$$\frac{d\tilde{\phi}}{dT} = \frac{\phi_1}{T} + \frac{k}{e} \ln \frac{1}{\sum_i f_i \exp(-e\,\delta\phi_i/kT)} - \frac{1}{T} \frac{\sum_i \phi_i f_i \exp(-e\delta\phi_i/kT)}{\sum_i f_i \exp(-e\delta\phi_i/kT)} \quad (D.8)$$

where f_i is the fraction of the surface occupied by the ith type of patch, and $\delta\phi_i = \phi_i - \phi_1$. Of course, the differences of $d\tilde{\phi}/dT$ can also be obtained by constructing a retarding potential curve for the particular choice of patches, and finding the contact potential between the constructed curve and the curve for a uniform surface. Putting this contact potential, together with the value of ϕ^{**}, into eq. (D.6), one can obtain the temperature derivative in the same way as were the experimental values of column 4 of table VIII. Since it was desired to observe the degree of falling away from the break-point associated with the two-patch surfaces, the retarding potential curves for the constructed surfaces were plotted. For this purpose, the experimental 55° (112) curve of fig. 26 was used as typical of a uniform surface of work function 4.65 volts, and proper proportions of current calculated from two such curves, properly displaced in abscissae, were added to obtain a retarding potential curve for each of the calculated two-patch surfaces. Values of $d\tilde{\phi}/dT$ from these retarding potential plots were checked in a few cases by calculating $d\tilde{\phi}/dT$ from eq. (D.8). The agreement was sufficiently good that in general only the graphical method was used. In order to permit comparison with the experimental retarding potential curves of fig. 27 calculations were made for two-patch surfaces to match the 35° (111) for which $\phi^{**} = 4.39$, $A^{**} = 54$, and the 75° (116) for which $\phi^{**} = 4.30$, $A^{**} = 40$. In the following, $\delta\phi$ will refer to the difference in work function of the two patches, f will denote the frac-

tion of surface made up by the patch of lower work function ϕ_1, and $\delta\phi^{**} \equiv \phi^{**} - \phi_1$.

It is seen from fig. 12 of reference 8 that, in order to obtain a value of A** = 54 to match the (111) surface, a $\delta\phi \geq 0.35$ volts is required. Calculations were made for $\delta\phi$ of 0.4, 0.6, and 1.0. For each $\delta\phi$ there are two values of f giving A** = 54, but except in the case of $\delta\phi = 0.4$, the lower value would give much too high a value of $d\tilde{\phi}/dT$ (and incidentally would produce considerable curvature of the Richardson plot). Having the value of f, one can then obtain from fig. 12, reference 8, the $\delta\phi^{**}$, and thus the ϕ_1 and ϕ_2 for the two-patch surface. Finally, a retarding potential curve is calculated for the particular combination of patches. Comparison with the standard 55° (112) retarding potential curve then gives the contact potential and $d\tilde{\phi}/dT$ for the patchy surface. The numerical values obtained are given in table IX.

Table IX. Two-patch surfaces approximating the 35° (111).

$\delta\phi$	f	$\delta\phi^{**}$	ϕ_1	ϕ_2	C. Potential $\tilde{\phi}_s - \tilde{\phi}_p$	$d\tilde{\phi}/dT$	Graphed
0.4	0.1	0.09	4.30	4.70	0.07	9.6×10^{-5} v/°	+
0.4	0.27	0.033	4.36	4.76	0.11	7.5	0
0.6	0.4	0.01	4.38	4.98	0.14	6.0	△
1.0	0.45	0.00	4.39	5.39	0.16	5.0	□

The second patch combination gives a temperature derivative very nearly that of the experimental 35° (111) curve, which was 7.3×10^{-5} v/°. The retarding potential curve for each of the two-patch combinations is compared with the standard 55° (112) curve in fig. 28a.

Similar calculations were made for the 75° (116) surface. In this case, in order to obtain a value of A** = 40, a $\delta\phi \geq 0.4$ is required. Calculations were made for the higher value of f for $\delta\phi$ of 0.4, 0.6, and 1.0. The numerical values obtained are given in table X.

Table X. Two-patch surfaces approximating the 75° (116).

$\delta\phi$	f	ϕ^{**}	ϕ_1	ϕ_2	C. Potential $\tilde{\phi}_s - \tilde{\phi}_p$	$d\tilde{\phi}_p/dT$	Graphed
0.4	0.1	0.09	4.21	4.61	0.15	10.0×10^{-5} v/°	+
0.6	0.27	0.015	4.29	4.89	0.16	9.5	0
1.0	0.33	0.002	4.30	5.30	0.20	7.5	△

The second patch combination gives a temperature derivative very nearly that of the experimental 75° (116) curve, which was 9.0×10^{-5} v/°. The retarding potential curve for each of the two-patch combinations is compared with the standard 55° (112) curve in fig. 28b.

It is seen that the experimental values for both A** and $d\tilde{\phi}/dT$ can be obtained without much difficulty by proper choice of two-patch surfaces, taking the patch work functions to be temperature independent. Figures 28a and 28b of the two-patch retarding potential curves do show a significantly larger falling-off in the vicinity of the breakpoint than do the experimental curves of fig. 27a and 27c. Indeed, of the whole set of experimental curves*, only that for the 235° (112), given in fig. 29, shows a rounding-off as large as those for the two-patch curves.** However, it is not certain that a proper distribution of a

---

* Excluding the (110) direction, as has been done throughout this section.

** It is suspected that the 235° (112) surface examined includes one or more crystal "lakes" of the kind mentioned in Part I, giving a large scale patchiness, since the Schottky plot for the surface showed no indication of fine scale patchiness. The polar plots of fig. 18 show more emission from this direction than from the other (112) directions; this would not be unexpected if the surface were patchy. The higher A** value

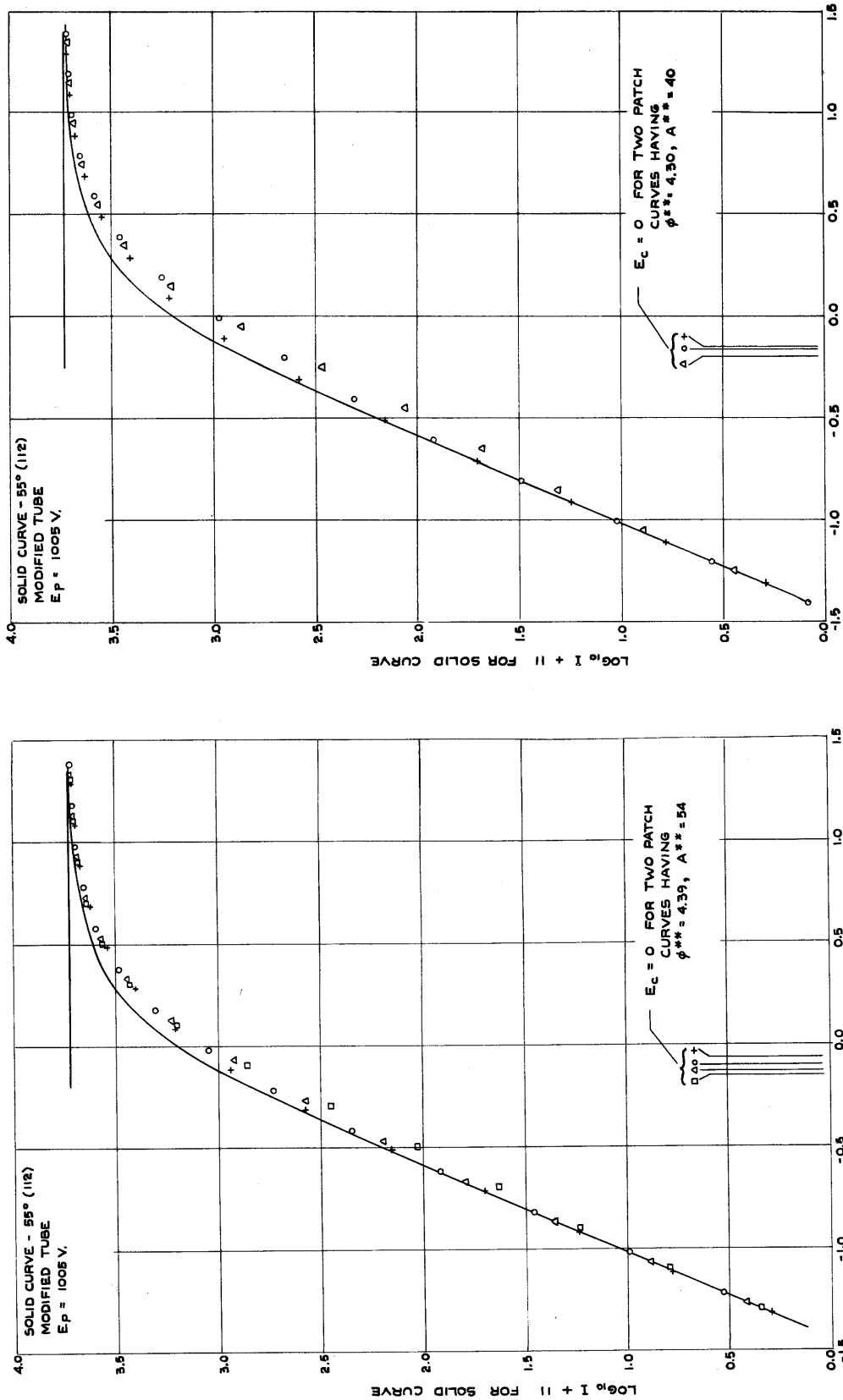

Fig. 28a. Two-patch retarding potential curves, temperature independent patches chosen to give $\phi^{**} = 4.39$, $A^{**} = 54$, as observed for the 35° (111) direction. Patch specifications given in table IX.

Fig. 28b. Two-patch retarding potential curves, temperature independent patches chosen to give $\phi^{**} = 4.30$, $A^{**} = 40$, as observed for the 75° (116) direction. Patch specifications given in table X.

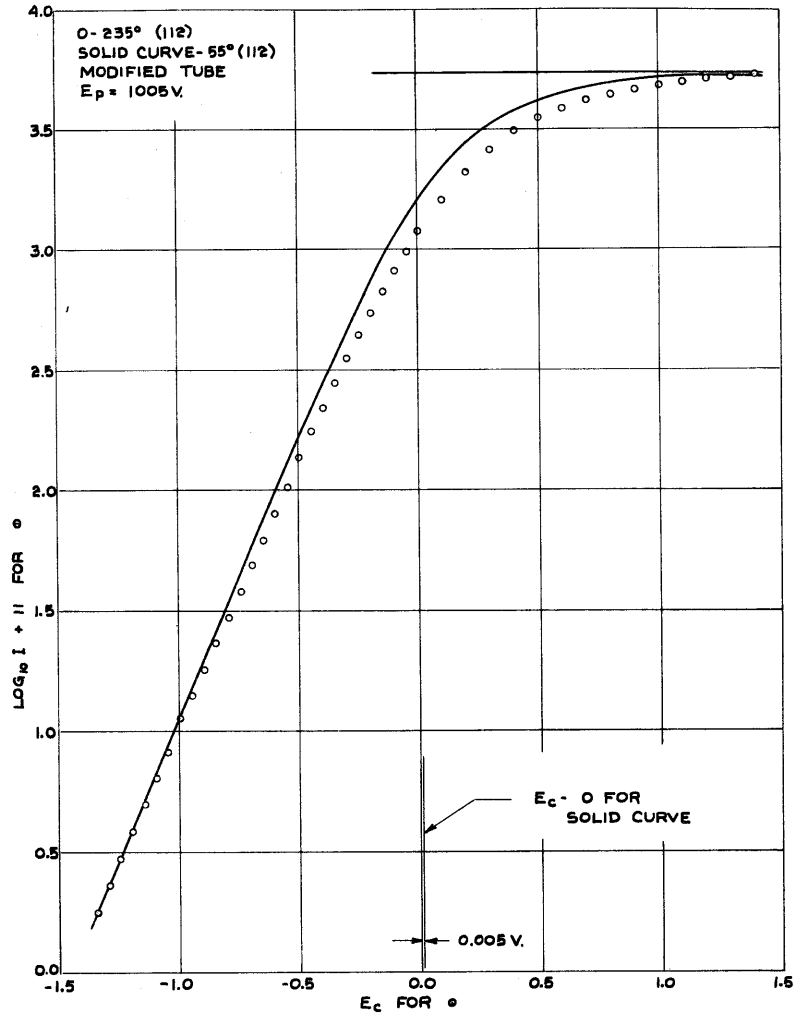

Fig. 29. Contact potential between the 235° (112) surface and the standard 55° (112) surface by superposition of retarding potential curves. This curve shows the largest falling-away observed among the surfaces measured (excluding the (110)), definitely indicating a patchy nature.

larger number of patches might not give the prescribed apparent emission constants and temperature derivative, and at the same time have a smaller departure in form from the uniform surface retarding potential curve. If one is not able to rule out patchiness of the (111) and (116) surfaces by other considerations, the fact that the experimental (111) and (116) retarding potential curves show less breaking away than do the constructed two-patch curves can hardly be considered as conclusive evidence that the (111) and (116) wire surfaces are not patchy.

Retarding potential curves taken with more favorable geometry in a tube designed for the purpose should be able to more clearly distinguish the presence or absence of a patchiness sufficient to account for the A** and $d\tilde{\phi}/dT$ observed in the (111) and (116) directions.

E. CONCLUSIONS TO PART II

To summarize the principal results of the investigation:
(a) Under an optical microscope, structure was observed in the (110), (112), and (001) directions (see Part I). This structure consisted of very faint shingling (minimized but not eliminated by choice of crystal) superimposed upon a "plateau" in each of these directions. Since the crystal investigated was always heated by alternating current, there was no evidence of "d.c. etch." Although the (110) shingling was less pronounced than the similar structure on a crystal investigated by Nichols (7), and although the structure on the (112) and (001) surfaces was not observed by Nichols, there was good agreement of observed emission data in all cases. It is believed that the structure visible in the three

---

of 133 for the 235° (112) direction is inconsistent with patchiness; as has been stated, however, the precision of A** values is about 10 percent.

directions does not indicate significant patchiness in those directions, other than the large scale patchiness due to exposure of different crystal directions by a single cylindrical crystal.

(b) In addition to showing the usual symmetric pattern, the polar plots of thermionic emission indicated the presence of "flats" of emission in the vicinity of the (110), (112), and (001) directions. These flats substantiate the visual observation of plateaus in those directions.

(c) Schottky plots for all principal directions except the (110), for which meaningful data were not available, failed to show departure from the mirror image Schottky line for field gradients down to 26,000 volts/cm. Since the single crystal itself would be expected to show tangential "patch" fields of the order of several hundred volts/cm, particularly near the minima of emission, there is no evidence of patchiness of smaller dimension than the spacing of the different crystal directions. Periodic deviations from the Schottky line for the different crystal directions were observed but not studied.

(d) Richardson plots for the directions giving maxima and minima of emission yielded apparent emission constants in good agreement with those reported by Nichols (7) in all directions but the (110). No curvature due to patchiness was observed in any direction.

(e) Anomalous behaviour of the measuring tube, the same tube as used by Nichols, was found to be responsible for the data obtained under normal operating conditions in the (110) direction. This anomalous behaviour accounts for both the departure from the Schottky line and the low emission constant, A**, reported by Nichols for the (110) direction and previously held to be indicative of a patchy surface. By partial

correction of this behaviour an upper limit to the true (110) emission was obtained, characterized by the apparent emission constants: $\phi^{**} = 4.72$, $A^{**} = 9.7$. By assuming that the departure of A** from 120 is entirely due to the anomalous behaviour, a completely corrected estimate of 5.26 volts was obtained for the (110) apparent work function.

(f) Except in the (112) and (001) directions, contact potentials, determined by comparing retarding potential curves taken in the different directions, failed to agree with apparent work function differences. This indicates a temperature dependence of the mean work function $\tilde{\phi}$ (as defined in reference 8) associated with the retarding potential curve, a temperature dependence which must vary from surface to surface over the single crystal. Retarding potential curves for the (111), (112), (116) and (001) directions have shapes not sufficiently different to establish that any of them are patchy in nature. However, among all of the curves, the 55° (112) direction has the sharpest breakpoint.

It has already been suggested by Herring and Nichols (8) that the (112) and (001) surfaces may be uniform and have practically no temperature dependence of their work functions. Evidence to this effect is the absence of indication of patchiness, and A** values near 120. The present investigation supports this evidence. Two reasonable hypotheses, each based on a uniform (112) surface with temperature independent work function are proposed to explain the observed temperature dependence of $\tilde{\phi}$ for the (111) and (116) directions: (a) assuming uniform surfaces with temperature dependent work functions, and (b) assuming patchy surfaces with temperature independent patch work functions.

When the observed temperature derivatives $d\tilde{\phi}/dT$ are used, under hypothesis (a), to adjust the observed A** values, the results lie within experimental error of 120 for all of the surfaces. Thus the first hypothesis offers a consistent explanation of all the data. However, the second hypothesis can also provide a consistent explanation, for two-patch surfaces are demonstrated which have both the apparent emission constants and the $d\tilde{\phi}/dT$ observed for the (111) and (116) directions. Although the two-patch surface retarding potential curves fall away at the breakpoint more than do the experimental (111) and (116) curves, it is not certain that an actual patch distribution might not give a smaller change in shape. Hence, unless it is felt that there is other sufficient evidence to preclude patchiness in the (111) and (116) directions, the second hypothesis must be admitted as satisfactory. Further work with a more suitable tube designed especially for contact potential measurements should give more information regarding the actual patch nature of the surfaces obtained on a single crystal.

APPENDIX I. History of Single Crystal Wire

Part	Temp. °K.	Duration	Evaporation g/cm²	Diameter cm	Tool	Remarks
0.	--	--	--	0.0127	Mike	Before polishing to remove die-marks.
	2095	15½ hrs	--	0.0111	Mike	Recrystallization in projection tube.
	2410	10 min	0.01×10^{-4}			--
	2610	15½ min	0.29			--
	2820	30 sec	0.13			--
	--	--	--			Projection tube pattern, fig. 1b.
						1st microscopic study of surface.
1.	2610	4 hrs	4.45			2nd projection tube.
	2720	30 min	2.28			--
	2820	10 min	2.58			--
	2915	2 min	1.51			--
	--	--	--			2nd microscopic study.
						Repolish wire to remove structure
2.	2940	3 sec	--	0.0110	Mike	--
	2985	2 sec	--			--
	2760	340 min	43.2			--
	2990	10 min	16.1			--
	--	--	--	0.0108	Weigh ends	3rd microscopic study.
3.	2725	45 min	3.64			1st evacuation, measuring tube.
	2680	120 min	5.40			--
	2750	51 min	5.71			(7 interspersed periods at 1900°K., each about 4 hrs; see Coomes (39).
	--	--	--			(1st tube data taken, temperatures below 2100°K., discarded due poor vacuum.

Part	Temp. °K.	Duration	Evaporation g/cm^2	Diameter cm	Tool	Remarks
3.	2820	4 min	1.06×10^{-4}			--
(cont.)	2850	1 min	0.36			--
	--	--	--			4th microscopic study; observe (112), (001) plateaus.
4.	2575	32 min	0.37			2nd evacuation, measuring tube.
	2775	$1\frac{1}{2}$ min }	5.45			3rd evacuation, measuring tube.
	2775	$33\frac{1}{2}$ min }				4th evacuation, measuring tube.
	--	--	--	0.010727	0.61 percent evap. to next value	Pre-end-guard data taken, temperatures below 2100°K.
5.	2785	$2\frac{1}{4}$ min }	6.70			--
	2785	$36\frac{1}{4}$ min }				5th evacuation, measuring tube.
	--	--	--	0.010662	0.25 percent evap. to next value	Final tube data taken, temperatures below 2100°K.
6.	3030	1 min	2.48			--
	2800	5 sec	0.02			--
	--	--	--	0.010635 ± 0.00002	Interferometer	Photomicrographs of surface structure

The history lists all treatment involving temperatures above 2100°K. Each of the principal data-taking periods (at temperatures below 2100°K.) is located in the schedule. The basic temperature scale used was the Forsythe and Watson scale, reference 23. The range of history covered by each value of diameter is indicated in the diameter column. Parts 1 and 2 of the history correspond with the heat treatment of tables I and II of the text.

The amount of evaporation associated with each item was calculated by use of the Jones and Langmuir tables, reference 12. Using their value for the density of tungsten given by the relation between wire weight and diameter, $d = 0.008112 \sqrt{w}$ (d in cm, w in mg/cm), one can easily calculate the corresponding increment in diameter for each amount of evaporation. This method was used to arrive at both final tube, and pre-end-guard tube diameters; corrections to the interferometer value were 0.25 and 0.86 percent respectively. Since these corrections are of the order of magnitude of the uncertainty in the interferometer measurement, 0.2 percent, no appreciable error is introduced by their use. However, from comparison with other methods of measuring the diameter, relatively accurate when larger amounts of tungsten have been evaporated, it appears that in general the evaporation calculations give values too large. For example, the total diameter reduction obtained by evaporation calculations using the data of parts 3,4,5, and 6 amounts to 3.0 percent, whereas a difference of only 1.7 percent is found between the weighed value and the interferometer value. Hence, of the two sets of reported data, the final set has slightly more reliable temperature measurements than the pre-end-guard set, which may be based on a wire

diameter a few tenths of a percent high. Temperature measurements based upon micrometer diameter determinations are of course subject to greater uncertainty.

APPENDIX II. Details of Evacuation Schedule for Measuring Tube.

1. Tube and trap were baked 3 hrs. at 470°C. using only first stage of Hg pump. Pressure was then about 10^{-5} mm Hg by McLeod gauge.
2. Tube and trap were baked 16 hours at 470°C. using both stages of Hg pump. Pressure was then "sticking" or about 10^{-7} mm Hg.
3. Pumping lead between trap and last stage diffusion pump, as well as McLeod gauge and Hg cut-off leads, was torched by hand; ovens were then removed. Liquid N_2 applied to trap before tube oven removed.
4. Anode assembly was raised to bright yellow heat by R.F. induction 4-1/2 hours. Other parts, except springs, etc., were held at bright red heat.
5. During 4, but with R.F. heating removed, the crystal was heated 7 min. at 2600°K.
6. During 4 both tantalum getters were heated by 1.6 amp. interspersed by 1 min. at 1.8 amp. and 2 min. at 1.9 amp. (by previous experiment it was found that 1.7 amp. produced appreciable evaporation).
7. During 4 the ion gauge was outgassed for one hour by 55 watts of electron bombardment, raising the grid and anode to a bright yellow color. At the conclusion of 4, with both getter and ion gauge hot, McLeod gauge indicated sticking pressure.
8. Rotor was "exercised" by constantly moving it, by external electromagnet, over the entire range of its travel for a total of 34 min.
9. The constriction for "sealing-off" was softened for 16 min. by torch.
10. Rebake of tube and trap 12-1/2 hours at 470°C., as per 2.
11. Torchout as per 3.

12. R.F. induction heating as per 4 for 5 hours.

13. During 12, but with R.F. heating removed, the crystal was heated 30 min. at 2785°K. After this heat treatment, the crystal was maintained at a temperature just visibly hotter than the surrounding anode for the remainder of the outgassing period.

14. During 12 both tantalum getters were heated by 1.7 amp. interspersed by 5 sec. flashes at 2.0, 2.0, 2.12, and 2.15 amp.

15. During 12 the ion gauge was outgassed 2 hours by 55 watts, the later part of this period coinciding with the end of 11.

16. Midway in 12, with R.F. heating removed, the seal-off constriction was softened for 25 minutes by torch.

17. Midway in 12, with R.F. heating removed, the rotor was exercised for 50 min., as per 8.

18. Liquid N_2 was raised to cover new portion of trap; R.F. induction heating was reduced slowly over a period of 30 min., with crystal, getters, ion gauge filaments all hot. Rotor was exercised 10 min.

19. With getters and ion gauge filaments hot, the tube was sealed off from the pumps. 3 ma. grid current was immediately applied to ion gauge to commence pumping action. Pressure in the tube at this time amounted to about 10^{-7} mm of Hg, which under the action of the ion gauge pumping had been reduced to 10^{-8} mm in 5 min., to 1.5×10^{-9} mm within a few hours.

20. One of the getters was heated at 1.8 amp. until, after 6 days, it evaporated sufficient tantalum to burn out.

APPENDIX III. Failure of Projection Properties of Measuring Tube at Low Fields.

In addition to small scale surface patchiness, two other effects can produce departure from the Schottky line at low applied field gradients. These effects are: (a) thermal velocities, and (b) large scale patchiness due to exposure of different crystal surfaces on a cylindrical crystal. It has been seen (sec. C.2.b) that thermal velocities become important for fields of 26,000 volts/cm or lower, since an upward departure from the (112) Schottky line is observed at E_p = 750 volts (fig. 20). Even a large-scale patchiness can produce only a downward departure from the Schottky line taken in the (112) direction, since the tangential patch fields are directed away from the high work function surfaces, and when they become important they will draw the normal (112) emission away from the (112) direction. However, the criterion for significance of either effect is essentially the same. If the current is measured at the center of the 6 degree "flat" in the (112) direction by a slit of 2 degree resolution, a tangential deviation of about 2 degrees in electron trajectories will be required to be significant. In the case of thermal velocities, a 2 degree tangential deviation for trajectories from the adjacent high emission wire patches would bring current into the slits; in the case of large-scale patch fields such a deviation would reduce the current collected through the slits.

(a) Thermal velocities. The effect of thermal energy will be greatest before the electron acquires appreciable energy from the applied radial field. If we assume plane geometry, 26,000 v/cm applied gradient, a tangential velocity corresponding to kT = 0.15 volt (1740°K.) and compute a tangential translation up until the time that the electron has acquired 15 ev from the applied field, we obtain 1.2×10^{-4} cm. For the 0.01 cm wire this amounts to about 1.5° in azimuth. Since this displacement takes place before the electron is more than 10 percent of the wire radius away from the wire the plane geometry is justified, and it is seen that thermal velocities do indeed become significant for applied fields of about 26,000 volts/cm.

(b) Large-scale Patchiness. In the case of cylindrical electrodes, a strip array of patches with strips parallel to the axis of the cylinder can produce a patch field which dies off only inversely with the radial distance from the surface (ref. 8 and chapt. IV of ref. 40). Assuming plane geometry with a patch field of 260 volts/cm extending only one wire radius ($1/2 \times 10^{-2}$cm) beyond the wire, one obtains under an applied field of 26,000 v/cm a tangential translation of $1/2 \times 10^{-4}$cm, or 0.6° in azimuth. It is seen that the tangential fields due to exposure of different crystal directions around the wire become important for only slightly lower applied gradients than 26,000 volts/cm.

REFERENCES

1. C. J. Smithells, Tungsten, 2nd edition (D. Van Nostrand Company, Inc., New York, 1932).

2. C. S. Robinson, J. App. Phys. 13, 647 (1942).

3. M. H. Nichols, Phys. Rev. 78, 158 (1950).

4. S. T. Martin, Phys. Rev. 56, 947 (1939).

5. R. P. Johnson, Phys. Rev. 54, 459 (1938).

6. R. W. Schmidt, Zeits. f. Physik 120, 69 (1943).

7. M. H. Nichols, Phys. Rev. 57, 297 (1940).

8. Conyers Herring and M. H. Nichols, Rev. Mod. Phys. 21, 185 (1949).

9. R. P. Johnson, A. B. White, and R. B. Nelson, Rev. Sci. Inst. 9, 253 (1938).

10. R. P. Johnson and W. Schockley, Phys. Rev. 49, 439 (1936).

11. K. B. Blodgett and I. Langmuir, Rev. Sci. Inst. 5, 321 (1934).

12. H. A. Jones and I. Langmuir, Gen. Elec. Rev. 30, 310,354,408 (1927).

13. E. W. Müller, Zeits. f. Physik 120, 261,270 (1943).

14. J. A. Becker, Bell System Tech. J. 30, 907 (1951); also by private communication.

15. W. P. Dyke, Phys. Rev. 85, 752 (1952).

16. Conyers Herring, J. App. Phys. 21, 301 (1950).

17. W. B. Nottingham, Phys. Rev. 55, 203 (1939).

18. R. T. Bayard and D. Alpert, Rev. Sci. Inst. 21, 571 (1950).

19. Saul Dushman, Scientific Foundations of Vacuum Technique, (J. Wiley and Sons, Inc., New York, 1949).

20. W. D. Urry, J. Am. Chem. Soc. 54, 3887 (1932).

21. W. H. Keesom, Helium, (O. Amsterdam, Elsevier, 1942).

22. R. P. Johnson and W. B. Nottingham, Rev. Sci. Inst. 5, 191 (1934).

23. W. E. Forsythe and E. M. Watson, J. Opt. Soc. Am. 24, 114 (1934).

24. I. Langmuir, S. MacLane, K. B. Blodgett, Phys. Rev. 35, 478 (1930).

25. H. Palevsky, R. K. Swank and R. Brenshik, Rev. Sci. Inst. 18, 298 (1947).

26. L. N. Ridenour and C. W. Lampson, Rev. Sci. Inst. 8, 162 (1937).

27. M. H. Nichols, M.I.T. Ph.D. Thesis (1939).

28. K. G. McKay, Advances in Electronics, volume 1 (Academic Press, Inc., New York, 1948).

29. Erick Rudberg, Phys. Rev. 50, 138 (1936).

30. L. J. Haworth, Phys. Rev. 48, 88 (1935).

31. L. R. Koller, Gen. Elec. Rev. 51, 33 (April), 50 (June), (1948).

32. R. L. E. Seifert and T. E. Phipps, Phys. Rev. 43, 1058 (1933).

33. D. Turnbull and T. E. Phipps, Phys. Rev. 56, 663 (1939).

34. W. B. Nottingham, Phys. Rev. 57, 935 (1940).

35. R. J. Munick, W. B. LaBerge, and E. A. Coomes, Phys. Rev. 80, 887 (1950).

36. W. Heinze and S. Wagener, Zeits. f. Physik 110, 164 (1938).

37. J. G. Potter, Phys. Rev. 58, 623 (1940).

38. W. B. Nottingham, as reported at Field Emission Seminar, Linfield College, McMinnville, Ore., Jan. 2, 1952.

39. E. A. Coomes, Phys. Rev. 55, 519 (1939).

40. W. R. Smythe, Static and Dynamic Electricity, (McGraw-Hill Book Company, Inc., New York, 1939).